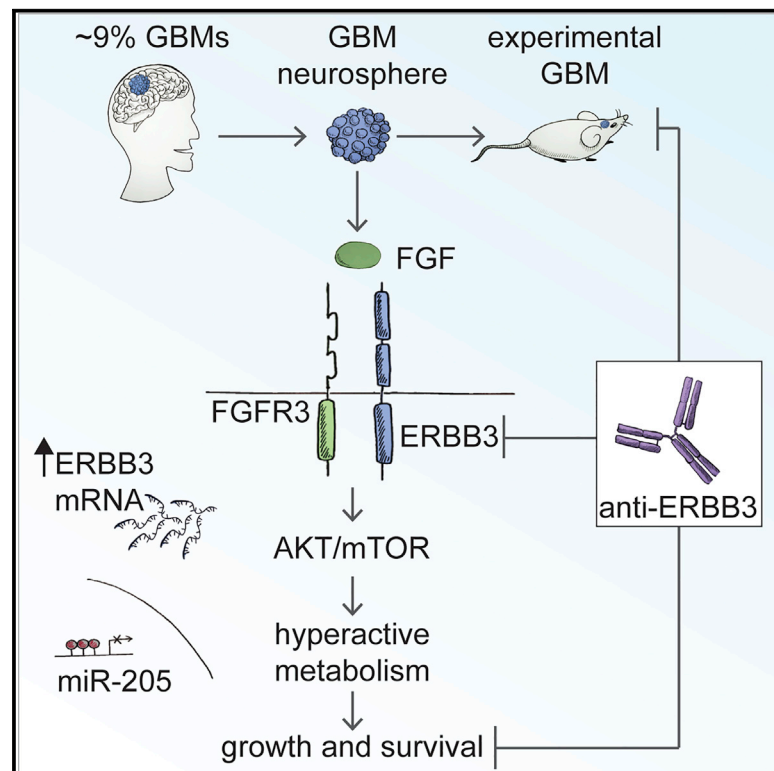


ERBB3 overexpression due to miR-205 inactivation confers sensitivity to FGF, metabolic activation, and liability to ERBB3 targeting in glioblastoma

Graphical abstract



Authors

Francesca De Bacco, Francesca Orzan, Jessica Erriquez, ..., Gaetano Finocchiaro, Paolo M. Comoglio, Carla Boccaccio

Correspondence

carla.boccaccio@ircc.it

In brief

Taking advantage of an integrated model based on patient-derived stem-like cells, De Bacco et al. identify a GBM subset characterized by ERBB3 overexpression, driven by an inheritable mechanism of miR-205 inactivation. By upregulating cell metabolism, overexpressed ERBB3 provides a selective advantage and a liability to be exploited for targeted therapy.

Highlights

- Total of ~9% of human GBMs feature ERBB3 overexpression and nuclear accumulation
- ERBB3 overexpression is sustained by miR-205 inactivation
- Overexpressed ERBB3 is activated by FGFR and upregulates cell metabolism
- ERBB3 targeting by a specific antibody inhibits growth of ERBB3-overexpressing GBMs



Article

ERBB3 overexpression due to miR-205 inactivation confers sensitivity to FGF, metabolic activation, and liability to ERBB3 targeting in glioblastoma

Francesca De Bacco,¹ Francesca Orzan,¹ Jessica Erriquez,² Elena Casanova,¹ Ludovic Barault,^{3,4} Raffaella Albano,² Antonio D'Ambrosio,¹ Viola Bigatto,^{1,12} Gigliola Reato,¹ Monica Patanè,⁵ Bianca Pollo,⁵ Geoffrey Kuesters,^{6,13} Carmine Dell'Aglio,^{7,8} Laura Casorzo,⁷ Serena Pellegatta,⁵ Gaetano Finocchiaro,^{5,9} Paolo M. Comoglio,^{10,11} and Carla Boccaccio^{1,4,14,*}

¹Laboratory of Cancer Stem Cell Research, Candiolo Cancer Institute, FPO-IRCCS, 10060 Candiolo, Turin, Italy

²Candiolo Cancer Institute, FPO-IRCCS, 10060 Candiolo, Turin, Italy

³Laboratory of Cancer Epigenetics, Candiolo Cancer Institute, FPO-IRCCS, 10060 Candiolo, Turin, Italy

⁴Department of Oncology, University of Torino Medical School, 10060 Candiolo, Turin, Italy

⁵Fondazione IRCCS Istituto Neurologico C. Besta, 20133 Milan, Italy

⁶Merrimack Pharmaceuticals, Inc., One Broadway, 14th floor, Cambridge, MA 02142, USA

⁷Unit of Pathology, Candiolo Cancer Institute, FPO-IRCCS, 10060 Candiolo, Turin, Italy

⁸Santa Croce e Carle Hospital, 12100 Cuneo, Italy

⁹Department of Neurology, IRCCS Ospedale San Raffaele, 20132, Milan, Italy

¹⁰Laboratory of Exploratory Research and Molecular Cancer Therapy, Candiolo Cancer Institute, FPO-IRCCS, 10060 Candiolo, Turin, Italy

¹¹FOM, FIRC Institute of Molecular Oncology, 20139 Milan, Italy

¹²Present address: Evotec, 37135 Verona, Italy

¹³Present address: Rubius Therapeutics, 399 Binney Street, Suite 300, Cambridge, MA 02139, USA

¹⁴Lead contact

*Correspondence: carla.boccaccio@ircc.it

<https://doi.org/10.1016/j.celrep.2021.109455>

SUMMARY

In glioblastoma (GBM), the most frequent and lethal brain tumor, therapies suppressing recurrently altered signaling pathways failed to extend survival. However, in patient subsets, specific genetic lesions can confer sensitivity to targeted agents. By exploiting an integrated model based on patient-derived stem-like cells, faithfully recapitulating the original GBMs *in vitro* and *in vivo*, here, we identify a human GBM subset (~9% of all GBMs) characterized by ERBB3 overexpression and nuclear accumulation. ERBB3 overexpression is driven by inheritable promoter methylation or post-transcriptional silencing of the oncosuppressor miR-205 and sustains the malignant phenotype. Overexpressed ERBB3 behaves as a specific signaling platform for fibroblast growth factor receptor (FGFR), driving PI3K/AKT/mTOR pathway hyperactivation, and overall metabolic upregulation. As a result, ERBB3 inhibition by specific antibodies is lethal for GBM stem-like cells and xenotransplants. These findings highlight a subset of patients eligible for ERBB3-targeted therapy.

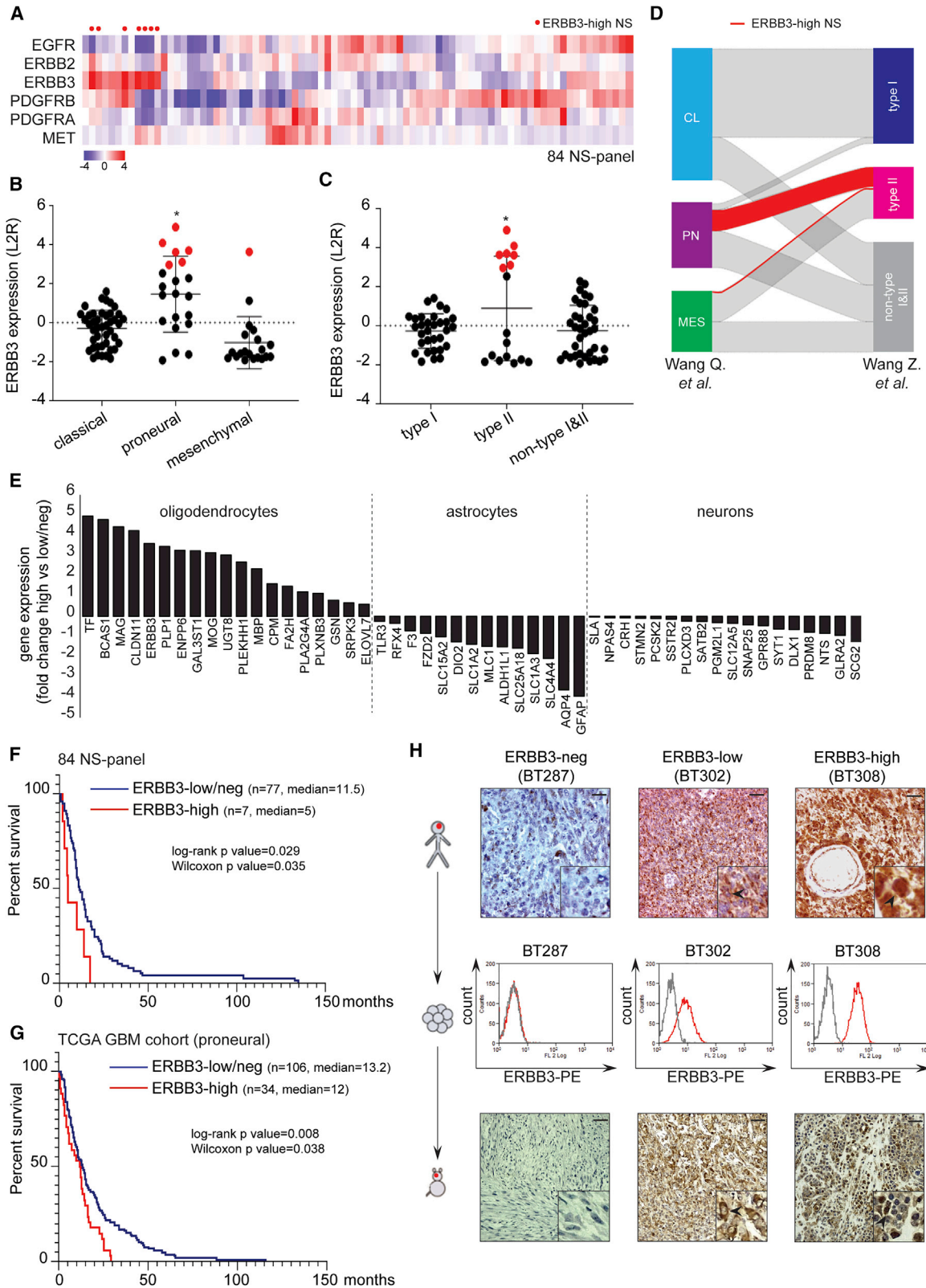
INTRODUCTION

Glioblastoma (GBM; WHO grade IV glioma) therapy is still based on a standard protocol established in 2005 that encompasses surgery, which is often suboptimal for the infiltrative nature of the tumor, followed by radiotherapy and chemotherapy with temozolomide (Hegi et al., 2005). GBM molecular characterization by transcriptional subtyping and identification of recurrent subtype-specific genetic alterations contributed to refining its diagnostic classification, but these methods have not helped to discern prognostic subgroups or to instruct new therapeutic protocols (Reifenberger et al., 2017). Intratumor genetic heterogeneity, including mosaic amplification of the main druggable targets such as receptor tyrosine kinases (RTKs), which overall occurs in more than 60% of patients (Brennan et al., 2013; Snu-

derl et al., 2011), sets the premises for resistance to therapeutic agents hitting a single target, likely ending up in positive selection of coexisting tumor subclones that rely on alternative genetic alterations. On the other hand, targeting a common signaling hub such as phosphatidylinositol 3-kinase (PI3K), presumptively hyperactivated by RTK alterations and/or *PTEN* biallelic loss, failed to provide a benefit for the high risk of generalized toxicity (Le Rhun et al., 2019).

Nevertheless, the principle of targeting genetic alterations has been beneficial in an ample spectrum of tumors, from lung cancers harboring alterations, such as *ALK* translocations, *epidermal growth factor receptor (EGFR)* mutations, or *MET* exon 14 skipping (Yang et al., 2020), to a small GBM-subset harboring *BRAF* mutations (Reifenberger et al., 2017). In such cases, the targeted alterations were likely selected during tumor





(legend on next page)

Darwinian evolution for providing benefits so essential to confer a dependence known as “oncogene addiction” (Sharma and Settleman, 2007).

To find out “addictive” GBM targets, it seems important to unearth the molecular mechanisms that are fixed by genetic alterations and challenge their requirement for tumor cell viability. To this aim, we exploited GBM neurospheres (NSs), long-term propagating cultures enriched in stem-like cells (GSCs), which faithfully retain the genomic landscape and the transcriptomic features of the original tumors and reliably recapitulate the tumor properties upon transplantation in the mouse (De Bacco et al., 2012, 2016; Li et al., 2008). By perusing a panel of 84 NSs in search for uncommon RTK alterations, we identified a subset that, by transcriptional profiling, was characterized by high ERBB3 gene expression and corresponded to patients with dismal prognosis. In this integrated model, we identified miR-205 epigenetic inactivation (i.e., transcriptional repression by promoter methylation or post-translational silencing) as a mechanism that sustains ERBB3 overexpression and is inheritable across tumor cell generations. Moreover, we found out that overexpressed ERBB3, an EGFR family member (Yarden and Pines, 2012), heterodimerizes with FGFR and orchestrates a chain of intracellular responses leading from FGF stimulation to enhanced energetic and biosynthetic metabolism. This feature is crucial to the malignant phenotype, conferring both a selective advantage and a liability so that, as we show, ERBB3 inhibition is lethal for GBM cells *in vitro* and *in vivo*.

RESULTS

ERBB3 overexpression defines a subset of proneural GBM with oligodendroglial features and dismal prognosis

In GBM, RTK overexpression, which is often sustained by gene amplification, significantly contributes to tumorigenesis and provides potential therapeutic targets (Reifenberger et al., 2017). To identify GBM subgroups characterized by altered expression of specific RTKs, we exploited a panel of 84 NSs (84 NS-panel), derived from as many primary GBMs. ERBB3 expression, previously associated with the proneural GBM subtype (Verhaak et al., 2010), was found remarkably high ($\log_2\text{ratio} > 2.5$) in a

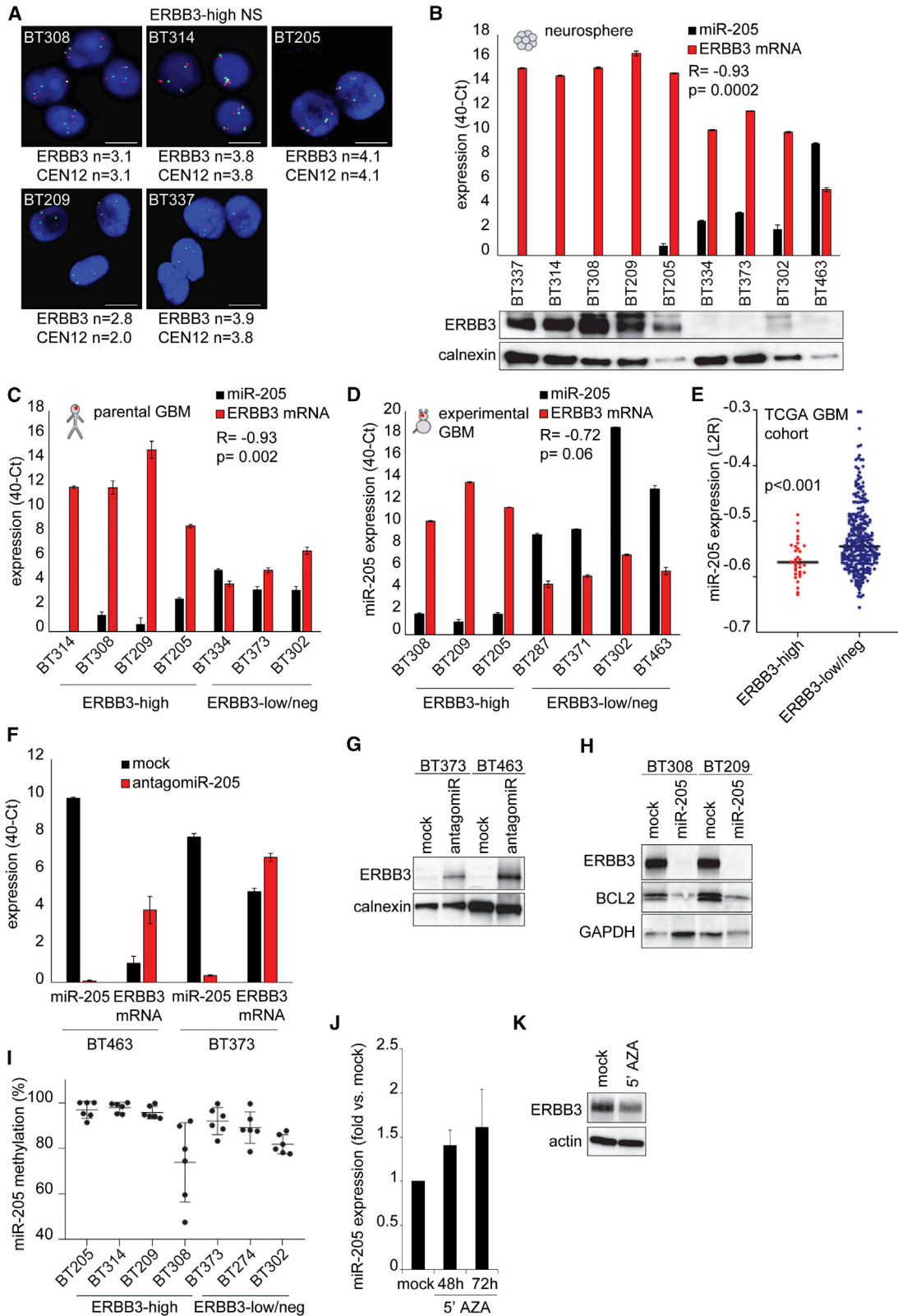
small subgroup of 7 NSs (8.4%, hereafter indicated as ERBB3-high NS), characterized by a globally very low expression of the main GBM-associated RTKs (EGFR, ERBB2, platelet derived growth factor receptor alpha [PDGFRA] and MET) (Figure 1A). These NSs were derived from tumors that displayed high ERBB3 expression as well (Figure S1A). An analysis of the The Cancer Genome Atlas (TCGA) GBM cohort ($n = 528$) identified a tumor subgroup (9.3%), classified as proneural, which displayed similar properties, i.e. high ERBB3 expression associated with low levels of the other RTKs except PDGFRA (Figure S1B).

According to the Verhaak’s signature (Wang et al., 2017), all NSs could be assigned either to a classical (32/84), proneural (30/84), or mesenchymal (22/84) subtype (Figure S1C; Table S1). Six out of 7 ERBB3-high NS were classified as proneural, and 1 as mesenchymal (Figure 1B). Moreover, we applied to the NS panel a new type I-type II stratification method, based on a signature including ERBB3 as a prominent type II marker (Wang et al., 2020). As result, 31/84 NSs were classified as type I, 17/84 as type II, and 36/84 remained defined as “non-type I&II” (Figure S1D; Table S1; Wang et al., 2020). Interestingly, 7/7 ERBB3-high NS were included in the type II subgroup (Figure 1C). A comparison between the Verhaak’s and the type I-type II assignments showed that type I mostly includes classical NSs, while type II comprises, beside proneural ERBB3-high NS, 9/22 mesenchymal NSs. Finally, the non-type I&II group includes similar percentages of proneural NSs expressing low ERBB3 levels (15/36), mesenchymal NSs (11/36), and classical NSs (10/36) (Figure 1D). NS assignments to type I and II, as well as to the Verhaak’s subtypes, reflected ratios reported in the TCGA GBM cohort (Wang et al., 2017, 2020), attesting that the 84 NS-panel reliably reflects the distribution of gene expression profiles in the patient population affected by GBM.

Consistent with assignment to the proneural/type II subsets, ERBB3-high NS displayed a specific and significant enrichment in an oligodendroglial gene expression signature (Figures 1E and S1E; Cahoy et al., 2008), reflecting a likely origin from an oligodendroglial progenitor (OPCs) (Wang et al., 2020). Moreover, in both the 84 NS-panel and TCGA GBM cohort, ERBB3 expression levels correlated with those of SRY-box transcription factor 10 (SOX10), a prominent ERBB3 transcriptional regulator (Prasad et al., 2011), and inversely correlated with those of the

Figure 1. ERBB3 overexpression defines a subset of proneural GBM with oligodendroglial features and dismal prognosis

- (A) Heatmap showing spontaneous clustering of the 84 NS-panel according to mRNA levels of the indicated genes (microarray). Red dots, ERBB3-high NS.
- (B) ERBB3 mRNA expression ($\log_2\text{ratio}$ [L2R], microarray) in NSs classified in the 3 GBM subtypes according to Wang et al. (2017). Red dots, ERBB3-high NS, preferentially falling in the proneural subtype (one-way ANOVA, $p = 0.03$). Mean \pm SEM.
- (C) ERBB3 mRNA expression (L2R, microarray) in NSs classified in the 3 subtypes identified by Wang et al. (2020). Red dots, ERBB3-high NS, all classified as type II (one-way ANOVA, $p < 0.001$). Mean \pm SEM.
- (D) Caleydo view of correspondence between the 84-NS panel classification according to Wang et al. (2017) (left) and Wang et al. (2020) (right). Red lines, ERBB3-high NS.
- (E) mRNA expression of oligodendrocyte, astrocyte, and neuron markers (according to Cahoy et al., 2008) significantly modulated in ERBB3-high versus ERBB3-low/neg NS (log fold change).
- (F) Survival curve of patients (all untreated) that originated the 84-NS panel, subdivided according to ERBB3 levels in matched NSs. ERBB3-high, patients matched with NSs displaying ERBB3 L2R > 2.5 ; ERBB3-low/neg, all other patients (NSs with ERBB3 L2R ≤ 2.5).
- (G) Survival curve in the TCGA cohort of untreated primary proneural patients with GBM ($n = 140$), subdivided according to ERBB3 expression. ERBB3-high, patients with ERBB3 mRNA levels falling in the upper quartile; ERBB3-low/neg, all other patients.
- (H) ERBB3 expression in representative patients (top panels, immunohistochemistry [IHC]) and matched NSs (middle panels, flow cytometry) and experimental GBMs obtained by NS orthotopic transplant (bottom panels, IHC). Insets, arrows, ERBB3 nuclear localization. Scale bar, 100 μm .
- See also Figures S1 and S2 and Tables S1, S2, and S3.



(legend on next page)

EGFR coexpressed SOX9 (Figures S1F and S1G), as previously reported (Wang et al., 2020).

Concerning genetic alterations, ERBB3-high NS displayed no statistically significant preferential association with any recurrent GBM gene mutation or copy number variation or with *ERBB3* amplification (Figures S1H and S1I). However, we could observe that ERBB3 overexpression tended (1) to co-occur with *PDGFR* and *CDK4* amplification or with *TP53* mutation; and (2) to be mutually exclusive with *EGFR* amplification and *CDKN2A* loss (Figures S1H and S1J). The same associations were statistically significant in ERBB3-high GBMs from the TCGA cohort (Figure S1K).

Interestingly, unlike overexpression of other RTKs, ERBB3 overexpression emerged as a strongly negative prognostic factor for patients with GBM. This prognostic correlation was observed either in the patient cohort matched to the 84 NS-panel or in the TCGA cohort of patients with GBM (proneural subgroup), in which the overall survival of ERBB3-overexpressing cases was significantly reduced (Figures 1F and 1G; Table S2). Consistently, experimental tumors generated by orthotopic transplantation of proneural ERBB3-high NS were significantly more aggressive than those formed by proneural NSs expressing normal ERBB3 levels, as shown by tumor take and proliferative index (Figures S1L and S1M).

ERBB3 overexpression is inheritable and sustained by epigenetic inactivation of the oncosuppressor miR-205

To establish an adequate model for investigating causes and consequences of ERBB3 overexpression, we further classified NSs based on ERBB3 mRNA levels. Among ERBB3-positive NSs, we discriminated the subgroup of 7 ERBB3-high NS from those that expressed lower but above-the-average ERBB3 levels (ERBB3-low NS, $0 \leq \log_2\text{ratio [L2R]} \leq 2.5$, $n = 29/84$). The remaining were classified as ERBB3-neg NS ($\text{L2R} < 0$, $n = 48/84$) (Figure S2A; Table S1). In the following experiments, BT308, BT209, BT314, and BT205 NSs were used as representatives of ERBB3-high; BT373 and BT302 as ERBB3-low; and BT463 and BT287 as ERBB3-neg (Figure S2B).

The ERBB3 protein levels in ERBB3-high NS were comparable to those observed in reference cell lines overexpressing ERBB3,

such as MCF7 (Figures S2C and S2D). Interestingly, by analysis of fractionated nuclear/cytoplasmic extracts and immunofluorescence, we observed that in ERBB3-high NS, ERBB3 localized also in the nucleus (Figures S2B and S2E). ERBB3 nuclear localization was previously described, but it has a still poorly understood functional significance (Reif et al., 2016).

Remarkably, ERBB3 protein levels remained stable in matched parental GBMs, NSs, and experimental tumors obtained by NS orthotopic transplant. In ERBB3-high cases, the ERBB3 protein was homogeneously overexpressed and localized in the nucleus within both parental and experimental tumor tissues and in NS cells as well (Figure 1H). ERBB3 overexpression was faithfully passed on throughout multiple cell generations, as shown by NS single-cell subcloning (Figures S2F and S2G), and it was not downregulated after NS culture in pro-differentiating conditions, unlike the expression of other genetically unaltered RTKs such as MET (Figure S2H; De Bacco et al., 2012). This evidence suggested that ERBB3 overexpression is fixed by inheritable genetic mechanisms.

By investigating such mechanisms, we ruled out alterations of the *ERBB3* gene, as (1) amplifications or translocations were unequivocally excluded by fluorescence in situ hybridization (FISH) (Figure 2A) in addition to qPCR (Figure S1I), and (2) mutations known to affect protein stability (Jaiswal et al., 2013) were absent (Figure S1H).

Considering the known mechanisms of ERBB3 post-translational control (Figure S3A) (Campbell et al., 2010), we excluded altered ERBB3 targeting to degradation, for lack of anti-correlation between ERBB3 and NEDD4 or NRDP1 ubiquitin ligase expression levels (Figure S3B).

We thus focused on miR-205, which is known as a major regulator of ERBB3 translation (Iorio et al., 2009; Campbell et al., 2010). We observed a strong anti-correlation between ERBB3 and miR-205 expression in NSs and parental and experimental tumors from our cohort and in the TCGA GBM cohort as well (Figures 2B–2E). The impact of miR-205 on ERBB3 protein translation was confirmed in NSs by complementary approaches such as (1) transduction of ERBB3-low/neg NS (BT463 and BT373) with an antagomiR-205, which upregulated ERBB3

Figure 2. ERBB3 overexpression is sustained by inactivation of the oncosuppressor miR-205

- (A) FISH analysis of *ERBB3* in 5 representative ERBB3-high NS (red dots, ERBB3 probe; green dots, chromosome 12 centromeric probe [CEN12]). n, average number of *ERBB3* gene copies evaluated in 100 nuclei. Scale bar, 12.5 μm .
- (B) miR-205 and ERBB3 mRNA expression (qPCR) and ERBB3 protein levels (western blot) in representative NSs. calnexin, loading control (Pearson correlation coefficient between miR-205 and ERBB3 mRNA: $R = -0.93$, $p = 0.0002$). Mean \pm SEM, $n = 3$.
- (C and D) miR-205 and ERBB3 expression (qPCR) in parental GBMs (C) that originated ERBB3-high or -low/neg NS and in experimental GBMs (D) generated by transplantation of ERBB3-high or -low/neg NS (Pearson correlation coefficient between miR-205 and ERBB3 expression: parental GBMs, $R = -0.93$, $p = 0.002$; experimental GBMs, $R = -0.72$, $p = 0.06$). Mean \pm SEM, $n = 3$.
- (E) miR-205 expression in GBMs from the TCGA cohort subdivided according to ERBB3 expression levels (ERBB3-high: patients with ERBB3 mRNA levels falling in the upper quartile; ERBB3-low/neg: all other patients; * $p < 0.001$, one-way ANOVA). Mean \pm SEM, $n = 339$.
- (F) miR-205 and ERBB3 mRNA expression (qPCR) in ERBB3-low/neg NS (BT463 and BT373) transfected with antagomiR-205. mock, mock-transfected cells. Mean \pm SEM, $n = 3$.
- (G) Western blot showing total ERBB3 protein in BT373 and BT463 transfected as in (F). calnexin, loading control.
- (H) ERBB3 protein expression in ERBB3-high NS (BT308 and BT209) transduced with miR-205. The known miR-205 target BCL2 was shown as positive control. GAPDH, loading control.
- (I) miR-205 promoter methylation ratio in ERBB3-high and -low/neg NS. ERBB3-high NS display higher methylation ratio versus ERBB3-low/neg (two-way ANOVA, $p < 0.0001$). Mean \pm SEM, $n = 6$.
- (J and K) miR-205 expression (qPCR) in ERBB3-high NS (BT209) treated with the demethylating agent 5'Aza-2-deoxycytidine (5' AZA) at the indicated time points after treatment (J) and ERBB3 protein in the same NS 72 h after treatment (K). actin, loading control; mock, PBS-treated cells. Mean \pm SEM, $n = 3$.
- See also Figure S3.

expression (Figures 2F and 2G); and (2) transduction of ERBB3-high NS (BT308 and BT209) with miR-205 (Figure S3C), which completely abolished ERBB3 protein expression (Figure 2H). Altogether, these data indicate that ERBB3 overexpression is likely due to the loss of miR-205 expression, and the latter should occur through inheritable genetic or epigenetic mechanisms.

Having excluded miR-205 genetic mutation by Sanger sequencing or loss by qPCR and FISH, we investigated whether miR-205 silencing could result from promoter hypermethylation, a frequently reported mechanism of miR-205 inactivation (Qin et al., 2013). We found that, indeed, the miR-205 promoter was hypermethylated in the majority of ERBB3-high NS, but not in ERBB3-low/neg NS (Figure 2I); accordingly, NS treatment with the de-methylating agent 5'-Aza-2'-deoxycytidine concomitantly increased miR-205 and decreased ERBB3 expression (Figures 2J and 2K). As a notable exception, ERBB3-high BT308 NS lacked miR-205 expression (Figure 2B) in the absence of promoter methylation (Figure 2I). In this case, we could correlate miR-205 silencing with overexpression of lnc-RNA SNHG5, which acts as a miR-205 sponge (Li et al., 2019), and was highly expressed in BT308 NS, as well as in matched parental and experimental GBMs (Figures S3D–S3F).

We also investigated whether other microRNAs (miRNAs) could be involved in ERBB3 targeting. By *in silico* analysis of ERBB3 3' UTR seed binding regions, we identified a list of miRNAs displaying a complementarity score similar to miR-205 (Figure S3G), which, however, did not display any anti-correlation with ERBB3 expression either in NSs or in the whole TCGA GBM cohort (Figures S3H and S3I).

We can conclude that, beside the known transcriptional activator SOX10, miR-205 is essential for controlling ERBB3 expression in GBM. Notably, the loss of miR-205 expression occurs through inheritable silencing mechanisms such as promoter hypermethylation or overexpression of the lnc-RNA SNHG5 (Figure S3J).

ERBB3 is overexpressed in the absence of other EGFR family members

ERBB3 is a member of the EGFR family devoid of intrinsic tyrosine kinase activity. ERBB3 signaling activation requires phosphorylation by a kinase-competent dimerization partner, namely another EGFR family member (Yarden and Pines, 2012). Such heterodimerization is usually induced either by the ERBB3 ligand Neuregulin 1 (NRG1) or by EGF-like ligands that bind EGFR (Yarden and Pines, 2012). However, transcriptomic analysis of the 84 NS-panel and TCGA GBM cohort showed that ERBB3 expression is mutually exclusive with *EGFR* amplification (Figures S1J and S1K) or expression (Figures S4A and S4B), which are both known to be mostly associated with the classical subtype (Verhaak et al., 2010). Concerning expression of the other EGFR family members, ERBB2 was anti-correlated with ERBB3 in the TCGA GBM cohort and only weakly associated ($R = 0.047$, $p = 0.67$) with ERBB3 in the 84 NS-panel; ERBB4 was instead significantly coexpressed with ERBB3 in the TCGA cohort, but it was not expressed in NSs, which is consistent with preferential expression of this RTK in differentiated neural and glial cells (Figures S4A and S4B) (Duhem-Tonnelle et al., 2010). By western blot and flow cytometry, we confirmed that in

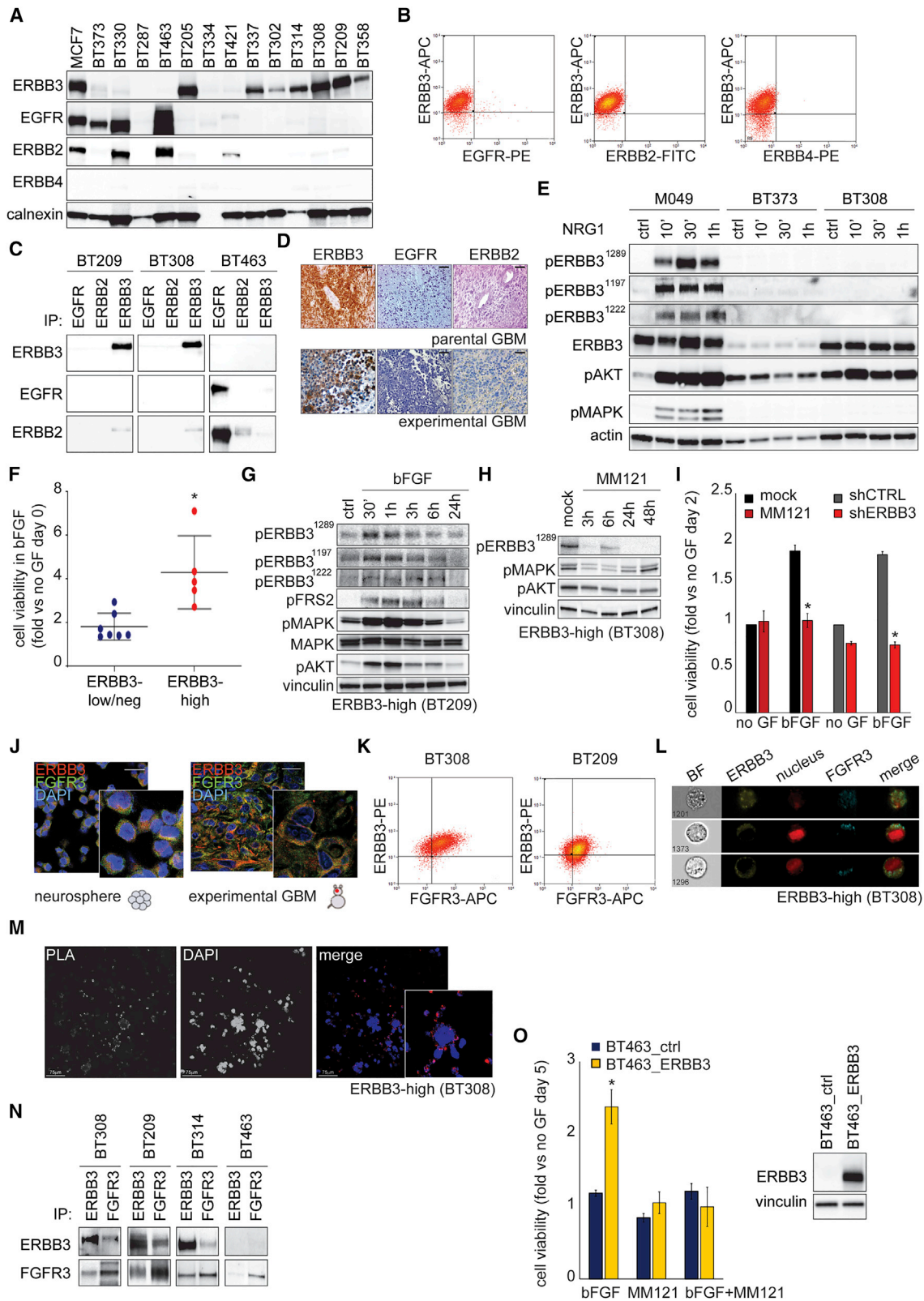
ERBB3-high NS, the ERBB3 conventional partners EGFR, ERBB2, or ERBB4 were neither coexpressed nor coprecipitated with ERBB3 in the presence of the ligands EGF or NRG1 (Figures 3A–3C and S4C). The lack of EGFR and ERBB2 protein expression was confirmed in ERBB3-high parental and experimental GBMs (Figure 3D), as well as in ERBB3-high TCGA GBM tissues assessed by The Human Protein Atlas (Figures S4D and S4E). Consistently, in ERBB3-high NS (kept in the absence of exogenous growth factors for 48 h), NRG1 stimulation failed to induce phosphorylation of multiple ERBB3 tyrosines and activation of downstream transducers (mitogen-activated protein [MAP] kinase and AKT), which were instead observed in spheres from colorectal cancers coexpressing EGFR and ERBB3 and assessed under the same conditions (Figure 3E; Luraghi et al., 2018), and in representative conventional cell lines (Figure S4F). In ERBB3-high NS, the lack of ERBB3 activation by NRG1 was mirrored by a lack of proliferative response to NRG1 (Figure S4G); no biochemical or biological response to EGF was observed as well (Figures S4F–S4H). Overall, these experiments indicated that, in NSs as well as in GBMs, ERBB3 is overexpressed in the absence of other EGFR family members. Moreover, in NSs, ERBB3 is insensitive to its conventional ligand NRG1 or to the EGFR ligand EGF.

Overexpressed ERBB3 is activated by bFGF through FGFR3

The above experiments implied that proliferation of ERBB3-high NS, which were selected and long-term propagated in a standard stem-cell medium (i.e. containing EGF and bFGF as the sole growth factors), relied specifically on bFGF. Indeed, ERBB3-high NS significantly responded to bFGF (Figure 3F), without additive effects by EGF or NRG1 (Figure S4G). The complete dependence of ERBB3-high NS proliferation on bFGF was further confirmed by treatment of NSs cultured in the standard medium with the pan-FGFR inhibitor BGJ398 (Figure S5A).

On these premises, we investigated whether, in ERBB3-high NS, bFGF stimulation could activate ERBB3 signaling. We indeed showed that bFGF, added as the sole growth factor, induced not only FGFR activation (as shown by phosphorylation of its specific fibroblast receptor substrate 2 [FRS2]) but also ERBB3 phosphorylation, which was followed by MAPK and AKT activation (Figures 3G and S5B), and prevented by FGFR inhibition with BGJ398 (Figure S5C). To investigate whether the downstream signaling response elicited by bFGF depended on ERBB3, we treated ERBB3-high NS with the specific ERBB3 inhibitory antibody seribantumab (also known and hereafter indicated as MM121), which is capable of inducing ERBB3 prolonged downregulation from the cell surface and degradation (Figures S5D and S5E), as previously described (Schoeberl et al., 2017). In ERBB3-high BT308, MM121 quenched downstream signaling sustained by bFGF in the standard medium (Figure 3H) and abolished the proliferative response to bFGF (Figure 3I). The same inhibition was obtained by targeting ERBB3 with a specific small hairpin RNA (shRNA) (Figure 3I).

We thus investigated whether ERBB3 could be a direct FGFR dimerization partner and phosphorylation substrate. Among the 4 FGFR family members, we focused on FGFR3 based on the following evidence: (1) in the 84-NS panel, only FGFR3 (and



(legend on next page)

FGFR4) mRNA levels positively correlated with those of ERBB3 (Figure S5F); (2) in ERBB3-high NS, FGFR3 (and FGFR4) levels were significantly higher than FGFR1 and FGFR2 mRNA levels; conversely, all FGFRs were poorly expressed in ERBB3-low/neg NS (Figure S5G); and (3) only FGFR3 was consistently expressed at high protein levels in representative ERBB3-high NS (Figures S5H and S5I). The FGFR3 critical role in mediating the bFGF signal in ERBB3-high NS was confirmed by FGFR3 expression silencing through shRNA, which fully abolished the proliferative response to bFGF (Figure S5J). Colocalization between ERBB3 and FGFR3 was shown in both ERBB3-high NS and experimental GBMs by immunofluorescence (Figure 3J), and in NS by flow-cytometric analysis (Figure 3K) and single-cell imaging (Figure 3L and S5K). A physical interaction between ERBB3 and FGFR3 was indicated by proximity-ligation assays (Figure 3M and S5L) and by ERBB3-FGFR3 coprecipitation in ERBB3-high NS (Figure 3N).

Moreover, we showed that forced ERBB3 overexpression could enable ERBB3-low/neg NS to respond to bFGF. Indeed, ERBB3-neg/low NS, although expressing FGFR family members (Figures 3N and S5M), were poorly sensitive to bFGF (Figure 3F) and mostly relied on EGF for their proliferation (Figure S5N). The proliferative response of ERBB3-neg BT463 transduced with ERBB3 was similar to that of ERBB3-high NS and fully counteracted by MM121 (Figure 3O).

Finally, we investigated whether overexpressed ERBB3 could be activated by other RTKs, including KIT and NTRK2, which

were highly expressed in ERBB3-high NS and TCGA GBMs, and MET and PDGFR, expressed at lower levels, but well-known to heterodimerize with ERBB3 (Figures S6A–S6C; Engelman et al., 2007; Song et al., 2018). However, the involvement of the above receptors was ruled out as their respective ligands failed to induce ERBB3 phosphorylation or receptor coprecipitation (Figure S6D).

Altogether, these data indicate that overexpressed ERBB3 is specifically activated by bFGF through heterodimerization with FGFR3 and can sensitize NSs to bFGF.

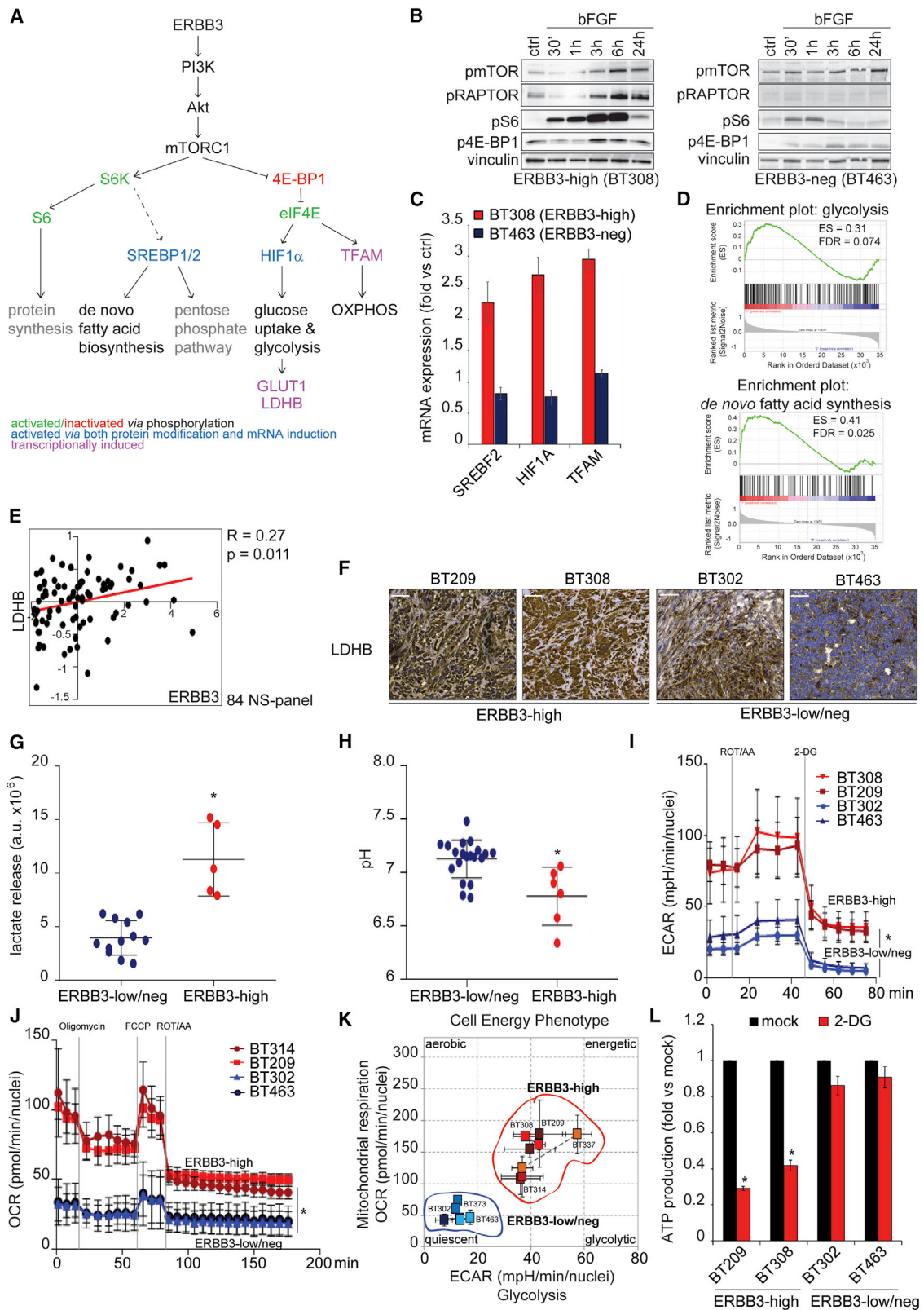
In ERBB3-overexpressing NSs, bFGF sustains the PI3K/AKT/mTOR pathway and metabolic hyperactivation

By harboring six consensus sequences for binding p85, the regulatory PI3K subunit (Schulze et al., 2005), ERBB3 is a powerful activator of the PI3K/AKT/mTOR pathway (Goncalves et al., 2018; Saxton and Sabatini, 2017). This pathway is well known for coupling growth factor signaling with anabolic metabolism required for biomass accumulation and cell duplication (Saxton and Sabatini, 2017). Hyperactivation of this pathway is essential to cancer proliferation and can provide a target for therapeutic intervention (Bi et al., 2020). As depicted in Figure 4A, downstream the mTOR kinase complex 1 (mTORC1) the pathway splits into two main branches, namely, one mainly responsible for protein and fatty acid biosynthesis and the other for upregulation of glycolytic and/or oxidative metabolism. In particular, (1) S6 kinase (S6K) activates S6, a master regulator of protein

Figure 3. ERBB3 is overexpressed in the absence of the other EGFR family members and is activated by bFGF through FGFR3

- (A) Western blot showing expression of ERBB3 and the other EGFR family members (EGFR, ERBB2, and ERBB4) in representative NSs and breast cancer cell line MCF7 (antibody positive control).
- (B) Flow cytometry showing lack of ERBB3 coexpression with EGFR, ERBB2, or ERBB4 in a representative ERBB3-high NS (BT209).
- (C) Immunoprecipitation (IP) with antibodies against EGFR, ERBB2, and ERBB3 in representative ERBB3-high (BT209 and BT308) and -neg NS (BT463), followed by western blot with anti-ERBB3, -EGFR, or -ERBB2 showing lack of coexpression.
- (D) Representative IHC staining of ERBB3, EGFR, and ERBB2 in representative ERBB3-high parental (top panel) and experimental (bottom panel) BT308 GBMs. Scale bar, 100 μ m.
- (E) Western blot showing lack of ERBB3 phosphorylation on Tyr1289, Tyr1197, and Tyr1222 at the indicated time points after treatment with the ERBB3 ligand NRG1 in representative ERBB3-high (BT308) and -low (BT373) NSs. Activation of downstream transducers AKT and MAPK is also shown (in BT308 AKT is basally active owing to *PTEN* loss). A colosphere (colorectal cancer stem cell culture, M049) sensitive to NRG1 is used as positive control. actin, loading control.
- (F) Cell viability assay in ERBB3-low/neg ($n = 7$) and ERBB3-high-NS ($n = 5$), after 4 days in the presence of bFGF as the sole growth factor (* $p < 0.001$, one-way ANOVA). Mean \pm SEM.
- (G) Western blot showing phosphorylation (p) of ERBB3 on Tyr1289, AKT, and MAPK in ERBB3-high BT209 kept in the absence of any growth factor for 48 h and treated with bFGF. Phosphorylation of fibroblast receptor substrate 2 (FRS2) was shown as surrogate marker of FGFR activation. ctrl: PBS-treated cells; vinculin, loading control. The same vinculin immunoblot is shown in Figure S7A as part of the same experiment.
- (H) Western blot showing inhibition of ERBB3, MAPK, and AKT phosphorylation (p) at different time points after treatment with or without MM121 of ERBB3-high NS (BT308) kept in standard medium (EGF + bFGF). mock, PBS-treated cells; vinculin, loading control. The same vinculin immunoblot is shown in Figure 5A as part of the same experiment.
- (I) Cell viability of ERBB3-high BT308, kept in the absence of any growth factor for 48 h and treated with bFGF or control medium (no growth factor [GF]) for 2 days. NSs were either treated with MM121 or transduced with a specific ERBB3 shRNA (shERBB3). mock, PBS-treated cells (* $p < 0.001$, paired t test). Mean \pm SEM, $n = 6$.
- (J) Immunofluorescence showing ERBB3 and FGFR3 colocalization in representative ERBB3-high NS (BT308) and matched experimental GBM. DAPI, nuclear staining; inset, higher magnification. Scale bar, 25 μ m.
- (K) Flow cytometry showing ERBB3 coexpression with FGFR3 in representative ERBB3-high NS (BT308 and BT209).
- (L) Colocalization of ERBB3 and FGFR3 measured by Amnis ImageStream in single cells from representative ERBB3-high NS (BT308). Single and merged fluorescence antibody signals are shown. BF, bright field.
- (M) Proximity ligation assay (PLA) showing ERBB3-FGFR3 interaction in representative ERBB3-high NS (BT308). Scale bar, 75 μ m.
- (N) IP with antibodies against ERBB3 or FGFR3 in representative ERBB3-high (BT209, BT308, and BT314) and ERBB3-neg NS (BT463), and western blot with anti-ERBB3 or -FGFR3 showing coprecipitation in ERBB3-high NS.
- (O) Cell viability in representative ERBB3-neg NS transduced with ERBB3 (BT463_ERBB3) or not (BT463_ctrl), kept in the absence of any growth factor for 48 h and treated with bFGF, with or without MM121. ERBB3 protein in transduced BT463 is shown. vinculin, loading control (* $p < 0.001$, paired t test BT463_ERBB3 versus BT463_ctrl). Mean \pm SEM, $n = 6$.

See also Figures S4, S5, S6, and S11 (related to STAR Methods).



(legend on next page)

synthesis, and sterol regulatory element binding protein 1/2 (SREBP1/2), transcription factors driving expression of *de novo* fatty acid biosynthesis and pentose phosphate pathway genes (Düvel et al., 2010); and (2) 4E-BP1 releases elongation factor eIF4E; this, in turn, promotes accumulation of Hypoxia Inducible Factor-1 α (HIF-1 α), which upregulates transcription of glucose uptake and glycolysis genes, including Glucose Transporter 1 (GLUT1) and Lactate Dehydrogenase B (LDHB) (Düvel et al., 2010); moreover, eIF4E promotes accumulation of transcription factor A mitochondrial (TFAM), required for mitochondrial expression of oxidative phosphorylation (OXPHOS) genes (Morita et al., 2013). In NSs, we could specifically associate activation of the global PI3K/AKT/mTOR pathway with ERBB3 overexpression and bFGF stimulation. Indeed, in ERBB3-high NS treated with bFGF, but not in ERBB3-neg, we observed (1) activating phosphorylation of key signal transducers such as mTOR and its regulator RAPTOR, S6, and 4E-BP1 (Figures 4B and S7A), and (2) upregulation of target genes, including SREBF2 (encoding SREBP2), HIF1- α , and TFAM (Figures 4C and S7B). Accordingly, a statistically significant enrichment of the overall “*de novo* fatty acid biosynthesis” and “glycolysis” gene sets were observed in the transcriptome of the ERBB3-high NS panel versus all the remaining NSs kept in standard medium, namely, in the presence of bFGF and EGF (Figure 4D). In particular, ERBB3 expression levels directly correlated with those of LDHB either in NSs (Figure 4E) or in the experimental tumors (Figure 4F) or in the TCGA GBM cohort (Figure S7C).

Accordingly, during culture in standard medium, release of the LDHB product lactate was on average more than double in ERBB3-high compared with ERBB3-low/neg NS, and consistently, the culture medium was acidified (pH 6.8 versus 7.2) (Figures 4G and 4H). As a result, genes associated with low pH were overall induced in ERBB3-high versus all the remaining cases in both the 84 NS-panel and TCGA GBM cohort (Figures S7D and S7E). Overall, representative ERBB3-high NS displayed increased glycolytic as well as mitochondrial metabolism and a

global phenotype that was significantly more energetic, as compared with representative ERBB3-low/neg NS (Figures 4I–4K and S7F). Metabolic hyperactivity of ERBB3-high NS depended on bFGF, as shown by addition of the FGFR inhibitor BGJ398 to the standard medium, which dramatically quenched all metabolic parameters (Figures S7G–S7I). Consistent with cell viability experiments (Figure S5A), the ERBB3 low/neg NS metabolic activity was unaffected by the FGFR inhibitor (Figures S7H and S7I).

The hyperactive glycolytic metabolism of ERBB3-high NS was likely able to fuel a more aggressive cell growth and at the same time to cause energetic dependency from glycolysis. Indeed, specific blockade of glucose uptake by the GLUT1 inhibitor 2-deoxyglucose abated ATP production, and therefore cell viability, in ERBB3-high but not in ERBB3-low/neg NS (Figure 4L).

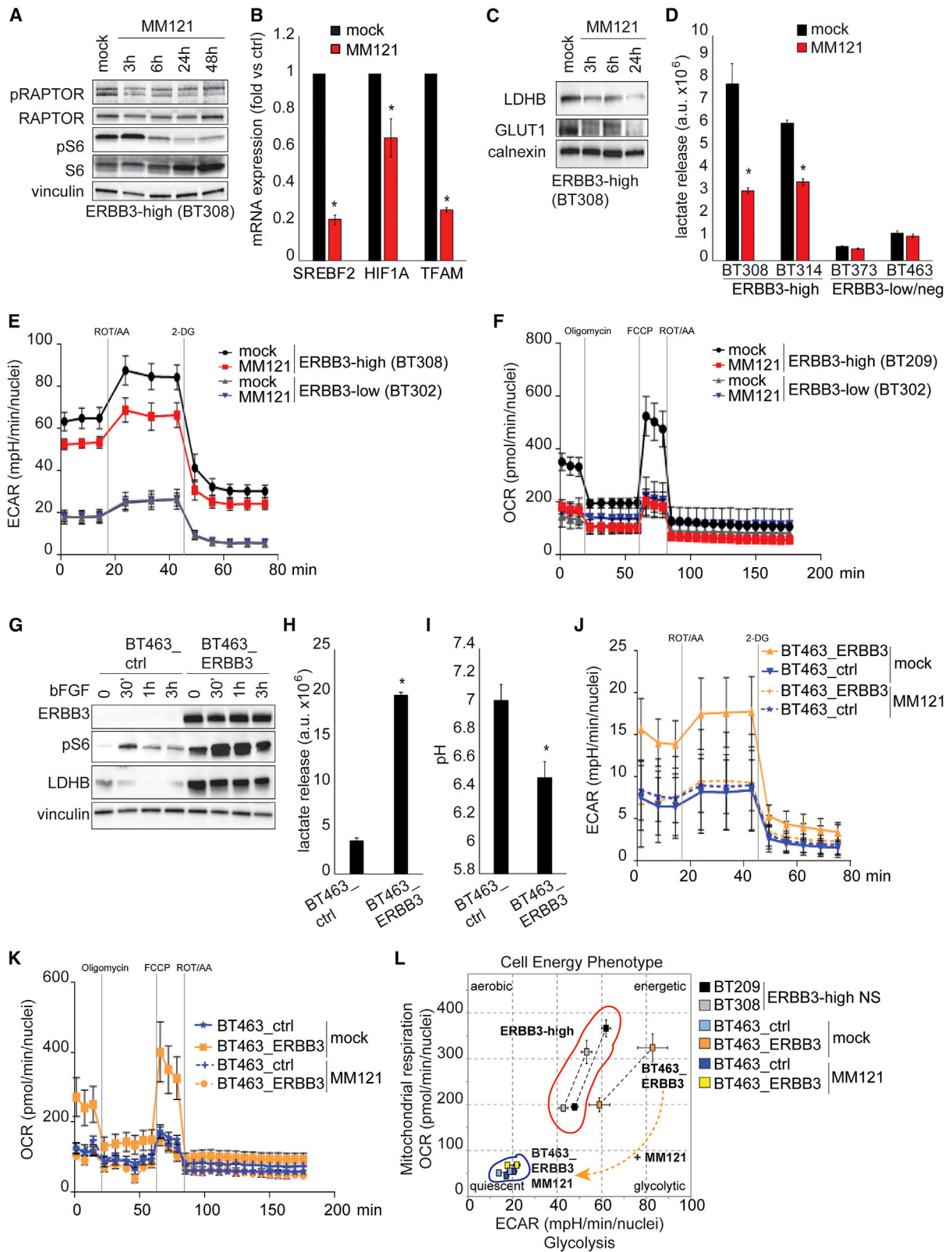
In summary, these data suggest that high levels of ERBB3 expression (supported by miR-205 silencing) enable GSCs to respond to bFGF with activation of the ERBB3-associated PI3K/AKT/mTOR pathway. In ERBB3-high GBMs, but not in those expressing low levels of the receptor, all the downstream effectors of the mTOR pathway, including genes responsible for *de novo* fatty acid synthesis and for glycolytic and mitochondrial metabolism, are functionally upregulated, leading to a highly energetic status. This may represent both an advantage and a liability, as glycolysis inhibition is detrimental for ERBB3-high GBMs.

ERBB3 overexpression is required for the PI3K/AKT/mTOR pathway and cell metabolism upregulation

To investigate whether ERBB3 overexpression is required for PI3K/AKT/mTOR pathway activation and the ensuing metabolic upregulation induced by bFGF, we treated representative NSs with MM121 (see above). When added to ERBB3-high NS growing in standard medium (EGF + bFGF), MM121 caused downregulation of pivotal mediators of the PI3K/AKT/mTOR signaling pathway (Figures 5A, 5B, and S8A) and downstream

Figure 4. In ERBB3-overexpressing NSs, bFGF sustains the PI3K/AKT/mTOR pathway and metabolic hyperactivation

- (A) Schematic representation of ERBB3/PI3K/AKT/mTOR pathway and cell metabolism control.
- (B) Western blot showing phosphorylation (p) of mTOR pathway effectors in ERBB3-high (left) and ERBB3-neg NS (right) kept in the absence of any growth factor for 48 h and treated with bFGF for the indicated time-points. ctrl, PBS-treated cells; vinculin, loading control. The same vinculin immunoblot is shown in Figure S5B as part of the same experiment.
- (C) Expression of mTOR target genes SREBF2, HIF1A, and TFAM in ERBB3-high (BT308) and ERBB3-neg NS (BT463) kept in the absence of any growth factor for 48 h and treated with bFGF for 24 h. Mean \pm SEM, n = 3.
- (D) Gene set enrichment analysis of ERBB3-high versus ERBB3-low/neg NS performed in the 84 NS-panel microarray. *De novo* fatty acid synthesis and glycolysis gene sets are significantly enriched in ERBB3-high NS. ES, enrichment score; FDR, false discovery rate.
- (E) Correlation plot between ERBB3 and LDHB mRNA expression (L2R) in the 84 NS-panel. Pearson correlation coefficient (R) and p value are reported.
- (F) Representative LDHB IHC staining in experimental GBMs generated by intracranially transplanted ERBB3-high (BT209 and BT308), -low (BT302), or -neg NS (BT463). Scale bar, 100 μ m.
- (G) Lactate release from ERBB3-low/neg (n = 12) and ERBB3-high (n = 5) NS after 3 days of culture in standard medium (EGF + bFGF) (*p < 0.05, one-way ANOVA). a.u., arbitrary units. Mean \pm SEM.
- (H) pH of ERBB3-low/neg (n = 20) and ERBB3-high (n = 6) NS standard medium after 3 days of culture (*p < 0.001, one-way ANOVA). Mean \pm SEM.
- (I) Extracellular acidification rate (ECAR) in representative ERBB3-high (BT308 and BT209) and ERBB3-low/neg NS (BT302 and BT463) in basal conditions (standard medium) (mean \pm SEM, n = 4; *p < 0.001, two-way ANOVA). ROT/AA, rotenone/antimycin A; 2-DG, 2-deoxy-d-glucose.
- (J) Oxygen consumption rate (OCR) of representative ERBB3-high (BT314 and BT209) and ERBB3-low/neg NS (BT302 and BT463) under basal conditions (standard medium) (mean \pm SEM, n = 4, *p < 0.001, two-way ANOVA).
- (K) Representative XF PhenoGram obtained by plotting basal OCR versus basal ECAR values obtained in the experiments shown in (J).
- (L) ATP production by ERBB3-high (BT209 and BT308) and ERBB3-low/neg NS (BT302 and BT463) 72 h after treatment with the glucose uptake inhibitor 2-DG in standard medium (*p < 0.05, one-way ANOVA). Mock, PBS-treated cells. Mean \pm SEM, n = 6.
- See also Figure S7 and Table S3.



(legend on next page)

target genes, including the key metabolic players GLUT1 and LDHB (Figure 5C). Consistently, within 24 h of treatment, MM121 significantly decreased lactate release (Figure 5D) and impaired both glycolytic and oxidative metabolism (Figures 5E, 5F, S8B, and S8C). In selected experiments (LDHB expression, lactate release, and medium acidification) overlapping results were obtained by knocking down ERBB3 with shRNA in representative ERBB3-high NS (Figures S8D–S8F). In ERBB3-low/neg, concomitantly assessed with ERBB3-high NS, MM121 did not exert any effect (Figures 5D–5F, S8B, and S8C). Conversely, forced ERBB3 overexpression enabled the representative ERBB3-neg BT463 to activate the mTOR signaling pathway (Figure 5G), to increase lactate release and medium acidification (Figures 5H and 5I), and to enhance the glycolytic and oxidative metabolism (ECAR and OCR) in response to bFGF (Figures 5J and 5K). The latter responses were fully abolished by MM121 (Figures 5J and 5K). Overall, the cell energy phenotype showed that ERBB3 overexpression is sufficient to switch NSs from the ERBB3-low/neg quiescent to the ERBB3-high energetic status, which can indeed be reverted by ERBB3 inhibition (Figure 5L).

Selective ERBB3 inhibition induces ERBB3-high NS apoptosis

ERBB3-dependent hyperactive metabolism emerged as a liability exploitable for destroying ERBB3-high NS. Indeed, prolonged treatment with MM121 induced cell death, as observed by (1) NS microscopic features (Figure 6A); (2) impaired cell viability (Figures 6B and S9A) and appearance of a sub-G0 cell fraction (Figures S9B and S9C); (3) annexin V incorporation (Figure 6C) and identification of early and late apoptotic subpopulations (Figure 6D); (4) transcriptional induction of apoptosis master regulator genes (Figure S9D) and induction of active, cleaved caspase 3 and poly(ADP-ribose) polymerase (PARP) proteins

(Figures 6E and 6F). A dramatic effect, overlapping to that of MM121, was obtained by transducing NSs with a specific ERBB3 shRNA or with miR-205 (Figures 6G, 6H, S9E, and S9F). Importantly, cell death was induced by MM121 or by ERBB3 silencing in ERBB3-high but not in ERBB3-low (and –neg) NS (Figures 6A–6E and S9A–S9H).

Overall, these data show that selective ERBB3 inhibition results in metabolic downregulation and cell death. These events specifically occur in ERBB3-high NS, in which ERBB3 overexpression is fixed by an inheritable mechanism and likely selected during tumor progression to provide an advantageous hyperactive metabolism. ERBB3 inhibition is instead ineffective in NSs that express normal ERBB3 levels, which do not display an ERBB3-dependent highly energetic metabolic profile.

ERBB3 antibodies inhibit ERBB3-high experimental GBMs

We next investigated the outcome of ERBB3 selective inhibition by MM121 in preclinical models generated by transplanting representative ERBB3-high (BT308 and BT209) and ERBB3-low (BT302) NS. These NSs could efficiently grow subcutis as well as orthotopically, retaining the parental tumor features, including ERBB3 nuclear localization in ERBB3-high cases (Figures 1H, 7A, and S10A).

Treatment of established ERBB3-overexpressing subcutaneous tumors with MM121 monotherapy over a 3-weeks course resulted in tumor volume stabilization, whereas in mock-treated mice, the tumor volume increased 5-fold (Figure 7B). Explanted tumors treated with MM121 revealed a loss of ki67 proliferative marker expression and appearance of TUNEL-positive (apoptotic) nuclei (Figures 7C and S10B). MM121 was instead ineffective in tumors generated by ERBB3-low NS, mirroring the *in vitro* response (Figures 7B and S10C). In ERBB3-high

Figure 5. ERBB3 overexpression is required for PI3K/AKT/mTOR pathway and cell metabolism upregulation

(A) Western blot showing inhibition of mTOR signaling pathway effectors at different time points after treatment with or without MM121 in ERBB3-high NS (BT308) kept in standard medium (EGF + bFGF). Mock, PBS-treated cells; vinculin, loading control. The same vinculin immunoblot is shown in Figure 3H as part of the same experiment.

(B) Expression of the mTOR target genes SREBF2, HIF1A, and TFAM 24 h after treatment with or without MM121 in ERBB3-high NS (BT308) kept in standard medium. Mock, PBS-treated cells. Mean \pm SEM, n = 3.

(C) Western blot showing downregulation of Lactate Dehydrogenase B (LDHB) and Glucose Transporter 1 (GLUT1) after treatment with or without MM-121 in ERBB3-high NS (BT308) kept in standard medium (EGF + bFGF). Mock, PBS-treated cells; calnexin, loading control.

(D) Lactate release from ERBB3-high (BT308 and BT314) and ERBB3-low/neg NS (BT373 and BT463) after 2 days of culture in standard medium with or without MM121 (*p < 0.05, paired t test). Mock, PBS-treated cells. Mean \pm SEM, n = 4.

(E) ECAR in representative ERBB3-high (BT308) and ERBB3-neg NS (BT302), treated with or without MM121 for 24 h in standard medium (mean \pm SEM, n = 4; paired t test mock versus MM121-treated NS, p < 0.001). mock, PBS-treated cells; ROT/AA, rotenone/antimycin A; 2-DG, 2-Deoxy-d-glucose.

(F) OCR in representative ERBB3-high (BT209) and ERBB3-low NS (BT302), treated with or without MM121 for 24 h in standard medium (mean \pm SEM, n = 4; paired t test mock versus MM121-treated NS, p < 0.001). mock, PBS-treated cells.

(G) Western blot showing S6 phosphorylation (pS6) and induction of LDHB expression in ERBB3-neg BT463 transduced with ERBB3 (BT463_ERBB3) or not (BT463_ctrl), kept in the absence of any growth factor for 48 h and treated with bFGF for the indicated times. Vinculin, loading control.

(H) Lactate release from BT463 transduced with ERBB3 (BT463_ERBB3) or not (BT463_ctrl) after 3 days culture in standard medium (*p < 0.001, paired t test). Mean \pm SEM, n = 3.

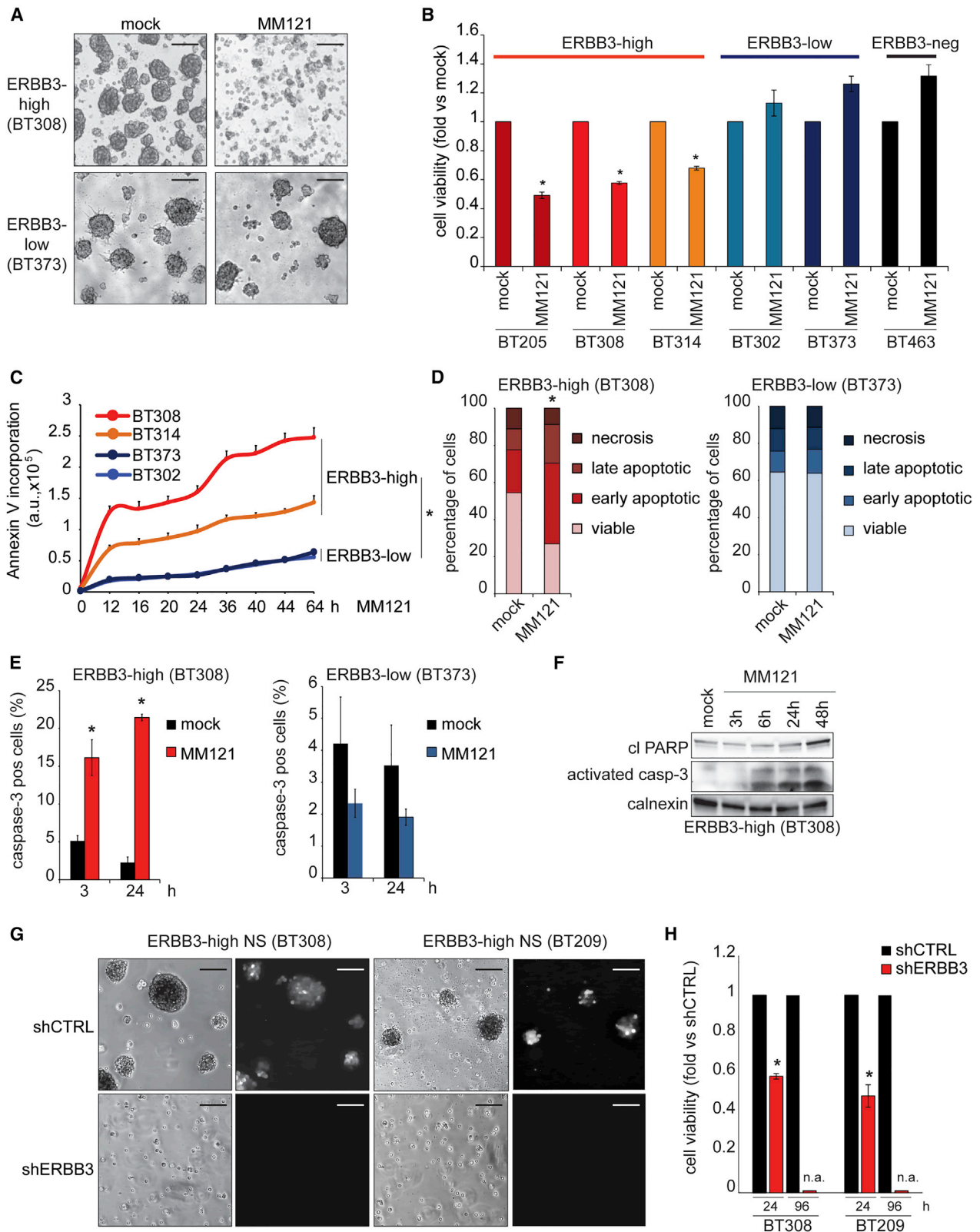
(I) pH of culture media from BT463 as in (H) (*p < 0.001, paired t test). Mean \pm SEM, n = 3.

(J) ECAR in BT463 transduced with ERBB3 (BT463_ERBB3) or not (BT463_ctrl), treated with or without MM121 in standard medium (mean \pm SEM, n = 5; two-way ANOVA, p < 0.005). Mock, PBS-treated cells.

(K) OCR in BT463 as in (J) (mean \pm SEM, n = 5; two-way ANOVA, p < 0.005).

(L) Representative XF PhenoGram obtained by plotting basal OCR versus basal ECAR values obtained in the experiment shown in (K). Representative ERBB3-high NS (BT209 and BT308, red circle) were tested in the same experiment for internal comparison. Arrow was added to indicate metabolic downregulation induced by MM121.

See also Figure S8.



(legend on next page)

tumors, as well as in ERBB3-high NS, MM121 caused downregulation of ERBB3 expression, loss of S6 phosphorylation (a surrogate marker of mTOR pathway activation), and decreased expression of the key mTOR-target gene LDHB (Figures 7D and S10D). The same therapeutic protocol, applied to established orthotopic tumors generated by luciferase-transduced ERBB3-high NS (BT308), similarly resulted in a significant tumor volume reduction, measured as bioluminescence (Figures 7E and 7F).

Overall, these data indicate that ERBB3-high experimental GBMs, generated by ERBB3-high NS and reproducing the features of the parental tumors, are sensitive to ERBB3 selective inhibition and display signs of ERBB3/PI3K/mTOR pathway downregulation. Remarkably, this sensitivity is confined to cases that express high levels of ERBB3, which is associated with the inheritable epigenetic mechanism of miR-205 silencing. This evidence confirms the principle by which only pathways genetically selected during tumor progression can be effectively exploited to target the tumor and advises that patients should be carefully stratified accordingly as to receive experimental ERBB3 therapy.

DISCUSSION

ERBB3 expression was associated with the GBM proneural subtype in the first systematic GBM transcriptional and mutational classification study (Verhaak et al., 2010). More recently, it was associated with the so-called type II GBM, identified as a descendent of OPCs (Wang et al., 2020). ERBB3 was known for being transcriptionally controlled by SOX10, a factor tightly required for the development of neural-crest-derived peripheral glia (in particular myelin-producing Schwann cells, the functional homolog of oligodendrocytes) (Britsch et al., 2001; Prasad et al., 2011). Among SOX10 targets, ERBB3 plays a prominent regulatory role as, upon NRG1 stimulation, it promotes glial cell fate specification (Shah et al., 1994). SOX10 then emerged as a transcription factor specifically expressed in the myelinating cell lineage in both the peripheral and central nervous system, and its coexpression with its targets ERBB3 (and PDGFR) can be considered as an unequivocal oligodendroglial-lineage signature (Laug et al., 2018).

The physiological role of ERBB3 in OPC-derived GBMs seems hardly adequate to provide a significant advantage in terms of tumor growth and survival. This scenario can dramatically change in case of *ERBB3* genetic alteration, which can unbalance the downstream signal toward pathways boosting tumor aggressiveness. Intratumor inheritable (i.e., evolutionary selectable) mechanisms of *ERBB3* alteration have been so far elusive, as the *ERBB3* gene is seldom affected by sequence alterations or copy number variations (Jaiswal et al., 2013). In this work, we report a mechanism of ERBB3 overexpression, based on miR-205 inactivation. This results from promoter methylation, which is inheritable, as shown by its transmission from the original tumors to the matched NSs and from these to both NS subclones and experimental tumors generated by NS transplantation. miR-205 is known to target ERBB3 in breast cancer cell lines (Iorio et al., 2009) and to downregulate a narrow set of pro-tumorigenic and pro-invasive players, such as epithelial-mesenchymal transition core transcription factors, thus behaving as an oncosuppressor (Gandellini et al., 2009; Gregory et al., 2008; Qin et al., 2013).

A second relevant finding reported in this study is activation of overexpressed ERBB3 by FGFR3. ERBB3 activation by an RTK outside the EGFR family is an absolute requirement; indeed, ERBB3 is kinase inactive, and the other EGFR family members are not coexpressed with ERBB3 in GBMs, as we showed by thorough scrutiny of the 84 NS-panel and the TCGA GBM cohort. ERBB3 interaction with a receptor belonging to a different RTK family is not surprising, as it has already been reported with MET and PDGFR (Engelman et al., 2007; Song et al., 2018). Concerning the ERBB3-FGFR interaction, a previous study characterizing the outcomes of FGFR2 amplification in lung cancer reported induction of ERBB3 phosphorylation, indicating that, in principle, the two receptors can cross-talk (Pearson et al., 2016). Based on our results, not only is the bFGF/FGFR3 pair required to activate ERBB3 but also ERBB3 is essential to confer responsiveness to bFGF. Like ERBB3, FGFR family activity has been associated with oligodendroglial early cell fate determination, and FGFR3 is known to counteract terminal differentiation (Fortin et al., 2005). Therefore, ERBB3-FGFR3 cooperation occurring in OPC-derived GBMs seems rooted in the innate properties of the cell of origin.

Figure 6. Selective ERBB3 inhibition induces ERBB3-high NS apoptosis

(A) Micrograph of ERBB3-high (BT308) and ERBB3-low NS (BT373) 24 h after treatment with or without MM121 in standard medium (EGF + bFGF). Mock, PBS-treated cells. Scale bar, 50 μ m.

(B) Cell viability of representative ERBB3-high, -low, and -neg NS 48 h after treatment with or without MM121 in standard medium. Mock, PBS-treated cells. (* $p < 0.05$, paired t test). Mean \pm SEM, $n = 6$.

(C) Cell apoptosis measured as annexin V incorporation (chemiluminescence) after treatment with or without MM121 of representative ERBB3-high (BT308 and BT314) and -low NS (BT373 and BT302) kept in standard medium (* $p < 0.001$, one-way ANOVA). Mean \pm SEM, $n = 8$.

(D) Cell apoptosis measured by flow cytometry of annexin V/DAPI incorporation in ERBB3-high (BT308) or ERBB3-low NS (BT373) 24 h after treatment with or without MM121 in standard medium (* $p < 0.05$, paired t test). Mock: PBS-treated cells.

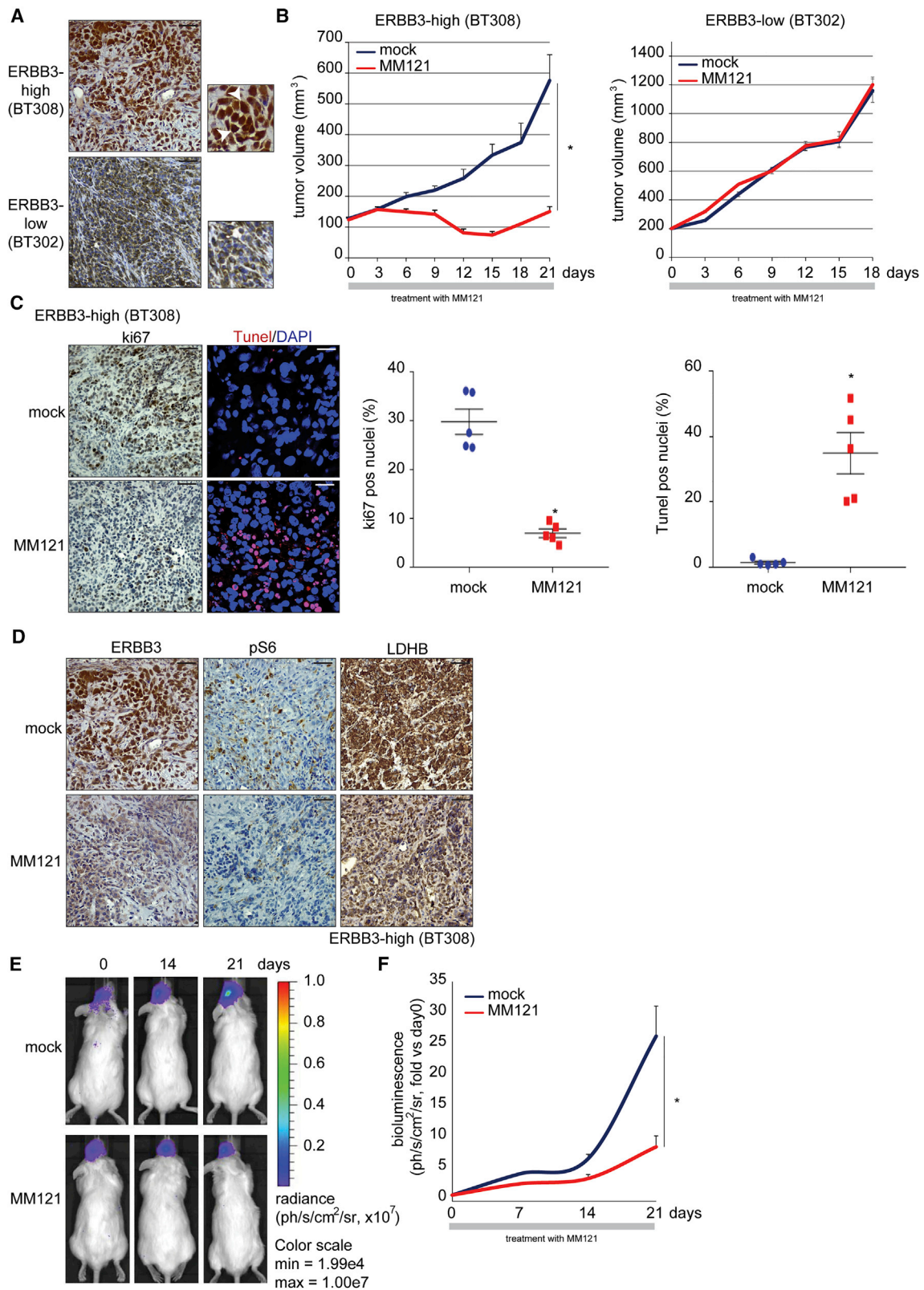
(E) Percentage of caspase-3 positive cells evaluated by flow cytometry in ERBB3-high (BT308) or ERBB3-low NS (BT373) after treatment with or without MM121 in standard medium (* $p < 0.05$, paired t test). Mock, PBS-treated cells. Mean \pm SEM, $n = 3$.

(F) Western blot showing activation of PARP (cleaved PARP [cl PARP]) and caspase-3 (casp-3) in a representative ERBB3-high NS (BT308) after treatment with or without MM121 in standard medium. Mock, PBS-treated cells; calnexin, loading control.

(G) Micrographs of ERBB3-high NS (BT308 and BT209) 72 h after shERBB3 transduction (bright field and fluorescein isothiocyanate [FITC] channel). Scale bar, 50 μ m.

(H) Cell viability measured in ERBB3-high NS (BT308 and BT209) 24 h and 96 h after shERBB3 transduction (* $p < 0.001$, paired t test). n.a., not assessable owing to complete cell death. Mean \pm SEM, $n = 10$.

See also Figure S9.



(legend on next page)

Fixation of ERBB3 overexpression by miR-205 inactivation could strongly contribute to retaining OPCs in an early stage, in which hyperactive signaling activities mediated by ERBB3 can boost high metabolic rate and vigorous cell expansion.

ERBB3 is known to be a privileged platform for PI3K activation (Schulze et al., 2005). This, in turn, activates the AKT/mTOR pathway, a master regulator of macromolecule biosynthesis, which is a prerequisite for cell growth, duplication, and proliferation (Goncalves et al., 2018; Saxton and Sabatini, 2017). As we showed, in the presence of overexpressed ERBB3, bFGF powerfully activates the PI3K/AKT/mTOR pathway, leading to upregulation of a complex metabolic network including the glycolytic pathway as a key element (Goncalves et al., 2018). As it is known, enhanced tumor anaerobic glycolysis in normoxic conditions (the renowned Warburg effect) is not merely an inefficient way to generate ATP; rather, it causes an accumulation of glycolytic pathway intermediates and end products, with the latter transformed by mitochondrial metabolism and all contributing to amino acid, nucleotide, and lipid synthesis (Zhu and Thompson, 2019). In ERBB3-high NS, together with glycolytic metabolism, increased mitochondrial activity was also evident, further highlighting the importance of the mitochondrial pathway in GBM, which was previously associated with *FGFR3-TACC* gene fusion (Frattini et al., 2018) and proposed as a therapeutic target (Shi et al., 2019).

The keen global metabolic enhancement in ERBB3-overexpressing GBM is likely a double-edge sword. On the one hand, it supports aggressive tumor growth, testified by the significantly reduced overall survival of patients overexpressing ERBB3 in both the whole 84 NS-panel and proneural TCGA patient cohorts. On the other hand, the mTOR pathway and metabolic shutdown caused by targeting ERBB3 with specific antibodies (seribantumab/MM121) was sufficient to induce cell death. This scenario represents a typical case of “oncogene addiction,” in which an alteration selected during tumor evolution (ERBB3 overexpression fixed by epigenetic miR-205 inactivation) confers cellular dependence on protein activity and destructive outcomes when the latter is impaired (Sharma and Settleman, 2007).

These observations are crucial to guide the possible exploitation of ERBB3 as a GBM therapeutic target. As we showed in NSs and experimental tumors, ERBB3 inhibition is effective only in cases for which ERBB3 overexpression is sustained by miR-205 inactivation but not in those for which ERBB3 is expressed at normal levels. Identification of patients eligible for targeted therapy is always critical and requires appropriate bio-

markers, whose definition can be difficult especially in the case of analogic variables such as protein expression levels. In the case of ERBB3 overexpression, a meaningful surrogate biomarker is ERBB3 nuclear localization, which was previously described and explained by the presence of an uncommon nuclear import signal in the ERBB3 sequence (Reif et al., 2016). Such nuclear accumulation can merely reflect excess protein production or hide still obscure functional properties linked with the ERBB3 ability to modulate gene transcription, which could further explain the dramatic effect of ERBB3 overexpression on the GBM phenotype.

STAR★METHODS

Detailed methods are provided in the online version of this paper and include the following:

- KEY RESOURCES TABLE
- RESOURCE AVAILABILITY
 - Lead contact
 - Materials availability
 - Data and code availability
- EXPERIMENTAL MODEL AND SUBJECT DETAILS
 - Neurosphere (NS) derivation from human patients
 - Neurosphere subcloning and cell treatment with growth factors
 - Generation of experimental tumors
 - Treatment of experimental tumors with MM121
 - Patients' data and survival analysis
- METHOD DETAILS
 - NS treatment with inhibitors
 - Nucleic acid extraction and retro-transcription
 - Gene copy number evaluation
 - Gene sequencing
 - Transcriptome analysis
 - Quantitative Real-Time PCR (qPCR)
 - Bisulfite treatment and methylation analysis
 - FISH analysis
 - Prediction of ERBB3 targeting miRNAs
 - NS transfection and transduction
 - Western blotting
 - Flow-cytometric analysis
 - Flow-cytometric single cell imaging
 - Immunofluorescence analysis
 - Immunohistochemistry and TUNEL assay

Figure 7. ERBB3 antibodies inhibit ERBB3-high experimental GBMs

(A) Representative ERBB3 IHC staining in tumors generated by subcutaneous transplant of ERBB3-high (BT308) or -low NS (BT302). ERBB3-high tumors display ERBB3 nuclear staining (arrows). Scale bar, 100 μ m.

(B) Growth curves of established tumors, generated by subcutaneous transplant of ERBB3-high (BT308, left) or -low NS (BT302, right) and treated with or without MM121 for 21 days (n = 6/group; *p = 0.0001, one-way ANOVA). Mock, PBS-treated tumors.

(C) Representative ki67 and TUNEL stainings of the same ERBB3-high tumors as in (B) at the experimental end point (left). Percentage of ki67- and TUNEL-positive cells (n = 10 HPF/condition; *p = 0.008, Kolmogorov-Smirnov test) (right). Scale bar, 100 μ m (ki67) and 25 μ m (TUNEL assay).

(D) Representative IHC staining of ERBB3, phospho-S6 (pS6), and LDHB in the same ERBB3-high tumors as in (B). Scale bar, 100 μ m.

(E) Luciferase radiance intensity in representative mice intracranially transplanted with ERBB3-high NS (BT308) transduced with GFP-luciferase and treated with or without MM121. Mock, PBS-treated mice.

(F) Bioluminescence measured in mice as in (E) (n = 6/group) (*p < 0.05, two-way ANOVA).
See also Figure S10.

- Duolink proximity ligation assay
- Lactate release and pH measurement
- Extracellular Acidification (ECAR) and Oxygen Consumption Rates (OCR)
- Cell proliferation, viability and apoptosis assays
- Annexin V and caspase 3 activity evaluation by flow-cytometry
- Cell cycle analysis
- **QUANTIFICATION AND STATISTICAL ANALYSIS**

SUPPLEMENTAL INFORMATION

Supplemental information can be found online at <https://doi.org/10.1016/j.celrep.2021.109455>.

ACKNOWLEDGMENTS

We thank Y. Yarden for discussion, L. Mancini (Accelera srl) for performing intracranial tumor studies, E. Anghileri for help with patients' data, G. Del Zotto for help with single-cell flow-cytometric analysis, M. Panero for FISH analysis, I. Sarotto and S. Giove for help with immunohistochemistry, C. Isella for help with bioinformatics analysis, M. Pipas for seribantumab, M. Rocchi and O. Capozzi for BAC clones probes, and F. Sassi and L. Trusolino for breast cancer PDX. This work was supported by AIRC - Italian Association for Cancer Research (Special Program Molecular Clinical Oncology 5 × 1000, N. 9970 and N. 21052, and Investigator grants N. 19933 to C.B. and N. 23820 to P.M.C.); FPRC 5 × 1000 '2014' Ministero della Salute, Italy; RC '2019', '2020' and '2021', Ministero della Salute, Italy; and Comitato per Albi98.

AUTHOR CONTRIBUTIONS

F.D.B. and C.B. conceived the project, planned experiments, interpreted data, and wrote the manuscript; F.D.B. performed or supervised all experiments; F.O. performed bioinformatic and genetic analysis; J.E. and A.D.A. performed *in vivo* experiments; E.C. performed flow-cytometric analysis; L.B. performed DNA methylation analysis; R.A. performed immunohistochemistry; V.B. helped with *in vitro* experiments; G.R. helped with molecular analysis; M.P. and B.P. performed histopathological diagnosis in patients and models; G.K. performed research and development of seribantumab and provided the antibody; C.D.A. and L.C. analyzed cytogenetics; S.P. and G.F. provided GBM neurospheres and patients' data; P.M.C. and C.B. supervised the project.

DECLARATION OF INTERESTS

G.K. is a shareholder of Merrimack stock. All the other authors declare no competing interests.

Received: September 21, 2020

Revised: June 10, 2021

Accepted: July 6, 2021

Published: July 27, 2021

SUPPORTING CITATIONS

The following reference appears in the supplemental information: [Kondo et al. \(2017\)](#).

REFERENCES

Agarwal, V., Bell, G.W., Nam, J.W., and Bartel, D.P. (2015). Predicting effective microRNA target sites in mammalian mRNAs. *eLife* 4, e05005.

Baralis, E., Bertotti, A., Fiori, A., and Grand, A. (2012). LAS: a software platform to support oncological data management. *J. Med. Syst.* 36, S81–S90.

Bi, J., Chowdhry, S., Wu, S., Zhang, W., Masui, K., and Mischel, P.S. (2020). Altered cellular metabolism in gliomas—an emerging landscape of actionable co-dependency targets. *Nat. Rev. Cancer* 20, 57–70.

Bowman, R.L., Wang, Q., Carro, A., Verhaak, R.G., and Squatrito, M. (2017). GlioVis data portal for visualization and analysis of brain tumor expression datasets. *Neuro-oncol.* 19, 139–141.

Brennan, C.W., Verhaak, R.G., McKenna, A., Campos, B., Noushmehr, H., Salama, S.R., Zheng, S., Chakravarty, D., Sanborn, J.Z., Berman, S.H., et al.; TCGA Research Network (2013). The somatic genomic landscape of glioblastoma. *Cell* 155, 462–477.

Britsch, S., Goerich, D.E., Riethmacher, D., Peirano, R.I., Rossner, M., Nave, K.A., Birchmeier, C., and Wegner, M. (2001). The transcription factor Sox10 is a key regulator of peripheral glial development. *Genes Dev.* 15, 66–78.

Cahoy, J.D., Emery, B., Kaushal, A., Foo, L.C., Zamanian, J.L., Christopherson, K.S., Xing, Y., Lubischer, J.L., Krieg, P.A., Krupenko, S.A., et al. (2008). A transcriptome database for astrocytes, neurons, and oligodendrocytes: a new resource for understanding brain development and function. *J. Neurosci.* 28, 264–278.

Campbell, M.R., Amin, D., and Moasser, M.M. (2010). HER3 comes of age: new insights into its functions and role in signaling, tumor biology, and cancer therapy. *Clin. Cancer Res.* 16, 1373–1383.

Cerami, E., Gao, J., Dogrusoz, U., Gross, B.E., Sumer, S.O., Aksoy, B.A., Jacobsen, A., Byrne, C.J., Heuer, M.L., Larsson, E., et al. (2012). The cBio cancer genomics portal: an open platform for exploring multidimensional cancer genomics data. *Cancer Discov.* 2, 401–404.

De Bacco, F., Casanova, E., Medico, E., Pellegatta, S., Orzan, F., Albano, R., Luraghi, P., Reato, G., D'Ambrosio, A., Porrati, P., et al. (2012). The MET oncogene is a functional marker of a glioblastoma stem cell subtype. *Cancer Res.* 72, 4537–4550.

De Bacco, F., D'Ambrosio, A., Casanova, E., Orzan, F., Neggia, R., Albano, R., Verginelli, F., Cominelli, M., Poliani, P.L., Luraghi, P., et al. (2016). MET inhibition overcomes radiation resistance of glioblastoma stem-like cells. *EMBO Mol. Med.* 8, 550–568.

Duhem-Tonnelle, V., Bièche, I., Vacher, S., Loyens, A., Muraige, C.A., Collier, F., Baroncini, M., Blond, S., Prevot, V., and Sharif, A. (2010). Differential distribution of erbB receptors in human glioblastoma multiforme: expression of erbB3 in CD133-positive putative cancer stem cells. *J. Neuropathol. Exp. Neurol.* 69, 606–622.

Düvel, K., Yecies, J.L., Menon, S., Raman, P., Lipovsky, A.I., Souza, A.L., Triantafellow, E., Ma, Q., Gorski, R., Cleaver, S., et al. (2010). Activation of a metabolic gene regulatory network downstream of mTOR complex 1. *Mol. Cell* 39, 171–183.

Engelman, J.A., Zejnullahu, K., Mitsudomi, T., Song, Y., Hyland, C., Park, J.O., Lindeman, N., Gale, C.M., Zhao, X., Christensen, J., et al. (2007). MET amplification leads to gefitinib resistance in lung cancer by activating ERBB3 signaling. *Science* 316, 1039–1043.

Fortin, D., Rom, E., Sun, H., Yayon, A., and Bansal, R. (2005). Distinct fibroblast growth factor (FGF)/FGF receptor signaling pairs initiate diverse cellular responses in the oligodendrocyte lineage. *J. Neurosci.* 25, 7470–7479.

Frattini, V., Pagnotta, S.M., Tala, F., Fan, J.J., Russo, M.V., Lee, S.B., Garofano, L., Zhang, J., Shi, P., Lewis, G., et al. (2018). A metabolic function of FGFR3-TACC3 gene fusions in cancer. *Nature* 553, 222–227.

Fu, L., and Medico, E. (2007). FLAME, a novel fuzzy clustering method for the analysis of DNA microarray data. *BMC Bioinformatics* 8, 3.

Gandellini, P., Folini, M., Longoni, N., Pennati, M., Binda, M., Colecchia, M., Salvioni, R., Supino, R., Moretti, R., Limonta, P., et al. (2009). miR-205 Exerts tumor-suppressive functions in human prostate through down-regulation of protein kinase Cepsilon. *Cancer Res.* 69, 2287–2295.

Goncalves, M.D., Hopkins, B.D., and Cantley, L.C. (2018). Phosphatidylinositol 3-Kinase, Growth Disorders, and Cancer. *N. Engl. J. Med.* 379, 2052–2062.

Gregory, P.A., Bert, A.G., Paterson, E.L., Barry, S.C., Tsykin, A., Farshid, G., Vadas, M.A., Khew-Goodall, Y., and Goodall, G.J. (2008). The miR-200 family

- and miR-205 regulate epithelial to mesenchymal transition by targeting ZEB1 and SIP1. *Nat. Cell Biol.* **10**, 593–601.
- Hegi, M.E., Diserens, A.C., Gorlia, T., Hamou, M.F., de Tribolet, N., Weller, M., Kros, J.M., Hainfellner, J.A., Mason, W., Mariani, L., et al. (2005). MGMT gene silencing and benefit from temozolomide in glioblastoma. *N. Engl. J. Med.* **352**, 997–1003.
- Hoshida, Y. (2010). Nearest template prediction: a single-sample-based flexible class prediction with confidence assessment. *PLoS One* **5**, e15543.
- Hulspas, R., O’Gorman, M.R., Wood, B.L., Gratama, J.W., and Sutherland, D.R. (2009). Considerations for the control of background fluorescence in clinical flow cytometry. *Cytometry B Clin. Cytom.* **76**, 355–364.
- Iorio, M.V., Casalini, P., Piovan, C., Di Leva, G., Merlo, A., Triulzi, T., Ménard, S., Croce, C.M., and Tagliabue, E. (2009). microRNA-205 regulates HER3 in human breast cancer. *Cancer Res.* **69**, 2195–2200.
- Jaiswal, B.S., Kijavín, N.M., Stawiski, E.W., Chan, E., Parikh, C., Durinck, S., Chaudhuri, S., Pujara, K., Guillory, J., Edgar, K.A., et al. (2013). Oncogenic ERBB3 mutations in human cancers. *Cancer Cell* **23**, 603–617.
- Kondo, A., Yamamoto, S., Nakaki, R., Shimamura, T., Hamakubo, T., Sakai, J., Kodama, T., Yoshida, T., Aburatani, H., and Osawa, T. (2017). Extracellular Acidic pH Activates the Sterol Regulatory Element-Binding Protein 2 to Promote Tumor Progression. *Cell Rep.* **18**, 2228–2242.
- Laug, D., Glasgow, S.M., and Deneen, B. (2018). A glial blueprint for gliomagenesis. *Nat. Rev. Neurosci.* **19**, 393–403.
- Le Rhun, E., Preusser, M., Roth, P., Reardon, D.A., van den Bent, M., Wen, P., Reifenberger, G., and Weller, M. (2019). Molecular targeted therapy of glioblastoma. *Cancer Treat. Rev.* **80**, 101896.
- Lewis, B.P., Burge, C.B., and Bartel, D.P. (2005). Conserved seed pairing, often flanked by adenosines, indicates that thousands of human genes are microRNA targets. *Cell* **120**, 15–20.
- Li, A., Walling, J., Kotliarov, Y., Center, A., Steed, M.E., Ahn, S.J., Rosenblum, M., Mikkelsen, T., Zenklusen, J.C., and Fine, H.A. (2008). Genomic changes and gene expression profiles reveal that established glioma cell lines are poorly representative of primary human gliomas. *Mol. Cancer Res.* **6**, 21–30.
- Li, X., Liu, L., Luo, Y., Cui, S., Chen, W., Zeng, A., Shi, Y., and Luo, L. (2019). Long non-coding RNA SNHG5 promotes glioma progression via miR-205/E2F3 axis. *Biosci. Rep.* **39**, BSR20190668.
- Luraghi, P., Bigatto, V., Cipriano, E., Reato, G., Orzan, F., Sassi, F., De Bacco, F., Isella, C., Bellomo, S.E., Medico, E., et al. (2018). A Molecularly Annotated Model of Patient-Derived Colon Cancer Stem-Like Cells to Assess Genetic and Nongenetic Mechanisms of Resistance to Anti-EGFR Therapy. *Clin. Cancer Res.* **24**, 807–820.
- Maecker, H.T., and Trotter, J. (2006). Flow cytometry controls, instrument setup, and the determination of positivity. *Cytometry A* **69**, 1037–1042.
- Morita, M., Gravel, S.P., Chénard, V., Sikström, K., Zheng, L., Alain, T., Gandin, V., Avizonis, D., Arguello, M., Zakaria, C., et al. (2013). mTORC1 controls mitochondrial activity and biogenesis through 4E-BP-dependent translational regulation. *Cell Metab.* **18**, 698–711.
- Pearson, A., Smyth, E., Babina, I.S., Herrera-Abreu, M.T., Tarazona, N., Peckitt, C., Kilgour, E., Smith, N.R., Geh, C., Rooney, C., et al. (2016). High-Level Clonal FGFR Amplification and Response to FGFR Inhibition in a Translational Clinical Trial. *Cancer Discov.* **6**, 838–851.
- Pietrantonio, F., Perrone, F., de Braud, F., Castano, A., Maggi, C., Bossi, I., Gevorgyan, A., Biondani, P., Pacifici, M., Busico, A., et al. (2014). Activity of temozolomide in patients with advanced chemorefractory colorectal cancer and MGMT promoter methylation. *Ann. Oncol.* **25**, 404–408.
- Prasad, M.K., Reed, X., Gorkin, D.U., Cronin, J.C., McAdow, A.R., Chain, K., Hodonsky, C.J., Jones, E.A., Svaren, J., Antonellis, A., et al. (2011). SOX10 directly modulates ERBB3 transcription via an intronic neural crest enhancer. *BMC Dev. Biol.* **11**, 40.
- Prat, M., Crepaldi, T., Pennacchietti, S., Bussolino, F., and Comoglio, P.M. (1998). Agonistic monoclonal antibodies against the Met receptor dissect the biological responses to HGF. *J. Cell Sci.* **111**, 237–247.
- Qin, A.Y., Zhang, X.W., Liu, L., Yu, J.P., Li, H., Wang, S.Z., Ren, X.B., and Cao, S. (2013). MiR-205 in cancer: an angel or a devil? *Eur. J. Cell Biol.* **92**, 54–60.
- Reif, R., Adawy, A., Vartak, N., Schröder, J., Günther, G., Ghallab, A., Schmidt, M., Schormann, W., and Hengstler, J.G. (2016). Activated ErbB3 Translocates to the Nucleus via Clathrin-independent Endocytosis, Which Is Associated with Proliferating Cells. *J. Biol. Chem.* **291**, 3837–3847.
- Reifenberger, G., Wirsching, H.G., Knobbe-Thomsen, C.B., and Weller, M. (2017). Advances in the molecular genetics of gliomas—implications for classification and therapy. *Nat. Rev. Clin. Oncol.* **14**, 434–452.
- Saxton, R.A., and Sabatini, D.M. (2017). mTOR Signaling in Growth, Metabolism, and Disease. *Cell* **168**, 960–976.
- Schoeberl, B., Kudla, A., Masson, K., Kalra, A., Curley, M., Finn, G., Pace, E., Harms, B., Kim, J., Kearns, J., et al. (2017). Systems biology driving drug development: from design to the clinical testing of the anti-ErbB3 antibody seribantumab (MM-121). *NPJ Syst. Biol. Appl.* **3**, 16034.
- Schulze, W.X., Deng, L., and Mann, M. (2005). Phosphotyrosine interactome of the ErbB-receptor kinase family. *Mol. Syst. Biol.* **1**, 2005.0008.
- Shah, N.M., Marchionni, M.A., Isaacs, I., Stroobant, P., and Anderson, D.J. (1994). Glial growth factor restricts mammalian neural crest stem cells to a glial fate. *Cell* **77**, 349–360.
- Sharma, S.V., and Settleman, J. (2007). Oncogene addiction: setting the stage for molecularly targeted cancer therapy. *Genes Dev.* **21**, 3214–3231.
- Shi, Y., Lim, S.K., Liang, Q., Iyer, S.V., Wang, H.Y., Wang, Z., Xie, X., Sun, D., Chen, Y.J., Tabar, V., et al. (2019). Gboxin is an oxidative phosphorylation inhibitor that targets glioblastoma. *Nature* **567**, 341–346.
- Snuderl, M., Fazlollahi, L., Le, L.P., Nitta, M., Zhelyazkova, B.H., Davidson, C.J., Akhavanfar, S., Cahill, D.P., Aldape, K.D., Betensky, R.A., et al. (2011). Mosaic amplification of multiple receptor tyrosine kinase genes in glioblastoma. *Cancer Cell* **20**, 810–817.
- Song, K., Yuan, Y., Lin, Y., Wang, Y.X., Zhou, J., Gai, Q.J., Zhang, L., Mao, M., Yao, X.X., Qin, Y., et al. (2018). ERBB3, IGF1R, and TGFBR2 expression correlate with PDGFR expression in glioblastoma and participate in PDGFR inhibitor resistance of glioblastoma cells. *Am. J. Cancer Res.* **8**, 792–809.
- Uhlen, M., Oksvold, P., Fagerberg, L., Lundberg, E., Jonasson, K., Forsberg, M., Zvalnen, M., Kampf, C., Wester, K., Hober, S., et al. (2010). Towards a knowledge-based Human Protein Atlas. *Nat. Biotechnol.* **28**, 1248–1250.
- Verhaak, R.G., Hoadley, K.A., Purdom, E., Wang, V., Qi, Y., Wilkerson, M.D., Miller, C.R., Ding, L., Golub, T., Mesirov, J.P., et al.; Cancer Genome Atlas Research Network (2010). Integrated genomic analysis identifies clinically relevant subtypes of glioblastoma characterized by abnormalities in PDGFRA, IDH1, EGFR, and NF1. *Cancer Cell* **17**, 98–110.
- Wang, Q., Hu, B., Hu, X., Kim, H., Squatrito, M., Scarpace, L., deCarvalho, A.C., Lyu, S., Li, P., Li, Y., et al. (2017). Tumor Evolution of Glioma-Intrinsic Gene Expression Subtypes Associates with Immunological Changes in the Microenvironment. *Cancer Cell* **32**, 42–56.e6.
- Wang, Z., Sun, D., Chen, Y.J., Xie, X., Shi, Y., Tabar, V., Brennan, C.W., Bale, T.A., Jayewickreme, C.D., Laks, D.R., et al. (2020). Cell Lineage-Based Stratification for Glioblastoma. *Cancer Cell* **38**, 366–379.e8.
- Yang, S.R., Schultheis, A.M., Yu, H., Mandelker, D., Ladanyi, M., and Büttner, R. (2020). Precision medicine in non-small cell lung cancer: Current applications and future directions. *Semin. Cancer Biol.*, S1044-579X(20)30164-4.
- Yarden, Y., and Pines, G. (2012). The ERBB network: at last, cancer therapy meets systems biology. *Nat. Rev. Cancer* **12**, 553–563.
- Zhu, J., and Thompson, C.B. (2019). Metabolic regulation of cell growth and proliferation. *Nat. Rev. Mol. Cell Biol.* **20**, 436–450.

STAR★METHODS

KEY RESOURCES TABLE

REAGENT or RESOURCE	SOURCE	IDENTIFIER
Antibodies		
anti-ERBB3 (1B2) antibodies	Cell Signaling Technology	#4754; RRID:AB_10691324 (WB 1:1000, IF 1:100)
anti-ERBB3 (2F12) antibodies	Millipore	#05-390; RRID:AB_309713 (4 μg/ml)
anti-ERBB3 antibodies	Sigma-Aldrich	#ab-1328; RRID:AB_10621903 (IHC 1:100)
anti-ERBB3 antibodies	ATLAS antibodies	#HPA045396; RRID:AB_2679312 (IHC 1:20)
anti-ERBB3-PE (REA508) antibodies	Miltenyi Biotec GmbH	#130-107-899; RRID:AB_2651655 (1:20)
anti-ERBB3-APC (1B4c3) antibodies	Biologend	#324708; RRID:AB_2099567 (1:100)
anti-phospho-ERBB3 Tyr1197 antibodies	Cell Signaling Technology	#4561; RRID:AB_2099707 (WB 1:1000)
anti-phospho-ERBB3 Tyr1222 antibodies	Cell Signaling Technology	#4784; RRID:AB_659920 (WB 1:1000)
anti-phospho-ERBB3 Tyr1289 antibodies	Cell Signaling Technology	#4791; RRID:AB_2099709 (WB 1:1000)
anti-ERBB2 (e2-4001) antibodies	Thermo Fisher Scientific	MA5-13105; RRID:AB_10988194 (WB 2 μg/ml)
anti-ERBB2 (Trastuzumab) antibodies	Roche	RRID:AB_2489608 (IP 2 μg/ml)
anti-ERBB2 antibodies	Agilent	A0485; RRID:AB_2335701 (IHC 1:600)
anti-ERBB2-FITC (5D3) antibodies	Biologend	#324404; RRID:AB_756120 (1:20)
anti-ERBB4 (111B2) antibodies	Cell Signaling Technology	#4795; RRID:AB_2099883 (WB 1:1000, IP 1:50)
anti-ERBB4-PE antibodies	R&D System	#AF1131; RRID:AB_354620 (1:20)
anti-EGFR (D38B1) antibodies	Cell Signaling Technology	#4267; RRID:AB_2246311 (WB 1:1000, IP 1:50)
anti-EGFR (Ab10 111.6) antibodies	Thermo Fisher Scientific	#OPA1-10100; RRID:AB_325381 (IHC 1:100)
anti-EGFR-PE (EGFR.1) antibodies	BD Bioscience	#555997; RRID:AB_396281 (1:20)
anti-FGFR1 antibodies	Cell Signaling Technology	#3472; RRID:AB_2103374 (WB 1:1000)
anti-FGFR2 (D4H9) antibodies	Cell Signaling Technology	#11835; RRID:AB_2797742 (WB 1:1000)
anti-FGFR2-APC (98725) antibodies	R&D System	#FAB684A; RRID:AB_894678 (1:10)
anti-FGFR3 (2H10B4) antibodies	NovusBio	NBP2-52468; RRID:AB_2782964 (WB 1:500, IF 1:100)
anti-FGFR3 (OT11B10) antibodies	NovusBio	NBP2-45716 (IP 5 μg/ml)
anti-FGFR3-APC (136334) antibodies	R&D System	#FAB766A; RRID:AB_11129249 (1:20)
anti-FGFR4 antibodies	Cell Signaling Technology	#2894; RRID:AB_2293993 (WB 1:1000)
anti-FGFR4-APC (240929) antibodies	R&D System	#FAB6852A; RRID:AB_10971830 (1:20)
anti-PDGFR4 (D1E1E) antibodies	Cell Signaling Technology	#3174; RRID:AB_2162345 (WB 1:1000, IP 1:50)
anti-PDGFR4-PE (16A1) antibodies	Biologend	#323506; RRID:AB_2268113 (1:10)
anti-PDGFRB (C82A3) antibodies	Cell Signaling Technology	#4564; RRID:AB_2236927 (WB 1:1000, IP 1:50)
anti-MET (DL21) antibodies	Prat et al., 1998	(WB 1:1500, IP 1:50)
anti-MET (DO24) antibodies	Prat et al., 1998	(IP 5 μg/ml)
anti-HGF R/MET-PE-Cy7 (95106) antibodies	R&D System	#MAB3582; RRID:AB_884334 (1:20)
anti-KIT antibodies	Cell Signaling Technology	#3074; RRID:AB_1147633 (WB 1:1000, IP 1:50)
anti-KIT-APC (104D2) antibodies	Immunological Science	#MAB-9117APC; RRID:AB_2892615
anti-NTRK2 antibodies	R&D System	#AF1494; RRID:AB_2155264 (WB 0.5 μg/μl, IP 5 μg/ml)
anti-NTRK2-AlexaF647 (72509) antibodies	R&D System	#FAB3971R; RRID:AB_2892614
anti-pan-phospho-tyr antibodies	Millipore	#05-321; RRID:AB_309678 (WB 1:1000)
anti-NEDD4 antibodies	Bethyl	#A303-254A-T; RRID:AB_10952871 (WB 1:1000)
anti-NRDP1 antibodies	NovusBio	#NB100-583; RRID:AB_2269715 (WB 1:10000)
anti-MAP2 antibodies	Cell Signaling Technology	#4542; RRID:AB_10693782 (WB 1:1000)
anti-BCL2 antibodies	Cell Signaling Technology	#4223; RRID:AB_1903909 (WB 1:1000)

(Continued on next page)

Continued

REAGENT or RESOURCE	SOURCE	IDENTIFIER
anti-phospho-42/44 MAPK antibodies	Cell Signaling Technology	#4370; RRID:AB_2315112 (WB 1:1000)
anti-phospho-AKT antibodies	Cell Signaling Technology	#3787; RRID:AB_331170 (WB 1:1000)
anti-phospho-FRS2 Tyr436 antibodies	Cell Signaling Technology	#3861; RRID:AB_2231950 (WB 1:500)
anti-phospho-mTOR (Ser2448) antibodies	Cell Signaling Technology	#2971; RRID:AB_330970 (WB 1:1000)
anti-phosphoRAPTOR(Ser792) antibodies	Cell Signaling Technology	#2083; RRID:AB_2249475 (WB 1:1000)
anti-RAPTOR (E6003A) antibodies	Cell Signaling Technology	#2280; RRID:AB_561245 (WB 1:1000)
anti-phospho-S6 antibodies	Cell Signaling Technology	#4858; RRID:AB_916156 (WB 1:1000, IHC 1:100)
anti-S6 antibodies	Cell Signaling Technology	#2217; RRID:AB_331355 (WB 1:1000)
anti-phospho-4EBP1 (Thr37/46) antibodies	Cell Signaling Technology	#2855; RRID:AB_560835 (WB 1:1000)
anti-LDHB antibodies	Abcam	#ab52488; RRID:AB_2134961 (WB 1:5000, IHC 1:500)
anti-GLUT1 (D3J3A) antibodies	Cell Signaling Technology	#12939; RRID:AB_2687899 (WB 1:1000)
anti-cleaved PARP antibodies	Cell Signaling Technology	#9541; RRID:AB_331426 (WB 1:1000)
anti-cleaved caspase 3 (asp175) antibodies	Cell Signaling Technology	#9661; RRID:AB_2341188
anti-b-actin antibodies	Cell Signaling Technology	#8457; RRID:AB_10950489 (WB 1:1000)
anti-calnexin antibodies	Cell Signaling Technology	#2679; RRID:AB_2228381 (WB 1:1000)
anti-TATA binding Protein antibodies	Millipore	#05-1531; RRID:AB_11212675
anti-GAPDH antibodies	Abcam	#ab9483; RRID:AB_307273
anti-vinculin antibodies	Sigma-Aldrich	#V9131; RRID:AB_477629
anti-ki67 antibodies	Agilent	M724001-2; RRID:AB_2631211

Biological samples

human glioblastoma tissues	Istituto Neurologico C. Besta	https://www.istituto-besta.it/
----------------------------	-------------------------------	-----------------------------------------------------------------------------

Chemicals, peptides and recombinant proteins

bFGF	PeptoTech	#100-18B, 20 ng/ml
EGF	Sigma-Aldrich	E5036, 20 ng/ml
NRG1	PeptoTech	#100-03, 50 ng/ml
PDGFBB	PeptoTech	#100-14B, 20 ng/ml
HGF	PeptoTech	#100-39H, 20 ng/ml
BDNF	PeptoTech	#450-02, 20 ng/ml
SCF1	PeptoTech	#300-07, 20 ng/ml
Seribantumab (MM121)	Merrimack	<i>in vitro</i> : 50 µg/ml; <i>in vivo</i> : 30 mg/kg
2-Deoxy-D-glucose (2-DG)	Sigma-Aldrich	D3179, 50mM
BGJ398	Selleckchem	#S2183, 5nM
5-aza-2'-deoxycytidine (5' AZA)	Sigma-Aldrich	#A3656, 5µM

Critical commercial assays

GenePrint® 10System	Promega	B9510
All Prep DNA/RNA Mini kit	QIAGEN	#80284
miRNeasy Mini kit	QIAGEN	#217084
RNeasy Mini kit	QIAGEN	#74004
Maxwell® RSC miRNA Tissue kit	Promega	#AS4500
Platinum® Taq Hot-Start DNA Polymerase	Thermo Fisher Scientific	#14966001
Platinum SuperFi II DNA Polymerase	Thermo Fisher Scientific	#12361010
Illumina® TotalPrep RNA Amplification Kit	Illumina	AMIL1791
EZ-DNA Methylation Gold Kit	ZYMO Research	#D5008
ERBB3/CEN 12 Dual Color Probe	Zytovision	#Z-2056-200
Nick translation reagent kit	Abbot Molecular Inc.	#07J00-001
TransIT-X2® Dynamic Delivery System	MirusBio	#miR6003
Protein A Mag Sepharose	GE Healthcare	#28951378

(Continued on next page)

Continued

REAGENT or RESOURCE	SOURCE	IDENTIFIER
DeadEnd Fluorometric TUNEL System	Promega	#G3250
Duolink PLA Technology	Sigma-Aldrich	#DUO92101
Lactate-GloAssay	Promega	#J5021
Glycolytic Rate Assay	Agilent	#103344-100
XF Cell Mito Stress	Agilent	#103015-100
Cultrex® BME PathClear®	Tema Ricerca	#3533-010-02
CellTiter-Glo®	Promega	#G7570
RealTime-Glo Annexin V Apopt and Nec Assay	Promega	#JA1011
eBioscience Annexin V Apopt Detection Kit	ThermoFisher Scientific	#BMS500FI-20

Deposited data

gene expression dataset	this paper	http://data.mendeley.com/login?redirectPath=/datasets/tyjf6km8y6/draft?a=505d1617-dc0d-4c42-b9c6-5a558578346c
gene expression dataset	this paper	GEO: GSE178236
raw data for western blots in Figures 2, 3, 4, 5, and 6	this paper	http://data.mendeley.com/login?redirectPath=/datasets/tyjf6km8y6/draft?a=505d1617-dc0d-4c42-b9c6-5a558578346c

Experimental models: Cell lines

glioblastoma neurospheres	this paper	Table S1
colosphere M049	Luraghi et al., 2018	N/A
U87MG	ATCC	ATCC® HTB-14
A549	ATCC	ATCC® CCL-185
A2780	ECACC	93112519-1VL
A375	ATCC	ATCC® CRL-1619
K562	NCI-60 cancer panel	N/A
OE21	ECACC	96062201-1VL
MDA468	NCI-60 cancer panel	N/A
HeLa	ATCC	ATCC® CCL-2
T47D	NCI-60 cancer panel	N/A
MCF7	NCI-60 cancer panel	N/A
BT474	DMSZ	ACC 64

Experimental models: Organisms/strains

NOD.CB17-Prkdcscid/J	Charles River Laboratories	N/A
----------------------	----------------------------	-----

Oligonucleotides

primers	this paper	Table S4
ERBB3	Thermo Fisher Scientific	Hs00187734_cn
CDKN2A	Thermo Fisher Scientific	Hs03714372_cn
EGFR	Thermo Fisher Scientific	Hs04942325_cn
HGF	Thermo Fisher Scientific	Hs02789622_cn
PDGFRA	Thermo Fisher Scientific	Hs05935655_cn
PTEN	Thermo Fisher Scientific	Hs02599450_cn
CDK4	Thermo Fisher Scientific	Hs01071103_cn
CDK6	Thermo Fisher Scientific	Hs04934380_cn
MDM2	Thermo Fisher Scientific	Hs02904108_cn
MIR205HG	Thermo Fisher Scientific	Hs07483345_cn
RNaseP CNV	Thermo Fisher Scientific	4403328
ERBB3	Thermo Fisher Scientific	Hs00176538_m1
SNHG5	Thermo Fisher Scientific	Hs05037597_s1

(Continued on next page)

Continued

REAGENT or RESOURCE	SOURCE	IDENTIFIER
TFAM	Thermo Fisher Scientific	Hs00273372_s1
HIF1A	Thermo Fisher Scientific	Hs00936368_m1
SREBF2	Thermo Fisher Scientific	Hs01081784_m1
APAF1	Thermo Fisher Scientific	Hs00559441_m1
BAD	Thermo Fisher Scientific	Hs00188930_m1
BAK1	Thermo Fisher Scientific	Hs0083876_g1
BAX	Thermo Fisher Scientific	Hs00180269_m1
BID	Thermo Fisher Scientific	Hs01026792_m1
BIM (BCL2L1)	Thermo Fisher Scientific	Hs00708019_s1
BIK	Thermo Fisher Scientific	Hs00154189_m1
HRK	Thermo Fisher Scientific	Hs02621354_s1
NOXA (PMAIP1)	Thermo Fisher Scientific	Hs00560402_m1
PUMA (BBC3)	Thermo Fisher Scientific	Hs00248075_m1
B2M	Thermo Fisher Scientific	Hs00984230_m1
miR205	Thermo Fisher Scientific	hsa-miR 205_000509
miR22	Thermo Fisher Scientific	hsa-miR 22_000398
miR125a-5p	Thermo Fisher Scientific	has-miR 125a-5p_002198
miR125b	Thermo Fisher Scientific	has-miR 125b_000449
miR148a	Thermo Fisher Scientific	has-miR 148a_000470
miR152	Thermo Fisher Scientific	has-miR 152_000475
RNU48	Thermo Fisher Scientific	001006
Recombinant DNA		
human ERBB3 (pReceiver-Lv105-ERBB3)	GeneCopoeia	#Y2798
human ERBB3 shRNA lentiviral particle	OriGene Technologies	Locus ID 2065, TL320343V
human FGFR3 shRNA lentiviral particle	OriGene Technologies	Locus ID 2261, TL320355V
empty shRNA vector	OriGene Technologies	TL30021V
miRZIP Lentiviral-based anti-microRNAs	System Bioscience	#MZIP 205PA-1
anti-miR-205-5p miRCURY LNAinhibitor	QIAGEN	#4101508-001
Software and algorithms		
cBioPortal site for Cancer Genomics	Cerami et al., 2012	http://www.cbioportal.org/
GlioVis data portal	Bowman et al., 2017	http://gliovis.bioinfo.cnio.es/
Glioblastoma BioDiscovery Portal (miRNA)	NCI	http://gbm-biodp.nci.nih.gov/
The Human Protein Atlas	Uhlen et al., 2010	http://www.proteinatlas.org
GraphPad Prism 8.3.0	GraphPad software	https://www.graphpad.com:443/
Laboratory Assistance Suite (LAS)	Baralis et al., 2012	https://las.ircc.it:443/las/laslogin/
StudyLog® Version 4.2.1.3	StudyLog® Systems Inc.	N/A
Chromas Lite 2.01 software	Technelysium	http://technelysium.com.au/wp/chromas/
COSMIC	Sanger Institute	https://cancer.sanger.ac.uk/cosmic
Nearest Template Prediction algorithm	Hoshida, 2010	http://cloud.genepattern.org/
Caleydo 3.1.5	JKU Visual Data Science Lab	http://caleydo.org/
GSEA software v.4.0.2	Broad Institute	http://www.gsea-msigdb.org/gsea/index.jsp
GEDAS software	Fu and Medico, 2007	https://sourceforge.net/projects/gedas/
TargetScanHuman 7.2	Lewis et al., 2005	http://www.targetscan.org/vert_72/
CytoVision® software	Leica	N/A
Summit 4.3 software	Beckman Coulter	N/A
Amnis IDEAS 6.2 image analysis software	Luminex	N/A
Image Lab software	Biorad	N/A
Wave Controller 2.6 software	Agilent	N/A

RESOURCE AVAILABILITY

Lead contact

Further information and requests for resources and reagents should be directed to and will be fulfilled by the lead contact, Carla Boccaccio (carla.boccaccio@ircc.it).

Materials availability

Neurospheres are available upon institutional material transfer agreement approval after request by qualified academic investigators for non-commercial purposes.

Data and code availability

● The gene expression dataset (microarray) generated during this study has been deposited in the Gene Expression Omnibus Database (GEO) and is publicly available as of the date of publication. Accession number is listed in the [Key resources table](#). Gene expression dataset and original western blot images for [Figures 2, 3, 4, 5 and 6](#) have been deposited at Mendeley and are publicly available as of the date of publication. The DOI is listed in the [Key resources table](#).

- This paper does not report original code.
- Any additional information required to reanalyze the data reported in this paper is available from the lead contact upon request.

EXPERIMENTAL MODEL AND SUBJECT DETAILS

Neurosphere (NS) derivation from human patients

We derived 84 cultures enriched in stem-like cells (i.e., neurospheres, NS; hereafter overall referred as 84 NS-panel) starting from surgical samples of consecutive primary GBMs obtained at Fondazione IRCCS Istituto Neurologico C. Besta (see [Table S2](#) for patient's details), according to a protocol approved by the institutional Ethical Committee, as previously described ([De Bacco et al., 2012](#)). NS were propagated at clonal density in standard medium containing human bFGF (20 ng/ml, PeproTech) and EGF (20 ng/ml, Sigma-Aldrich).

Neurosphere subcloning and cell treatment with growth factors

Subclones from ERBB3-high NS were obtained by seeding single cell in standard medium in low-adherent conditions and were stabilized on average after 2 months. NS pseudo-differentiation was induced by culturing cells in a medium deprived of growth factors and supplemented with 1% FBS (Sigma-Aldrich) in pro-adherent conditions for 4 days. For characterization of growth factor biochemical and biological activities, cells were previously kept in the absence of any growth factor for 48 h; bFGF (20 ng/ml), NRG1 (50 ng/ml), BDNF (20 ng/ml), SCF-1 (20 ng/ml), HGF (20 ng/ml) and PDGFBB (20 ng/ml) (PeproTech), EGF (20 ng/ml, Sigma-Aldrich) were added as indicated. The colorectal cancer stem-like cells M049 (colosphere) ([Luraghi et al., 2018](#)) was used as positive control for NRG1 activation. Human cell lines (U138MG, A549, A2780, A375, K562, OE21, MDA468, BT474, HeLa, T47D and MCF7), used as positive controls of RTK expression and activation, were kept in culture according to manufacturer's instructions (see [Key resources table](#) for details), and re-authenticated soon before experiments by short tandem repeated profiling (GenePrint® 10System, Promega).

Generation of experimental tumors

All animal studies were performed according to ethical regulations and protocols approved by the Italian Ministry of Health. Experiments were performed on 6-8 weeks old male NOD.CB17-Prkdcscid/J mice (Charles River Laboratories). Mice were housed at a maximum of 6 per cage with a 12 h light/dark cycle at 22°C, and were monitored at a minimum of twice weekly for general performance status. NS intracranial transplantation was conducted as previously described ([De Bacco et al., 2016](#)). Briefly, 2.5×10^5 dissociated cells were stereotactically injected into the mouse brain (coordinates used were as follows: 0.7 mm anterior from bregma, 2 mm lateral from the midline and 2 mm below the pial surface). Mice were monitored and sacrificed at the appearance of evident suffering signs. For subcutaneous transplantation, 2.5×10^5 cells were resuspended in 100 μ l 1:1 v/v PBS/Matrigel (BD Biosciences) and injected into the right flank. Tumor diameters were evaluated twice/week by caliper and tumor volume was calculated using the formula: $4/3\pi \times (d/2)^2 \times (D/2)$, where d and D are the minor and the major tumor axis, respectively. Mice were euthanized when xenografts' volume reached $\sim 1600 \text{ mm}^3$, or they displayed signs of distress, or weight loss $\geq 20\%$.

Treatment of experimental tumors with MM121

For treatment of experimental subcutaneous GBMs with the specific anti-ERBB3 antibody MM121 (Merrimack) ([Schoeberl et al., 2017](#)), mice were randomized in mock-treated or MM121-treated groups starting from a wider cohort of established tumors (average volume 150 mm^3), using the Laboratory Assistant Suite ([Baralis et al., 2012](#)). For treatment of intracranial GBMs, ERBB3-high NS (BT308) were engineered to express luciferase and GFP as previously described ([De Bacco et al., 2016](#)) and *in vitro* bioluminescence was verified. Intracranial injection (as described above), tumor monitoring and treatment were performed by an external Contract Research Organization (Accelera srl, Italy). Mice were monitored by bioluminescence imaging (IVIS® Lumina System, Caliper Life

Sciences); at day 25, mice were randomized in two groups (mock-treated and MM121-treated) ($n = 7/\text{group}$) starting from a wider cohort and using StudyLog® Version 4.2.1.3 (StudyLog® Systems Inc.). For both subcutaneous and intracranial experimental GBMs, MM121 (30 mg/kg) was administered by intraperitoneal injection twice/week; mock-treated mice received PBS. At least 6 mice/group were used, in order to identify significant therapeutic responses with a statistical power of 90% (calculated by considering: volume variations of $\pm 15\%$ as random, volume variation of at least 20% as a therapeutic effect and a statistical significance of $p = 0.05$).

Patients' data and survival analysis

Clinical data of patients that generated the 84 NS-panel (Table S2) were obtained according to the requirements of the institutional Ethical Committee, and analyzed after patients de-identification. For the TCGA GBM cohort: (1) genetic data for correlation studies were obtained from the public cBioPortal website (<https://www.cbioportal.org/>; Cerami et al., 2012) and were selected as follow: Glioblastoma Multiforme TCGA Firehose Legacy; samples with mutations, CNV and expression data ($n = 136$). (2) Gene expression, classification and survival data were obtained from the public TCGA GBM Dataset (<http://gliovis.bioinfo.cnio.es/>); only primary untreated GBMs were included ($n = 479$). (3) miR expression data were obtained from the public TCGA GBM Dataset (<http://gbm-biodp.nci.nih.gov/>) ($n = 339$). (4) Immunohistochemical evaluation of EGFR family members in public tumors was obtained from the Human Protein Atlas ([http://www.proteinatlas.org](http://www.proteinatlas.org;); Uhlen et al., 2010). Survival curves were calculated using log-rank (Mantel-Cox) and Wilcoxon test with Prism v8.0 software (GraphPad). Patients originating the 84 NS-panel were defined as ERBB3-high when matched with NS displaying ERBB3 mRNA $\log_2\text{ratio} > 2.5$; patients in the TCGA GBM cohort were defined as ERBB3-high when ERBB3 mRNA level was in the upper quartile.

METHOD DETAILS

NS treatment with inhibitors

For *in vitro* ERBB3 targeting, the specific anti-ERBB3 antibody MM121 (Merrimack) (Schoeberl et al., 2017) was used at the dose of 50 $\mu\text{g}/\text{ml}$ in single administration, according to manufacturer's instructions. For FGFR inhibition, the pan-FGFR inhibitor BGJ398 (Selleckchem) was used at the dose of 5 nM. For glucose uptake inhibition, NS were treated with 2-Deoxy-D-glucose (2-DG, 50 mM, Sigma-Aldrich). For methylation inhibition, cells were treated with the demethylating agent 5-aza-2'-deoxycytidine (5' AZA, 5 μM , Sigma-Aldrich). In all the above treatments, NS were kept in complete standard medium containing EGF and bFGF (20 ng/ml each); mock-treated cells received equal volume of PBS or DMSO.

Nucleic acid extraction and retro-transcription

From NS, nucleic acids were extracted using All Prep DNA/RNA Mini Kit (QIAGEN) according to manufacturer's instructions with minor modifications for preserving miRNAs. Briefly, 1.5 volumes of Absolute ethanol were used in the RNA precipitation step and wash buffer RW1 was replaced by RWT buffer (QIAGEN). In some experiments either miRNeasy Mini Kit (QIAGEN) or RNeasy Mini Kit (QIAGEN) were used following manufacturer's instructions. In parental and experimental GBMs, RNA and miRNAs were extracted from 10 μm thick formalin-fixed paraffin embedded (FFPE) sections with Maxwell® RSC miRNA Tissue kit and apparatus (Promega) according to manufacturers' instructions. Purified mRNA and miRNAs were reverse transcribed starting from 150 or 250 ng of total RNA and using High-Capacity cDNA or TaqMan microRNA Reverse Transcription Kit and specific microRNA primers, respectively (Thermo Fisher Scientific).

Gene copy number evaluation

Gene copy number analysis was assessed by real-time PCR, using TaqMan Universal PCR Master MIX and the ABI PRISM 7900HT sequence detection system (Thermo Fisher Scientific). Primers for TaqMan copy number assays are reported in the Key resources table. Relative gene copy number data were calculated by normalizing against endogenous control (RNaseP). A normal diploid human gDNA (293T cell line, ATCC) was used as calibrator to obtain the $\Delta\Delta\text{Ct}$. The copy number of each gene was calculated with the formula $2 \times 2^{-\Delta\Delta\text{Ct}}$. To discriminate between real EGFR amplification and chr7 polysomy, the calculated copy number was normalized against the copy number of a gene mapped on chr7 and usually not amplified (HGF). EGFR amplification is defined when EGFR copy number is $> 3 + \text{HGF copy number}$.

Gene sequencing

PCR products used for gene sequencing were amplified either from gDNA (*TERT* promoter, *IDH1*, *MIR205HG*, *PIK3CA*, *TP53* and *PTEN*) or from cDNA (*ERBB3* and *EGFR* "CNS specific" alterations corresponding to aa 108/289/598 and surrounding sequences) using Platinum® Taq DNA Polymerase (Thermo Fisher Scientific); *TERT* promoter amplification was obtained using Platinum SuperFi DNA Polymerase plus GC enhancer (Thermo Fisher Scientific). Specific primer pairs used are listed in Table S4 and De Bacco et al. (2012). PCR conditions for *IDH1*, *MIR205HG*, *PIK3CA*, *PTEN* and *TP53* were as follows: 95°C for 3 min; 3 × [95°C for 15 s, 64°C for 30 s, and 70°C for 1 min]; 3 × [95°C for 15 s, 61°C for 30 s, and 70°C for 1 min]; 3 × [95°C for 15 s, 58°C for 30 s, and 70°C for 1 min]; 37 × [95°C for 15 s, 57°C for 30 s, and 70°C for 1 min]; and 70°C for 5 min. PCR conditions for *EGFR* and *ERBB3* were as follows: 95°C for 3 min; 40 × [95°C for 30 s, 63°C for 30 s, and 72°C for 30 s]; and 72°C for 5 min. PCR conditions for *TERT* promoter were as follows:

98°C for 30 s; 40 × [98°C for 10 s, 63.9°C for 10 s, and 72°C for 15 s]; and 72°C for 5 min. PCR products were purified using Exo-ProStar 1-Step (Illustra) according to manufacturer's instructions. Cycle sequencing was carried out using BigDye Terminator v3.1 Cycle Sequencing kit (Thermo Fisher Scientific). Sequencing products were purified using Agencourt CleanSeq (Agencourt Bioscience, Beckman Coulter) and analyzed on a 3730 DNA Analyzer ABI capillary electrophoresis system (Thermo Fisher Scientific). Sequences were then analyzed with Chromas Lite 2.01 software (<http://technelysium.com.au/wp/chromas/>) and compared with reference sequences from the *Homo sapiens* assembly GRCh37 (February 2009). All identified mutations were then compared with those reported in the Catalogue Of Somatic Mutations In Cancer (COSMIC, <https://cancer.sanger.ac.uk/cosmic>).

Transcriptome analysis

For gene expression profiling of the 84 NS-panel, biotin-labeled cRNA was synthesized from 500ng of total RNA with the Illumina® TotalPrep RNA Amplification Kit and hybridized on Human HT-12 v4 BeadChip (Illumina), according to manufacturer's instructions. The chip was labeled with streptavidin-Cy3 and the fluorescent signal was scanned with the Illumina BeadArray Reader. Raw data were summarized and cubic-spline normalized with the GenomeStudio software (Illumina). Data filtering and log2ratio transformation were carried out with Excel (Microsoft). When multiple probes mapped on the same gene, probe displaying the highest average signal was reported.

NS classification according to Wang et al. (2017) was performed by the tree way methodology available at <http://gliovis.bioinfo.cnio.es/>; NS classification according to Wang et al. (2020) was performed using Nearest Template Prediction algorithm (Hoshida, 2010) available at <https://cloud.genepattern.org/>. Correspondences between NS classifications were represented using Caleydo 3.1.5. Gene set enrichment analysis was performed using GSEA software v.4.0.2. Genes sets used in this study are reported in Table S3. Clustering and data representation were performed with the GEDAS software (Fu & Medico, 2007).

Quantitative Real-Time PCR (qPCR)

Real-time PCR for evaluation of gene mRNA and miRNA expression was performed using primer and probe sets (Thermo Fisher Scientific) listed in the Key resources table, with TaqMan Universal PCR Master Mix and an ABI PRISM 7900HT sequence detection system (Thermo Fisher Scientific). Expression levels were normalized against endogenous controls (β -actin and β 2 microglobulin for gene mRNA; RNU48 for miRNA); control cells were used as calibrators. Expression levels were reported as 40-Ct or as fold versus control cells, and are the mean \pm SEM of two independent experiments in triplicate.

Bisulfite treatment and methylation analysis

200ng of gDNA were bisulfite converted using the EZ-DNA Methylation Gold kit (ZYMO Research) according to manufacturer's instructions. Amplification was performed in replicate in a final volume of 20 μ L using 1.5 mM of Mg, 300 nM of dNTP, 200 nM of primer mix, and 0.4 Unit of Platinum Taq (Invitrogen), with 45 cycles using 58°C or 60°C as annealing temperature for miR205 promoter and miR205HG respectively. 10 μ M forward primer, 10 μ M biotinylated Tag and 1 μ M reverse primer were used for primer mix (primer sequences are reported in Table S4). Amplification products were purified and annealed with the sequencing primer using the pyromark Q24 Workstation, according to manufacturer's protocol, and were then sequenced on pyromark Q24 (QIAGEN). For evaluation of MGMT promoter methylation, NS gDNA was analyzed with BEAMing methodology as previously described (Pietrantonio et al., 2014). Briefly, MGMT amplification was first obtained using the Platinum® Taq (Life technologies) and specific primers listed in Table S4. PCR products were diluted (1:20000) and a second amplification step allowing physical separation and independent amplification of different templates was performed. PCR emulsion breaking and hybridization (sequences in Table S4) were carried out using Inostics reagents. Fluorescence was assessed on a CyAN flow-cytometer (Beckam-Coulter). The percentage of methylation was evaluated as follow: methylated specific signals/(methylated + unmethylated specific signals).

FISH analysis

For evaluation of ERBB3 gene amplification or translocation, FISH analysis was performed using ERBB3/CEN 12 Dual Color Probe (Zytovision), including a green fluorochrome probe specific for the alpha satellite centromeric region of chromosome 12 (D12Z3) and an orange fluorochrome probe specific for the human ERBB3 gene (12q13.2-q13.3). For evaluation of the MIR205HG genomic region (chr1:209,428,823-209,432,549, hg38), FISH analysis was performed using RP11-927D11 (chr1:209,409,153-209,605,505) and the centromeric clones RP11-57117 (chr1:207,554,754-207,751,766) and RP11-54717 (chr1:190,352,905-190,488,640), kindly provided by Prof. M. Rocchi (University of Bari). Briefly, BAC clones DNA were isolated and fluorescent dye incorporation was performed using Nick translation reagent kit [SpectrumGreen (RP11-927D11), SpectrumRed (RP11-57117), or SpectrumAqua (RP11-54717) conjugated dUTP] (Abbot Molecular inc.). FISH was carried out on interphase cells prepared according to standard techniques. Cells were incubated with the probe for 10 min at 75°C for co-denaturation and placed in a humidified chamber at 37°C overnight for the hybridization step. After washing with ISH Stringent Wash Buffer (Agilent), chromatin was counterstained with DAPI 150ng/ml (Zytovision). An average of 100 cells was analyzed using an Olympus BX61 microscope and CytoVision software. ERBB3 and miR205 status was defined by calculating the mean gene copy number (*ratio* copy number/nuclei), and considered increased if ≥ 3 .

Prediction of ERBB3 targeting miRNAs

For identification of putative miRNAs targeting ERBB3, the ERBB3 3' UTR sequence from ensembl (<http://www.ensembl.org/useast.ensembl.org/?redirectsrc=//www.ensembl.org%2F>, ENST00000267101.3) was analyzed with TargetScanHuman 7.2 (http://www.targetscan.org/vert_72/). miRNAs highly conserved and with a high context score (Agarwal et al., 2015; Lewis et al., 2005) were selected for further analysis.

NS transfection and transduction

For transfection with antagomiR-205 (anti-miR-205-5p miRCURY LNA microRNA inhibitor, Quiagen), NS were dissociated to single-cell suspensions, and 10^5 cells were transduced using TransIT-X2® Dynamic Delivery System (MirusBio) according to manufacturer's instructions and cells were assessed 48 h after transfection. For transduction, NS were dissociated to single-cell suspensions, and 10^5 cells were transduced in standard medium with miRZIP Lentivector-based Anti-MicroRNAs (System Bioscience), or human ERBB3 shRNA Lentiviral Particles (Locus ID 2065, OriGene Technologies) or FGFR3 shRNA Lentiviral Particles (Locus ID 2261, OriGene Technologies), or human ERBB3 (pReceiver-Lv105-ERBB3) lentivector (GeneCopoeia) at a Multiplicity Of Infection (MOI) of 5. Transduction efficiency was determined 72 h post-infection by fluorescent microscopy and quantitative Real Time PCR as above. Empty vectors were used as controls.

Western blotting

Protein expression was analyzed in whole cell-lysates solubilized in boiling Laemmli buffer (for total protein extraction) or RIPA (for single protein immunoprecipitation) or EB-extraction buffer (for protein co-immunoprecipitation), or in cytoplasmic and nuclear fractions obtained as previously described (De Bacco et al., 2016). Cell-lysates were sonicated, quantified using BCA method (Pierce), and 10 to 20 μ g were resolved by SDS-PAGE in reducing conditions (BioRad) and blotted onto nitrocellulose membrane (BioRad). After blocking, the following primary antibodies were used (see [Key resources table](#) for detail): anti-MET (DL21, Candiolo Cancer Institute), anti-ERBB3, anti-EGFR, anti-ERBB4, anti-PDGFR, anti-PDGFRB, anti-FGFR1, anti-FGFR2, anti-FGFR4, anti-MAP2, anti-BCL2, anti-phospho-ERBB3 (Tyr1289, Tyr1222, Tyr1197), anti-c-KIT, anti-phospho-p44/42 MAPK, anti-phospho-AKT (Ser473), anti-phospho-FRS2 (Tyr436), anti-phospho-mTOR, anti-phospho-RAPTOR, anti-RAPTOR, anti-phospho-S6, anti-S6, anti-phospho-4EBP1, anti-GLUT1, anti-cleaved PARP and anti-caspase 3 (Cell Signaling Technology), anti-ERBB2 (Thermo Fisher), anti-NTRK2 (R&D), anti-NEDD4 (Bethyl), anti-FGFR3 and anti-NRDP1 (NovusBio), anti-LDHB (abcam), anti-phospho-Tyr (Millipore), b-actin and Calnexin (Cell Signaling Technology), TATA binding Protein (TBP) and vinculin (Sigma-Aldrich), and GAPDH (Abcam) were used as protein loading control as indicated. For co-immunoprecipitation and ERBB3 phosphorylation, equal amounts of proteins were immunoprecipitated using the following antibodies: mouse monoclonal anti-ERBB3 (Millipore), anti-ERBB2 (Trastuzumab, Roche), anti-MET (DO24, Candiolo Cancer Institute), anti-EGFR, anti-PDGFR, anti-PDGFRB, anti-KIT (Cell Signaling Technology), anti-NTRK2 (R&D System), anti-FGFR3 (NovusBio), and analyzed by western blotting with anti-pan-phospho-Tyr antibodies (Millipore), and the above antibodies. For multiple protein detection in immunoprecipitates, membranes were stripped using stripping buffer solution (Thermo Fisher). After membrane incubation with HRP-conjugated secondary antibodies (Jackson Lab), enhanced chemiluminescence (Biorad) was used for detection; blot images were acquired with the ChemiDoc Touch™ Imaging System (Biorad) with Image Lab software. Results are representative of at least 2 independent experiments.

Flow-cytometric analysis

NS were manually dissociated and resuspended in PBS 1% BSA at a concentration of 2×10^6 cells/ml. For surface markers detection, cells were incubated for 15 min at room temperature with the following antibodies (see [Key resources table](#) for details): anti-ERBB3-PE (clone REA508, Miltenyi Biotec GmbH); anti-ERBB3-APC (clone 1B4c3) and anti-ERBB2 (clone 5D3) (Biolegend); anti-ERBB4 (polyclonal anti-goat, R&D System); anti-EGFR (clone EGFR.1, BD Bioscience); anti-FGFR2 (clone 98725), anti-FGFR3 (clone 136334) and anti-FGFR4 (clone 240929) (R&D System); anti-PDGFR (clone 16A1) (Biolegend); anti-HGF R/MET (clone 95106, R&D System); anti-NTRK2 (clone 72509, R&D System); anti-c-KIT (clone 104D2, Immunological Sciences). DAPI (Roche) was used for dead cells exclusion. Analysis was performed on a CyAn ADP (Beckman Coulter) equipped with 488nm, 405nm and 642nm solid state lasers and data were processed using Summit 4.3 software (Beckman Coulter). Whenever appropriate, the compensation matrices available with software, including the VisiComp scaling algorithm were applied in order to avoid overcompensation errors. For each antibody, unstained cells, obtained from the same NS culture and treated as stained cells, were used to determine background fluorescence and to set negative gates appropriately. In multicolor staining, the Fluorescence Minus One methodology was applied in order to avoid interferences (Hulspas et al., 2009; Maecker & Trotter, 2006). EGFR family antibodies validation and gating strategy are shown in [Figures S11A](#) and [S11B](#).

Flow-cytometric single cell imaging

Amnis ImageStream system were used to define co-localization of ERBB3 and FGFR3 in single cells obtained from ERBB3-high NS. NS were mechanically dissociated and 1×10^7 /ml cells were incubated for 30 min at room temperature with the following antibodies: anti-ERBB3-PE (clone REA508, Miltenyi Biotec GmbH, 1:10) and anti-FGFR3-APC (clone 136334, R&D System, 1:5). Hoechst 33342

Staining Dye Solution (Abcam) was used to identify nuclei. Data were acquired by an Amnis ImageStream®XMarkII (Luminex), equipped with 488 nM, 405 nM and 642 nM solid state lasers, and analysis were performed by Amnis IDEAS 6.2 image analysis software (Luminex).

Immunofluorescence analysis

Immunofluorescence analyses were performed either in NS or FFPE experimental tumor sections. Samples were fixed 10 min with PFA 4% at 4°C, permeabilized with Triton 0.2% for 10 min, washed and saturated with PBS-TWAIN BSA 5% for 1 h. Primary antibodies for anti-ERBB3 (Cell Signaling Technology) or anti-FGFR3 (NovusBio) (see [Key resources table](#)), were incubated for 1 h at room temperature and then overnight at 4°C. AlexaFluor conjugated anti-rabbit or anti-mouse secondary antibodies (1:1000, Thermo Fisher) were incubated for 1 h. DAPI was used for nuclear counterstaining. Images were acquired using a LEICA SPEII confocal microscope and are representative of at least three independent immunostainings.

Immunohistochemistry and TUNEL assay

Analysis of parental tumor samples was performed on ~3 μm section starting from Carnoy fixed, paraffin embedded samples. For ERBB3 and ERBB2 immunostaining, heat induced epitope retrieval (HIER) was performed in PT Link® pre-treatment module (Agilent) using Target retrieval solution high pH (Dako), and sections were then incubated with anti-ERBB2 (Agilent) or anti-ERBB3 antibodies (Sigma-Aldrich). For EGFR immunostaining with anti-EGFR (Thermo Fisher) no antigen retrieval was required. As secondary antibodies, anti-rabbit Envision® HRP-conjugated (Agilent) was used for ERBB3, while FLEX® HRP-conjugated was used for ERBB2 and EGFR antibodies. Staining was detected using the diaminobenzidine (DAB Substrate Chromogen System, Agilent) and counterstained with hematoxylin. ERBB3, ERBB2 and EGFR expression was evaluated by B.P. and M.P., and was scored semiquantitatively as 0, 1+ or 2+, based on the percentage of positive cells and staining intensity. Immunohistochemistry analysis on experimental GBMs was performed on ~2 μm FFPE sections collected on polarized slides. Haematoxylin-Eosin staining (H&E) was performed. ERBB2 and EGFR detection was performed as described above with appropriate staining controls: EGFR amplified GBM (#BT379) and ERBB2 amplified breast cancer PDX (kindly provided by Dr. Sassi and Prof. Trusolino) ([Figure S11C](#)). For ERBB3, phospho-S6 and ki-67 immunostaining, sections underwent heat-induced antigen retrieval via microwaves; for LDHB pre-heat water bath and citrate buffer were used. Sections were then incubated with primary antibody diluted in TBS 1% BSA overnight at 4°C. The following antibodies were used: anti-ERBB3 (Protein human Atlas), anti-phospho-S6 (Cell Signaling Technology), anti-LDHB (Abcam) and anti-ki-67 (Agilent) (see [Key resources table](#)). Sections were then incubated with the appropriate secondary HRP-conjugated antibodies and DAB (Dako).

Terminal deoxynucleotidyl transferase dUTP nick end labeling (TUNEL assay, Promega) was used to measure apoptotic index in experimental GBMs at the endpoint. FFPE tumors were sectioned according to manufacturer's instruction. TUNEL-positive cells were quantified by averaging the number of positive nuclei in six high-power fields (HPF, 400 × magnification) per mouse (n = 3/group), excluding necrotic areas.

Duolink proximity ligation assay

10⁴ NS cells were fixed as above and the Duolink proximity ligation assay (PLA) kit (Sigma-Aldrich) was used according to manufacturer's instructions. Briefly, primary antibodies (for dilutions and details see [Key resources table](#)) were incubated overnight at 4°C, then Duolink PLA probes detecting rabbit or mouse antibodies were incubated for 2 h. Secondary antibodies hybridized when the two different PLA probes (anti-rabbit minus probe and anti-mouse plus probe) were bound to proteins closer than 40 nm. After ligation and amplification steps, the signal generated by fluorescently labeled oligonucleotides was detected by fluorescence microscopy as a point-shaped signal. ERBB3-neg NS were used as specificity control, as well as cells stained with only ERBB3 or FGFR3 antibodies. Images were acquired as described above.

Lactate release and pH measurement

NS were kept in standard medium at clonal dilution for 3 days, with or without MM121, and then culture supernatants were collected and immediately analyzed. Lactate release was evaluated by Lactate-GloAssay and GloMax 96 Microplate Luminometer (Promega) according to manufacturer's instructions. pH was measured by a pHmeter (Basic 20, Crison), calibrated before each experiment with standard medium supplied with serial dilutions of HCl or NaOH. Technical and biological replicates were performed (n ≥ 3). Data were reported as mean ± SEM of at least two independent experiments (n > 6).

Extracellular Acidification (ECAR) and Oxygen Consumption Rates (OCR)

Glycolytic Rate Assay and XF Cell Mito Stress were used for evaluating ECAR and OCR respectively with the Seahorse XFe96 instrument (Agilent), according to manufacturer's instructions. Cells were dissociated from exponentially growing NS kept in standard medium and 1.2 × 10⁴ cells/well were plated in XF96 microplates (Agilent) coated with Cultrex® BME PathClear® (Tema Ricerca) in fresh standard medium for 24 h. The following day, medium was replaced with the Seahorse XF base medium supplemented with 1 mmol/L L-glutamine for ECAR or 10 mmol/L glucose, 2 mmol/L glutamine and 1 mmol/L pyruvate for OCR. For normalization, at the end of the experiments, cells were fixed, stained with DAPI and counted using Cytation 3 Cell Imaging Reader (BioTek Instrument).

Cell proliferation, viability and apoptosis assays

10^3 NS cells/well were seeded in a 96-well plate at day -2 in a medium devoid of any growth factor for measuring the response to growth factors, or in standard medium (EGF + bFGF) for experiments with ERBB3 or FGFR inhibitors, shRNA and miR-205. Growth factors and/or MM121 or BGJ398 were added at day 0 and ATP production was measured by CellTiter-Glo® (Promega) at the indicated time points. For apoptosis, Annexin V incorporation was measured by RealTime-GloAnnexin V Apopt and Nec Assay (Promega) according to manufacturer's instructions at the indicated time points. Assays were measured using a GloMax 96 Microplate Luminometer (Promega). Data were reported as mean \pm SEM of at least two independent experiments ($n > 6$).

Annexin V and caspase 3 activity evaluation by flow-cytometry

NS were kept in standard medium and MM121 for 24 h. To evaluate different apoptosis phases, eBioscience Annexin V Apoptosis Detection Kit (ThermoFisher) and DAPI (Roche) were used according to manufacturer instructions. Apoptosis phases were defined as follow: viable, annexin V^{neg}/DAPI^{neg} cells; early apoptotic, annexin V^{pos}/DAPI^{neg}; late apoptotic, annexin V^{pos}/DAPI^{pos}; necrotic, annexin V^{neg}/DAPI^{pos}. For flow cytometric evaluation of activated caspase-3, NS were permeabilized with FIX&PERM® Kit (Nordic-MU-Bio) according to manufacturer's instructions, and then were incubated with purified rabbit anti-active caspase-3 (BD Biosciences). Reported values are the mean \pm SEM of two independent experiments.

Cell cycle analysis

Cell cycle was analyzed as previously described (De Bacco et al., 2016). Briefly, 10^6 cells were fixed overnight with 70% ethanol, stained with Propidium Iodide (PI, 50 μ g/ml) in RNaseA (100 μ g/ml) solution (DNAcon3 kit ConsulTS) for 3 hours at 4°C, and analyzed by flow-cytometry. Data are the mean \pm SEM of at least two independent experiments.

QUANTIFICATION AND STATISTICAL ANALYSIS

Data were expressed as mean \pm standard error of the mean (SEM) of at least two independent experiments. Statistical comparisons were performed using the parametric Student's t test, one-way Analysis of Variance (ANOVA) and Pearson's correlation, or the non-parametric Mann-Whitney test, 2-way ANOVA, and Kolmogorov-Smirnov test. Survival curves were analyzed using the Kaplan-Meier method with groups compared by respective median survival; the non-parametric Mantel-Cox and Wilcoxon tests were used for calculating log-rank p values. A *p-value* < 0.05 was considered significant. All statistical tests were performed with Prism v8.0 software (GraphPad). Statistical details of all experiments can be found in the figure legends, including exact number (n) of cell samples or mice.

Supplemental information

**ERBB3 overexpression due to miR-205 inactivation
confers sensitivity to FGF, metabolic activation,
and liability to ERBB3 targeting in glioblastoma**

Francesca De Bacco, Francesca Orzan, Jessica Erriquez, Elena Casanova, Ludovic Barault, Raffaella Albano, Antonio D'Ambrosio, Viola Bigatto, Gigliola Reato, Monica Patanè, Bianca Pollo, Geoffrey Kuesters, Carmine Dell'Aglio, Laura Casorzo, Serena Pellegatta, Gaetano Finocchiaro, Paolo M. Comoglio, and Carla Boccaccio

INVENTORY OF SUPPLEMENTAL INFORMATION

1.

Supplemental Figures

Figure S1, related to Figure 1

Figure S2, related to Figure 1

Figure S3, related to Figure 2

Figure S4, related to Figure 3

Figure S5, related to Figure 3

Figure S6, related to Figure 3

Figure S7, related to Figure 4

Figure S8, related to Figure 5

Figure S9, related to Figure 6

Figure S10, related to Figure 7

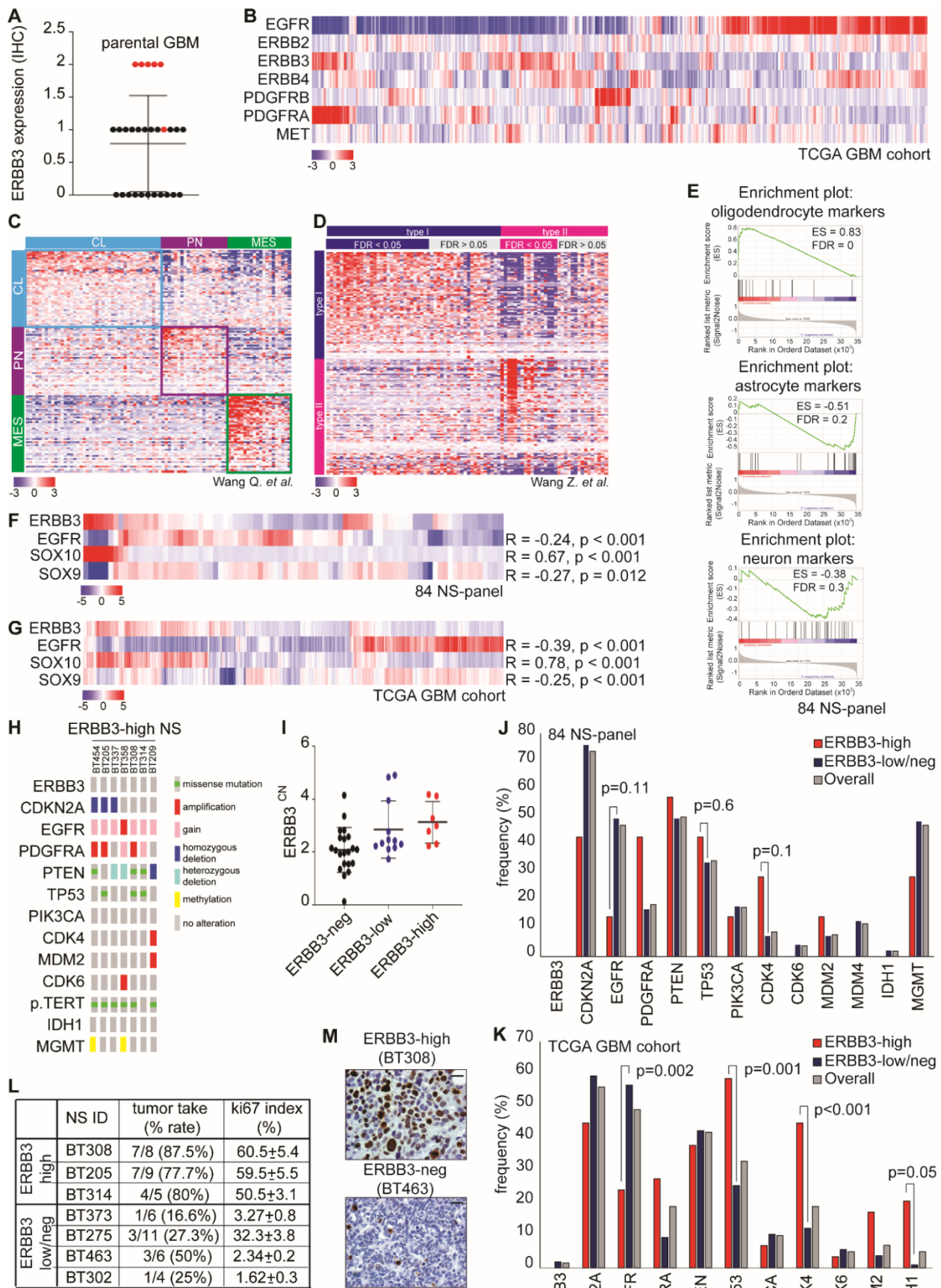
Figure S11, related to STAR Methods

2.

Supplemental Tables

Table S1, related to Figure 1

Table S2, related to Figure 1



De Bacco et al., Figure S1, related to Figure 1

Figure S1. ERBB3 overexpression defines a subset of proneural GBMs with oligodendroglial features and dismal prognosis, related to Figure 1

(A) ERBB3 expression measured by IHC in representative GBMs from the cohort that originated the 84-NS panel (n = 28). Red dots, patients matched with ERBB3-high NS.

(B) Heatmap showing spontaneous clustering of primary GBMs (TCGA, n = 497) according to mRNA levels of the indicated genes.

(C) Heatmap showing subtyping of the 84 NS-panel according to the classical (CL), proneural (PN) and mesenchymal (MES) classification system (Wang Q. *et al.*, 2017).

(D) Heatmap showing Nearest Template Prediction algorithm (NTP) subtyping of the 84 NS-panel according to the Type I and Type II classification system (Wang Z. *et al.*, 2020). NS with FDR > 0.05 were classified as non-Type I&II.

(E) Gene set enrichment analysis of oligodendrocyte, astrocyte and neuron markers in ERBB3-high versus ERBB3-low/neg NS performed in the 84-NS panel microarray. In ERBB3-high NS oligodendrocyte markers are significantly enriched, while astrocyte markers are significantly anticorrelated. ES, enrichment score; FDR, false discovery rate.

(F and G) Heatmaps showing mRNA levels (microarray) of the indicated genes in the 84 NS-panel (F) and in the TCGA GBM cohort (n = 497) (G). Pearson correlation coefficient (R) with ERBB3 and relative p-values are reported.

(H) Mutational profile (oncoprint) and O-6-methylguanine-DNA methyltransferase (*MGMT*) promoter methylation status of ERBB3-high NS. Colored rectangles indicate copy number variations, colored dots sequence alterations (see legend). *p.TERT*, *TERT* promoter.

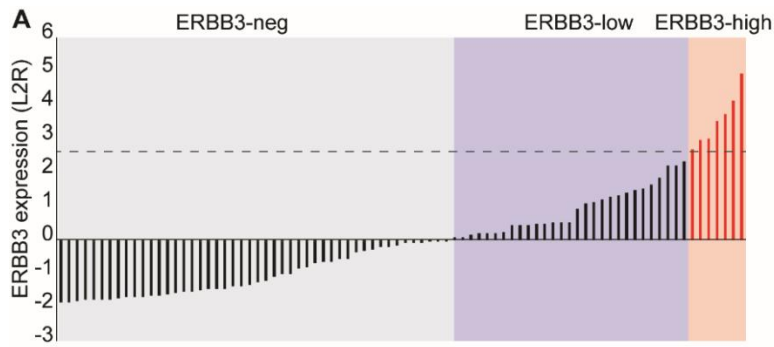
(I) *ERBB3* gene copy number measured by qPCR in 84 NS-panel gDNA, showing no significant variation in any NS subgroup. CN, copy number. Mean \pm SEM (n = 20 ERBB3-neg, n = 12 ERBB3-low, n = 7 ERBB3-high).

(J and K) Frequency of alterations (mutations and/or copy number variations) of the indicated GBM driver genes in ERBB3-high and ERBB3-low/neg cases (according to ERBB3 mRNA levels), in the 84-NS panel (J) and TCGA GBM cohort (K). Overall alteration frequency is also shown. Preferential association or anticorrelation between genetic alterations and ERBB3 expression was evaluated by Fisher's exact test. Significant p values in the TCGA GBM cohort and the corresponding p values in the 84 NS-panel are reported. *ERBB3*, *EGFR*: amplification and mutation; *CDKN2A*: homozygous deletion; *PDGFRA*, *CDK4*, *CDK6*, *MDM2*, *MDM4*: amplification; *PTEN*: homozygous deletion and mutation; *TP53*, *PIK3CA*, *IDH1*: mutation; *MGMT*: promoter methylation.

(L) Tumor take and ki67 index (positive cells/nuclei, mean \pm SEM, n = 5) in experimental GBMs obtained by orthotopic transplantation of proneural ERBB3-high or -low/neg NS. The mesenchymal ERBB3-low NS BT302 used for further *in vivo* experiments is also shown. ERBB3-high NS are significantly more aggressive than ERBB3-low/neg NS (unpaired t test with Welch's correction, p = 0.0027).

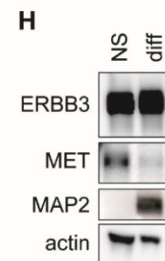
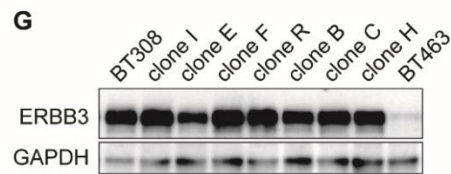
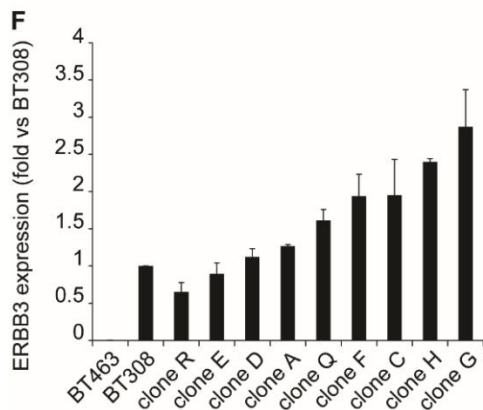
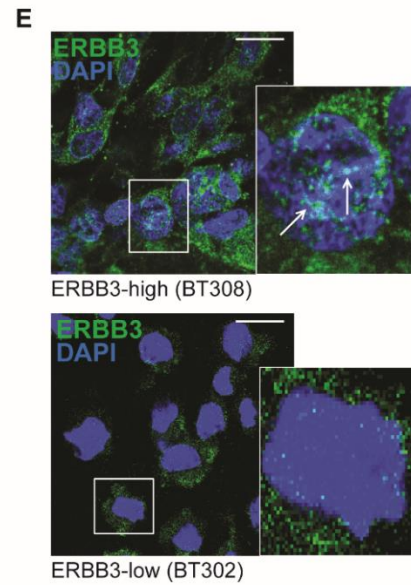
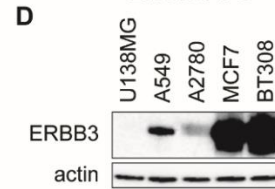
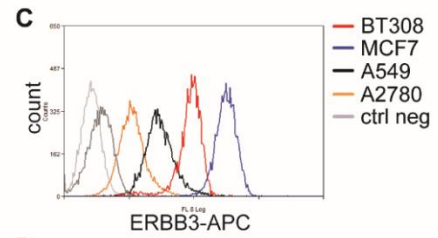
(M) ki67 staining in representative tumors obtained as in (L) with an ERBB3-high (BT308) or ERBB3-neg NS (BT463). Scale bar, 50 μ m.

See also Table S1-S2-S3.



B

	NS ID	mRNA		WB			flow-cytometry		IF																		
		-2.5	0	2.5	5	tot	cyt	nuc		ERBB3	TBP	98.84%	MFI 202.25	99.70%	MFI 117.65	99.91%	MFI 131.11	99.45%	MFI 146.12	48.84%	MFI 23.16	41.48%	MFI 12.99	0%	0%		
ERBB3-high	BT308																										
	BT209																										
	BT314																										
	BT205																										
ERBB3-low	BT373																										
	BT302																										
ERBB3-neg	BT463																										
	BT287																										



De Bacco *et al.*, Figure S2, related to Figure 1

Figure S2. ERBB3 expression in the 84-NS panel, related to Figure 1.

(A) ERBB3 mRNA expression levels (qPCR) shown as log₂ ratio (L2R) in the 84 NS-panel. Dotted line, threshold (L2R = 2.5) to discriminate ERBB3-high NS (red columns) from ERBB3-low ($0 < \text{L2R} \leq 2.5$) and ERBB3-neg (L2R < 0). Expression values for each NS are reported in Table S1.

(B) ERBB3 expression in representative ERBB3-high, -low and -neg NS evaluated at mRNA (L2R, qPCR) and protein level (WB, western blot of total, cytoplasmic and nuclear extracts; flow-cytometry; and IF, immunofluorescence). Percentages of ERBB3 positive cells and mean fluorescence intensity (MFI) measured by flow-cytometry are reported. TATA Binding Protein (TBP), loading control; DAPI, nuclear staining. Scale bar, 25 μm . IF higher magnification is shown in (E).

(C and D) ERBB3 protein expression in a representative ERBB3-high NS (BT308) compared with the indicated cancer cell lines, measured by flow-cytometry (C) and western blot (D). actin, loading control.

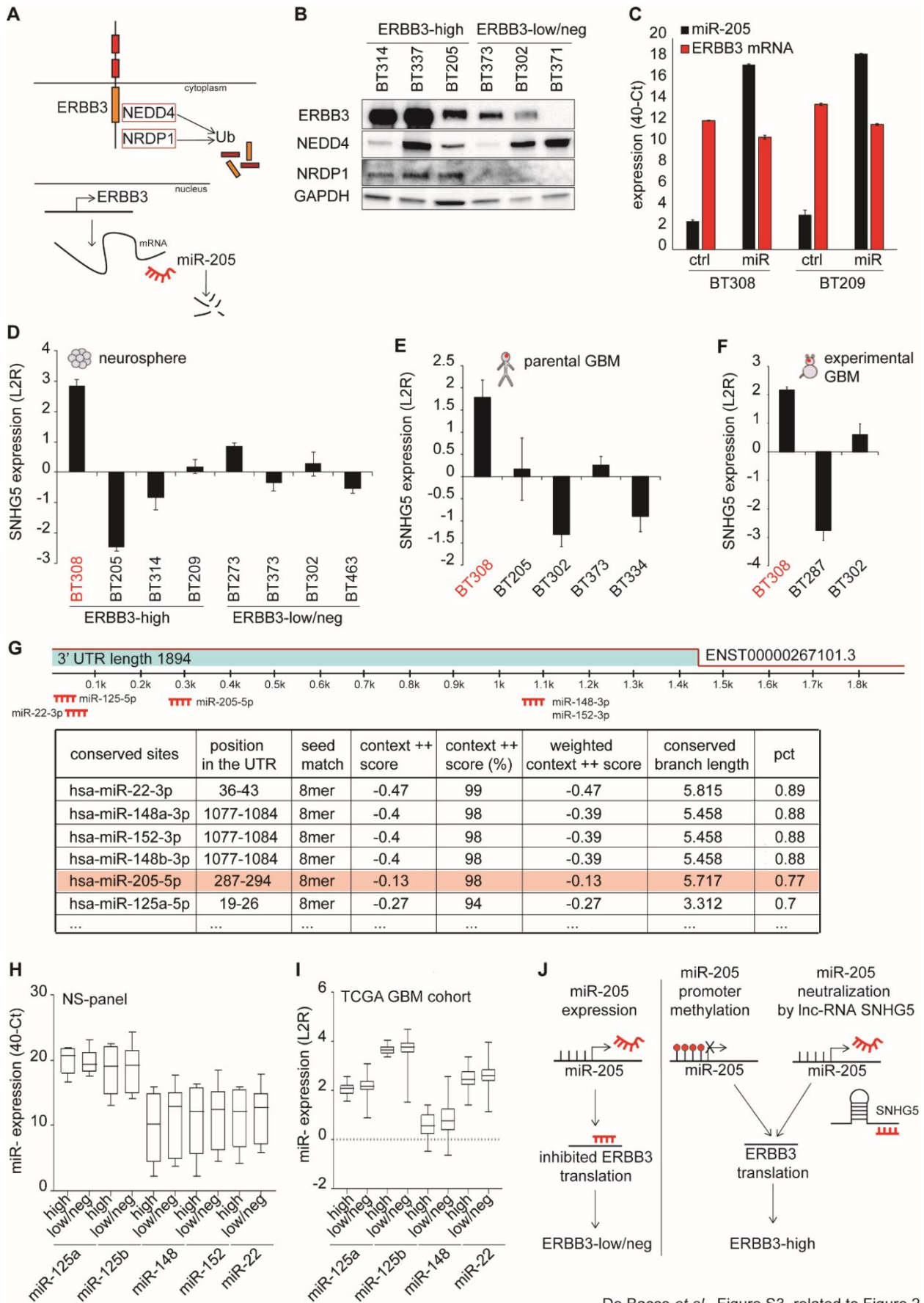
(E) ERBB3 localization evaluated by IF in ERBB3-high (BT308) and ERBB3-low NS (BT302). In magnified micrographs (right), arrows indicate nuclear clusters. Scale bar, 12.5 μm .

(F) ERBB3 mRNA expression (qPCR) in clones derived from subcloning of an ERBB3-high NS (BT308). Results are shown as fold versus parental BT308 expression (mean \pm SEM, n = 3). BT463 (ERBB3-neg NS), negative control.

(G) Western blot showing similar levels of ERBB3 protein in BT308 and its subclones. BT463 (ERBB3-neg NS), negative control; GAPDH, loading control.

(H) Western blot showing ERBB3 expression in NS and their progeny grown in pseudodifferentiating conditions (diff) for 4 days. MAP2 is used as differentiation marker, MET as positive control of RTK downregulation during differentiation; actin, loading control.

See also Table S1.



De Bacco *et al.*, Figure S3, related to Figure 2

Figure S3. ERBB3 overexpression is sustained by inactivation of the oncosuppressor miR-205, related to Figure 2.

(A) Possible mechanism(s) responsible for ERBB3 post-transcriptional downregulation: protein targeting to ubiquitination (Ub) by NEDD4 or NRDP1, or mRNA degradation by miR-205.

(B) Western blot showing lack of inverse correlation between ERBB3 and NEDD4 or NRDP1 expression in representative ERBB3-high and –low/neg NS. GAPDH, loading control.

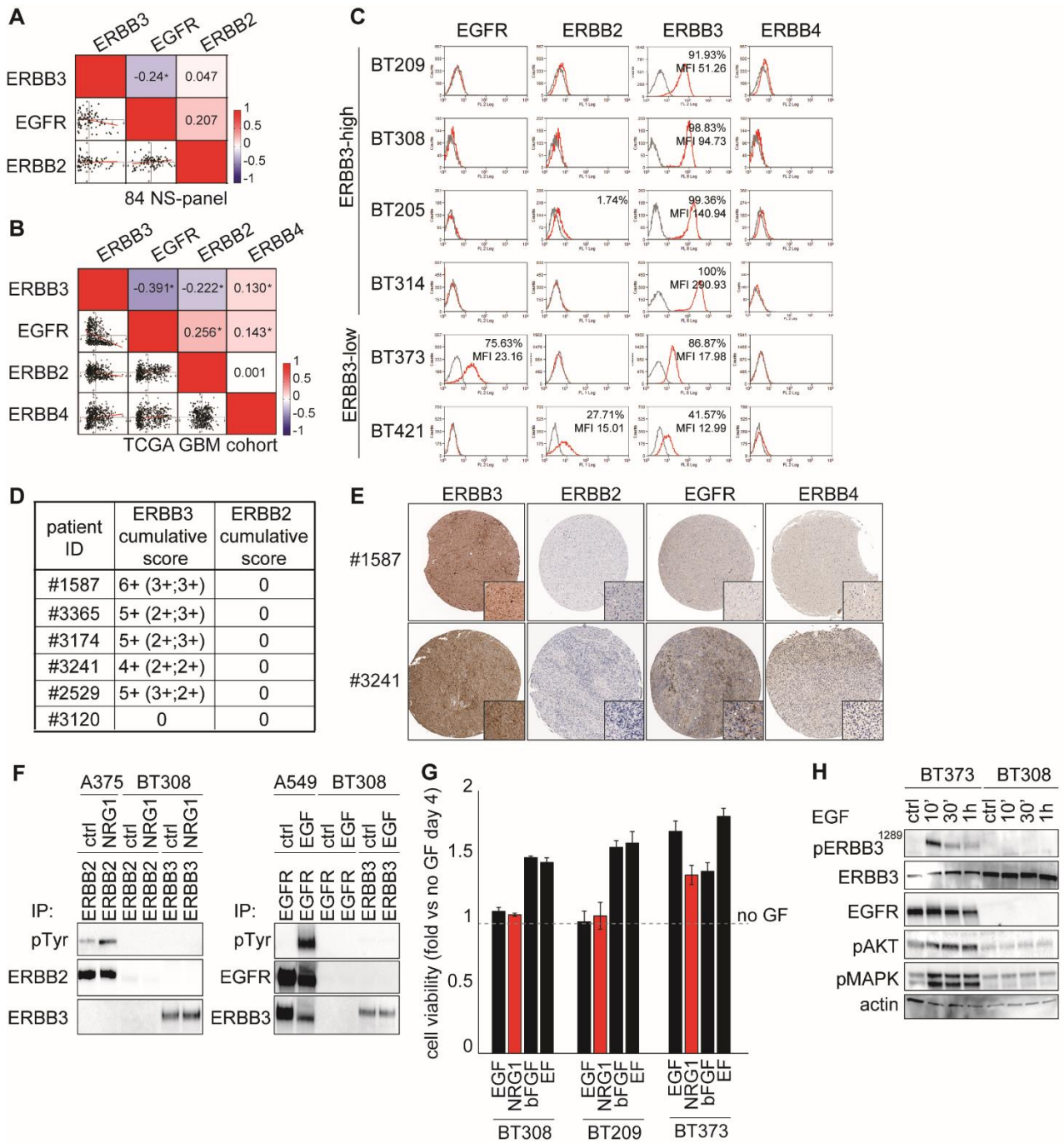
(C) miR-205 and ERBB3 expression (qPCR) in ERBB3-high NS (BT308 and BT209) transduced with miR-205. Mean \pm SEM, n = 3.

(D-F) lnc-RNA SNHG5 expression (qPCR) in representative ERBB3-high and –low/neg NS (D), parental (E) and experimental (F) GBMs. L2R, log₂ratio. Mean \pm SEM, n = 3.

(G) Seed binding regions located in the ERBB3 3'UTR (ENST00000267101.3). Highly conserved miRNAs displaying high complementary score ($\geq 90\%$) were shown (TargetScanHuman).

(H-I) miR-125a/b, -148, -152 and -22 expression in representative ERBB3-high (n = 5) and –low/neg (n = 6) NS (H) and in the TCGA GBM cohort (n = 339) subdivided according to ERBB3 expression (I). No significant correlation between ERBB3 expression and any of these miRNAs has been observed (one-way ANOVA, in all cases p > 0.5). Mean \pm SEM.

(J) Alternative mechanisms (promoter methylation or neutralization by lnc-RNA SNHG5) for miR-205 silencing and ensuing ERBB3 overexpression in GBM and NS.



De Bacco *et al.*, Figure S4, related to Figure 3

Figure S4. ERBB3 is overexpressed in the absence of other EGFR family members, related to Figure 3.

(A-B) Heatmap showing matrix correlation of ERBB3 with the other EGFR family members in the 84 NS-panel (n = 84) (A) and in the TCGA GBM cohort (n = 497) (B). Pearson coefficients (R) and correlation plots are shown (* p < 0.05).

(C) Flow-cytometry showing expression of EGFR family members in representative ERBB3-high and -low NS. Mean fluorescence intensity (MFI) and % of positive cells are reported.

(D) Table showing the cumulative score (resulting from staining intensity + percentage of positive cells) after ERBB3 or ERBB2 IHC of GBMs from the TCGA cohort evaluated by the Human Protein Atlas. All available cases co-stained for ERBB3 and ERBB2 were included. No GBM displays ERBB3-ERBB2 co-staining.

(E) Representative IHC showing ERBB3, ERBB2, EGFR or ERBB4 staining of the same GBM tissues from the TCGA cohort performed by the Human Protein Atlas. Inset, higher magnification. Image credit: Human Protein Atlas.

(F) Stimulation of ERBB3-high NS, kept in the absence of any growth factor for 48 h, with NRG1 (left) or EGF (right) for 30', followed by immunoprecipitation and western blot with the indicated antibodies, showing no ERBB3 phosphorylation or coprecipitation with ERBB2 or EGFR. Cancer cell lines A549 and A375 were used as positive controls. ctrl, PBS treated cells; pTyr, anti-pan-phosphotyrosine.

(G) Cell viability in response to the indicated growth factors measured 4 days after treatment in representative ERBB3-high (BT308 and BT209) or -low NS (BT373). Dotted line, fold-increase versus cells kept in the absence of growth factors (no GF) = 1. Mean \pm SEM, n = 5.

(H) Western blot showing lack of ERBB3 phosphorylation on Tyr1289 at the indicated time points after treatment with the EGFR ligand EGF in representative ERBB3-high/EGFR-neg NS (BT308).

Activation of downstream signaling transducers AKT and MAPK is also shown. ERBB3-low/EGFR-high NS (BT373) sensitive to EGF was used as positive control. actin, loading control.

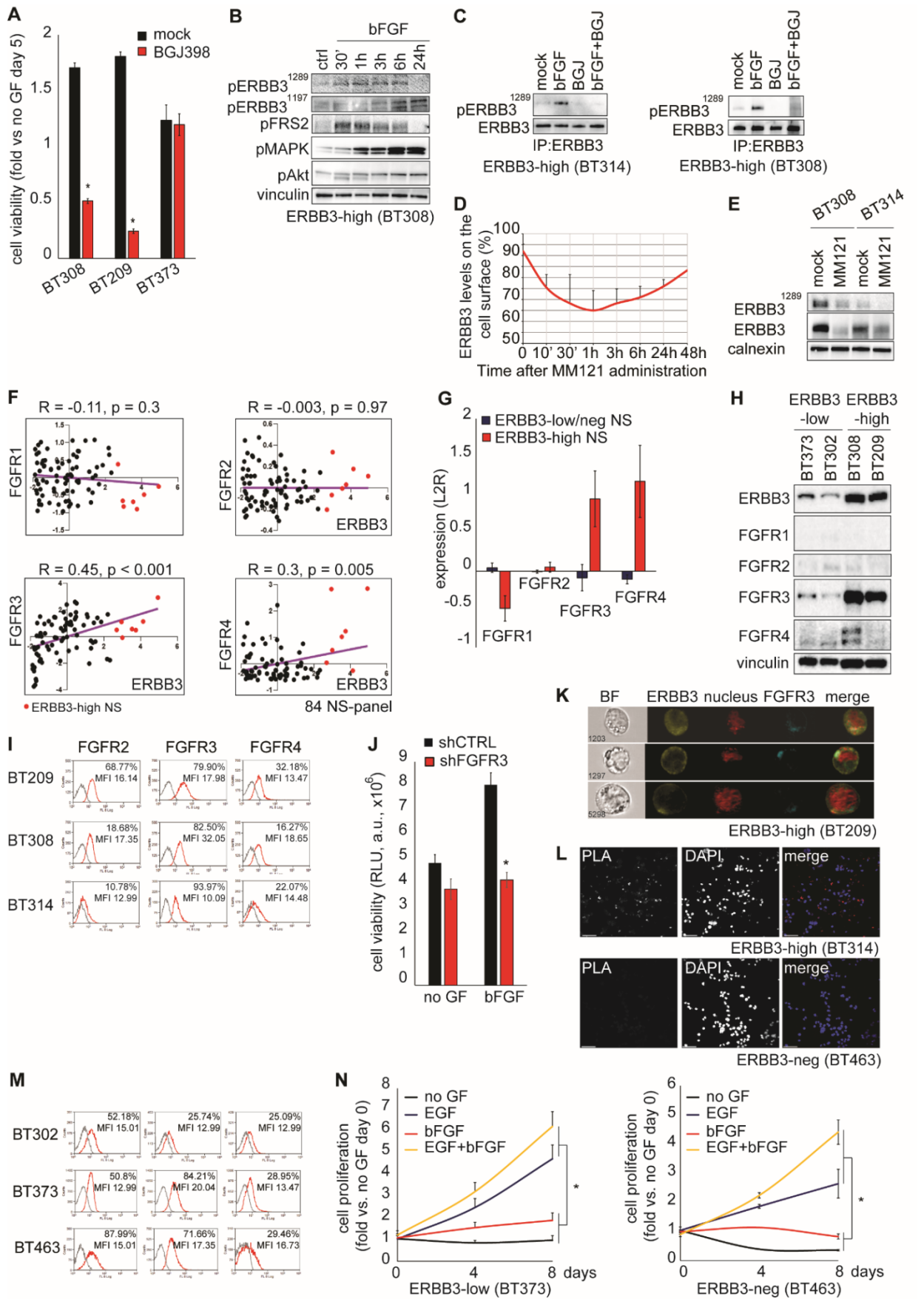


Figure S5. Overexpressed ERBB3 is activated by bFGF via FGFR3, related to Figure 3.

(A) Cell viability in representative ERBB3-high (BT308 and BT209) or –low NS (BT373) measured 5 days after treatment with or without pan-FGFR inhibitor BGJ398 in the presence of bFGF. Mock, PBS-treated cells (* $p < 0.001$, paired t test). Mean \pm SEM, $n = 6$.

(B) Western blot showing phosphorylation (p) of ERBB3 on Tyr1289 and Tyr1197, AKT and MAPK in ERBB3-high NS BT308 kept in the absence of any growth factor for 48 h and treated with bFGF for the indicated time-points. FRS2 phosphorylation was shown as surrogate marker of FGFR activation. ctrl, PBS treated cells; vinculin, loading control. The same vinculin immunoblot is shown in Figure 4B as part of the same experiment.

(C) Immunoprecipitation with anti-ERBB3 antibodies and western blot showing ERBB3 phosphorylation on Tyr1289 and ERBB3 total protein in ERBB3-high NS (left, BT314; right, BT308) pre-treated with or without the pan-FGFR inhibitor BGJ398 (BGJ) and supplied with bFGF. NS were kept in the absence of any growth factors for 48 h prior to treatment. Mock, PBS treated cells.

(D) Flow-cytometric quantification of the ERBB3 relative amount exposed at the cell surface (%) at different time points after treatment with MM121 in ERBB3-high NS (BT308). Mean \pm SEM, $n = 3$.

(E) Western blot showing ERBB3 phosphorylation on Tyr1289 and total protein levels after treatment with MM121 in ERBB3-high NS (BT308 and BT314) kept in standard medium (EGF + bFGF). Mock, PBS-treated cells; calnexin, loading control.

(F) Correlation plots between ERBB3 and FGFR1, FGFR2, FGFR3, or FGFR4 mRNA expression (L2R) in the 84-NS panel. Pearson correlation coefficients (R) and p-values are reported. Red dots, ERBB3-high NS.

(G) FGFR1-4 mRNA expression (microarray) in ERBB3-high ($n = 7$) and –low/neg NS ($n = 77$) (L2R).

(H) Western blot showing FGFR family members in representative ERBB3-low (BT373 and BT302) and ERBB3-high NS (BT308 and BT209). Vinculin, loading control.

(I) Flow-cytometry showing FGFR2, FGFR3 and FGFR4 expression in representative ERBB3-high NS (BT209, BT308 and BT314). Mean fluorescence intensity (MFI) and % of positive cells are reported.

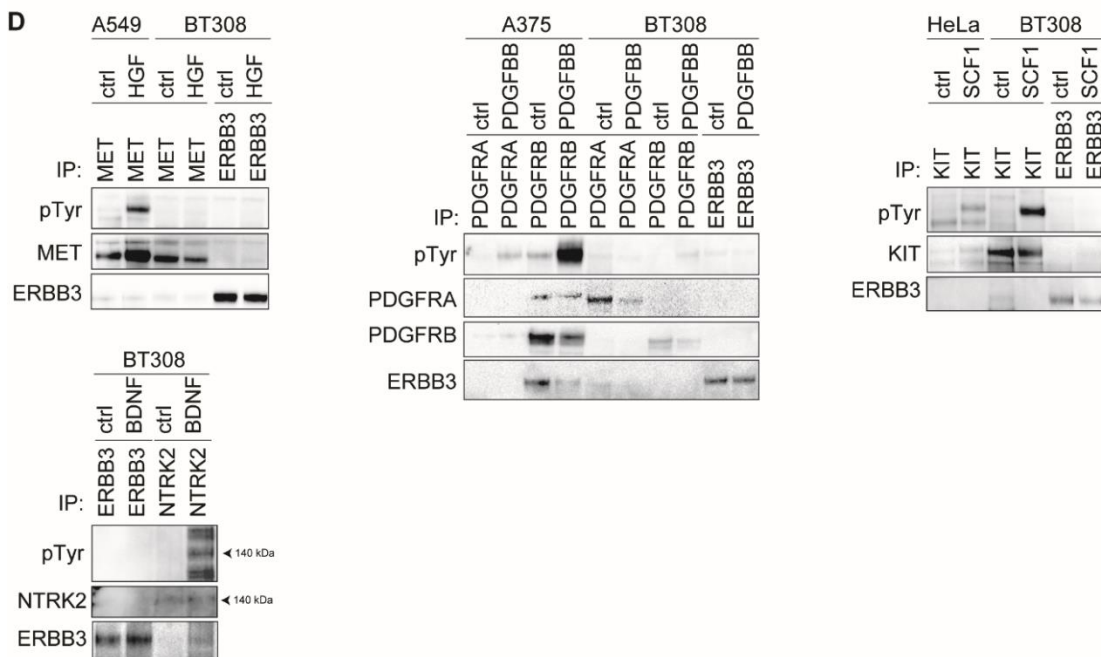
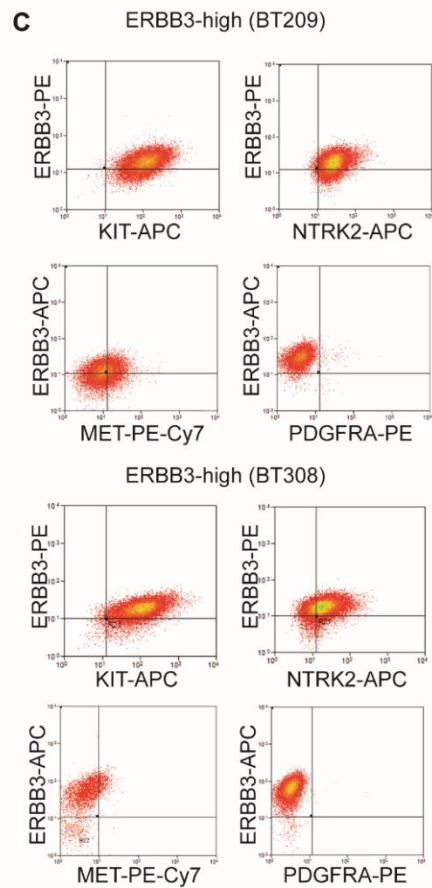
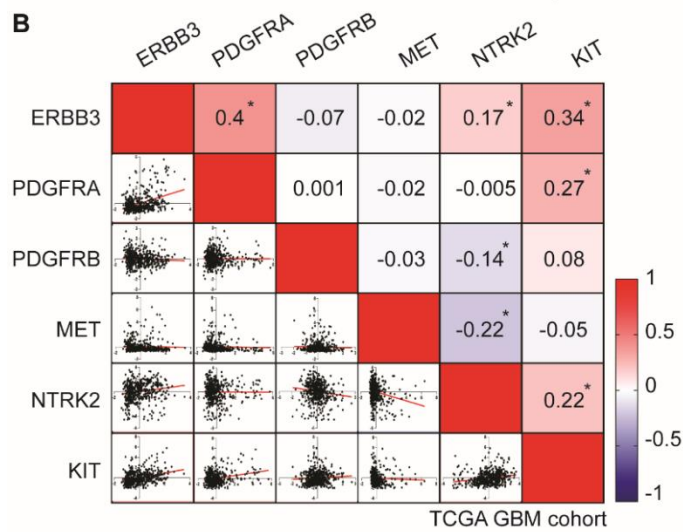
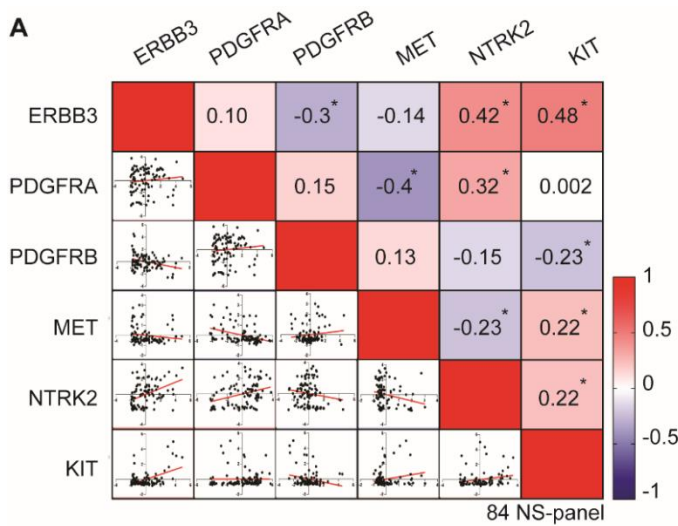
(J) Cell viability of ERBB3-high BT308, kept in the absence of any growth factor for 48 h, transduced with a specific FGFR3 shRNA (shFGFR3) and supplied with bFGF for 2 days. a.u., arbitrary units (* $p < 0.001$, shFGFR3 versus shCTRL paired t test). Mean \pm SEM, $n = 6$.

(K) Co-localization of ERBB3 and FGFR3 measured by Amnis ImageStream in single cells from representative ERBB3-high-NS (BT209). Single and merged fluorescent antibody signals are shown. BF, bright field.

(L) Proximity ligation assay (PLA) showing ERBB3-FGFR3 interaction in representative ERBB3-high NS (BT314). ERBB3-neg NS (BT463) is used as negative control. DAPI, nuclear staining. Scale bar, 75 μm .

(M) Flow-cytometry showing FGFR2, FGFR3 and FGFR4 expression in representative ERBB3-low (BT302 and BT373) and -neg NS (BT463). Mean fluorescence intensity (MFI) and % of positive cells are reported.

(N) Cell viability in representative ERBB3-low (BT373) and -neg (BT463) NS measured at the indicated time points in the presence of EGF or bFGF or both (EGF + bFGF) (* $p < 0.001$, paired t test). Mean \pm SEM, $n = 6$.



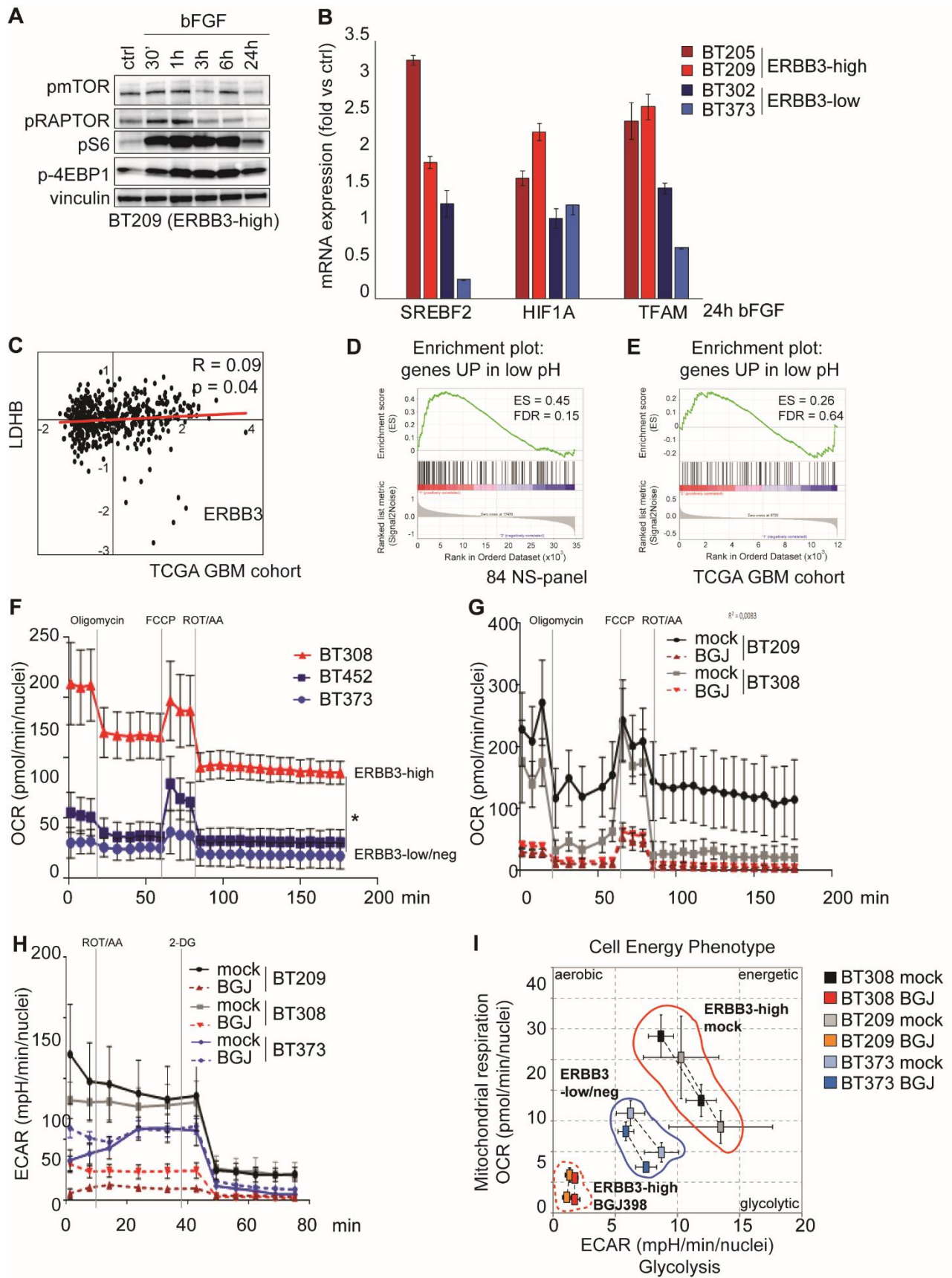
De Bacco *et al.*, Figure S6, related to Figure 3

Figure S6. Lack of ERBB3 activation by MET, PDGFRs, KIT and NTRK2, related to Figure 3.

(A and B) Heatmap showing matrix correlation of ERBB3 with the indicated RTKs in the 84 NS-panel (n = 84) (A) and in the TCGA GBM cohort (n = 497) (B). Pearson coefficients (R) and correlation plots are reported (* p < 0.05).

(C) Flow-cytometry showing ERBB3 co-expression with different RTKs in representative ERBB3-high NS (BT209 and BT308).

(D) Stimulation of ERBB3-high NS, kept in the absence of any growth factor for 48 h, with hepatocyte growth factor (HGF, MET ligand), or platelet derived growth factor BB (PDGFBB, PDGFRA and -B ligand), or stem cell factor 1 (SCF1, KIT ligand) or brain derived neurotrophic factor (BDNF, NTRK2 ligand) for 30', followed by immunoprecipitation and western blot with the indicated antibodies, showing no ERBB3 phosphorylation or coprecipitation with any of the above receptors. Cancer cell lines A549, A375 and HeLa were used as positive controls for receptor immunoprecipitation. Ctrl, PBS treated cells; pTyr, anti-pan-phosphotyrosine.



De Bacco *et al.*, Figure S7, related to Figure 4

Figure S7. In ERBB3 overexpressing NS, bFGF sustains the PI3-K/AKT/mTOR pathway and metabolic hyperactivation, related to Figure 4.

(A) Western blot showing phosphorylation (p) of mTOR pathway effectors in ERBB3-high NS (BT209) kept in the absence of any growth factor for 48 h and treated with bFGF for the indicated time-points. Ctrl, PBS-treated cells; vinculin, loading control. The same vinculin immunoblot is shown in Figure 3G as part of the same experiment.

(B) Expression of mTOR target genes SREBF2, HIF1A and TFAM in ERBB3-high (BT205 and BT209) and ERBB3-low NS (BT302 and BT373) kept in the absence of any growth factor for 48 h and treated with bFGF for 24 h. Mean \pm SEM, n = 3.

(C) Correlation plots between ERBB3 and LDHB mRNA expression (L2R) in the TCGA GBM cohort (n = 497). Pearson correlation coefficient (R) and p-value are reported.

(D and E) Gene set enrichment analysis of ERBB3-high versus ERBB3-low/neg cases performed in the 84 NS-panel (n = 84) (D) and in the TCGA GBM cohort (n = 497) (E), showing that genes upregulated in low pH conditions are prominently enriched in ERBB3-high NS and GBMs.

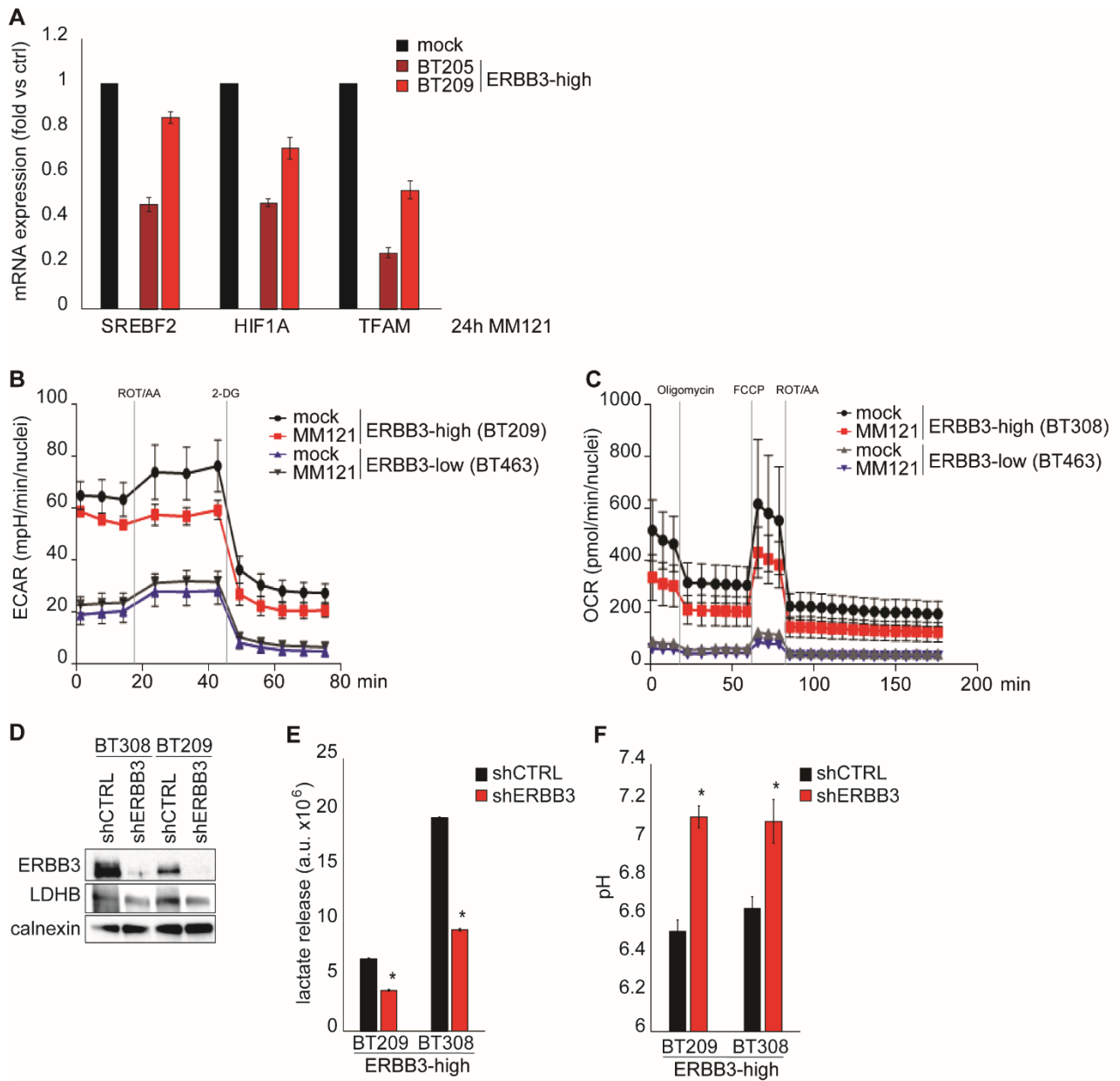
(F) Oxygen Consumption Rate (OCR) measured by Seahorse mitochondrial stress assay of representative ERBB3-high (BT308) and ERBB3-low/neg NS (BT452 and BT373) assessed in basal conditions (standard medium, EGF + bFGF) (mean \pm SEM, n = 4; * p < 0.001, two-way ANOVA). ROT/AA: rotenone/antimycin A.

(G) OCR measured as in (F) in representative ERBB3-high NS (BT209 and BT308) assessed 24 h after treatment with or without BGJ398 in standard medium (EGF + bFGF) (mean \pm SEM, n = 6; paired t test mock versus BGJ treated NS, p < 0.001). Mock, PBS-treated cells.

(H) Extracellular Acidification Rate (ECAR) in representative ERBB3-high NS (BT209 and BT308) and ERBB3-low/neg NS (BT373) assessed as in (G) (mean \pm SEM, n = 5, paired t test mock versus BGJ treated NS, p < 0.001. BT373: not significant, p = 0.56). Mock, PBS-treated cells; 2-DG: 2-Deoxy-D-glucose.

(I) Representative XF PhenoGram obtained by plotting basal OCR versus basal ECAR values obtained in the experiments shown in (H).

See also Table S3.



De Bacco *et al.*, Figure S8, related to Figure 5

Figure S8. ERBB3 overexpression is required for the PI3-K/AKT/mTOR pathway and cell metabolism upregulation, related to Figure 5.

(A) Expression of the mTOR target genes SREBF2, HIF1A and TFAM 24 h after treatment with or without MM121 in ERBB3-high NS (BT205 and BT209) kept in standard medium (EGF + bFGF). Mock, PBS-treated cells. Mean \pm SEM, n = 3.

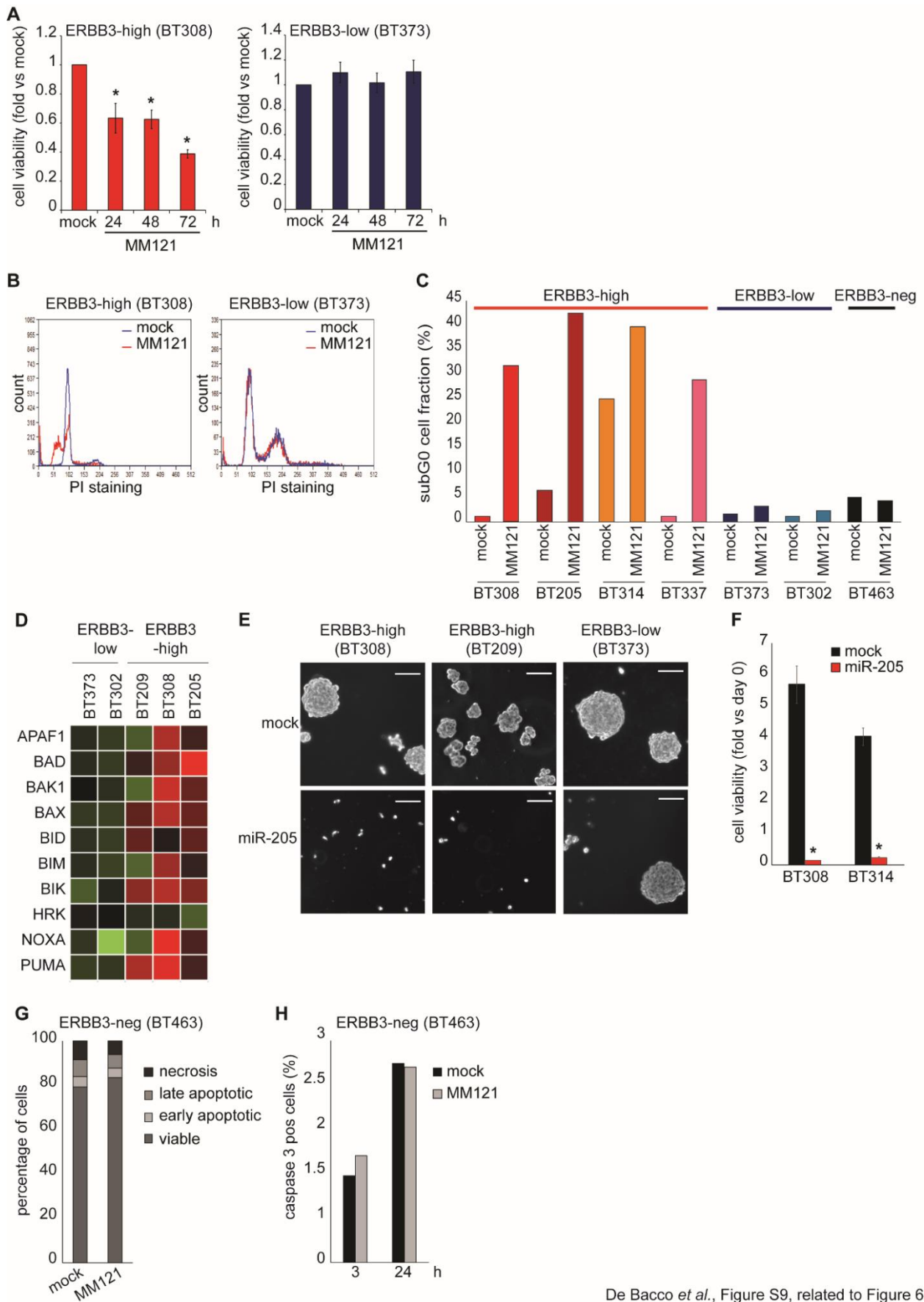
(B) Extracellular Acidification Rate (ECAR) measured by Seahorse glycolytic rate assay in representative ERBB3-high (BT209) and ERBB3-low NS (BT463), assessed 24 h after treatment with or without MM121 in standard medium (EGF + bFGF) (mean \pm SEM, n = 4; two-way ANOVA, $p < 0.001$). Mock, PBS-treated cells; ROT/AA: rotenone/antimycin A; 2-DG: 2-Deoxy-d-glucose.

(C) Oxygen Consumption Rate (OCR) measured by Seahorse mitochondrial stress assay in representative ERBB3-high (BT308) and ERBB3-low NS (BT463), assessed 24 h after treatment with or without MM121 in standard medium (EGF + bFGF) (mean \pm SEM, n = 4; two-way ANOVA, $p < 0.001$). Mock, PBS-treated cells.

(D) Western blot showing ERBB3 and LDHB expression in representative ERBB3-high NS (BT308 and BT209) transduced with a specific ERBB3 shRNA (shERBB3; shCTRL, mock-transduced NS) and kept in standard medium (EGF + bFGF). calnexin: loading control.

(E) Lactate release in culture media from NS treated as in (D) (* $p < 0.005$, paired t test). a.u., arbitrary units. Mean \pm SEM, n = 3.

(F) pH of culture media from NS treated as in (D) (* $p < 0.05$, paired t test,). Mean \pm SEM, n = 3.



De Bacco *et al.*, Figure S9, related to Figure 6

Figure S9. Selective ERBB3 inhibition induces ERBB3-high NS apoptosis, related to Figure 6.

(A) Cell viability measured in ERBB3-high (BT308) or -low NS (BT373) at the indicated time points after treatment with or without MM121 in standard medium (EGF + bFGF). Mock, PBS-treated cells. (* $p < 0.05$, paired t test). Mean \pm SEM, $n = 6$.

(B) Cell distribution in different cell cycle phases evaluated by flow-cytometry in ERBB3-high (BT308) or ERBB3-low NS (BT373) 24 h after treatment with or without MM121 in standard medium (EGF + bFGF). Mock, PBS-treated cells.

(C) Percentage of cells in the subG0 phase evaluated as in (B) in representative ERBB3-high, -low and -neg NS. Mock, PBS-treated cells.

(D) Induction of pro-apoptotic genes in ERBB3-low (BT373 and BT302) and ERBB3-high NS (BT209, BT308 and BT205) 24 h after treatment with MM121 in standard medium (EGF + bFGF).

Data (qPCR) are expressed as fold versus PBS-treated cells, mean \pm SEM, $n = 3$.

(E) Micrographs of ERBB3-high (BT308 and BT209) and ERBB3-low NS (BT373) 96 h after miR-205 transduction. Mock, non-transduced cells. Scale bar, 50 μ m.

(F) Cell viability measured in ERBB3-high NS (BT308 and BT314) 96 h after miR-205 transduction (* $p < 0.05$, paired t test). Mock, non-transduced cells. Mean \pm SEM, $n = 6$.

(G and H) Cell apoptosis measured as Annexin V/DAPI incorporation (G) and Caspase-3 activation (H) in ERBB3-neg NS (BT463).

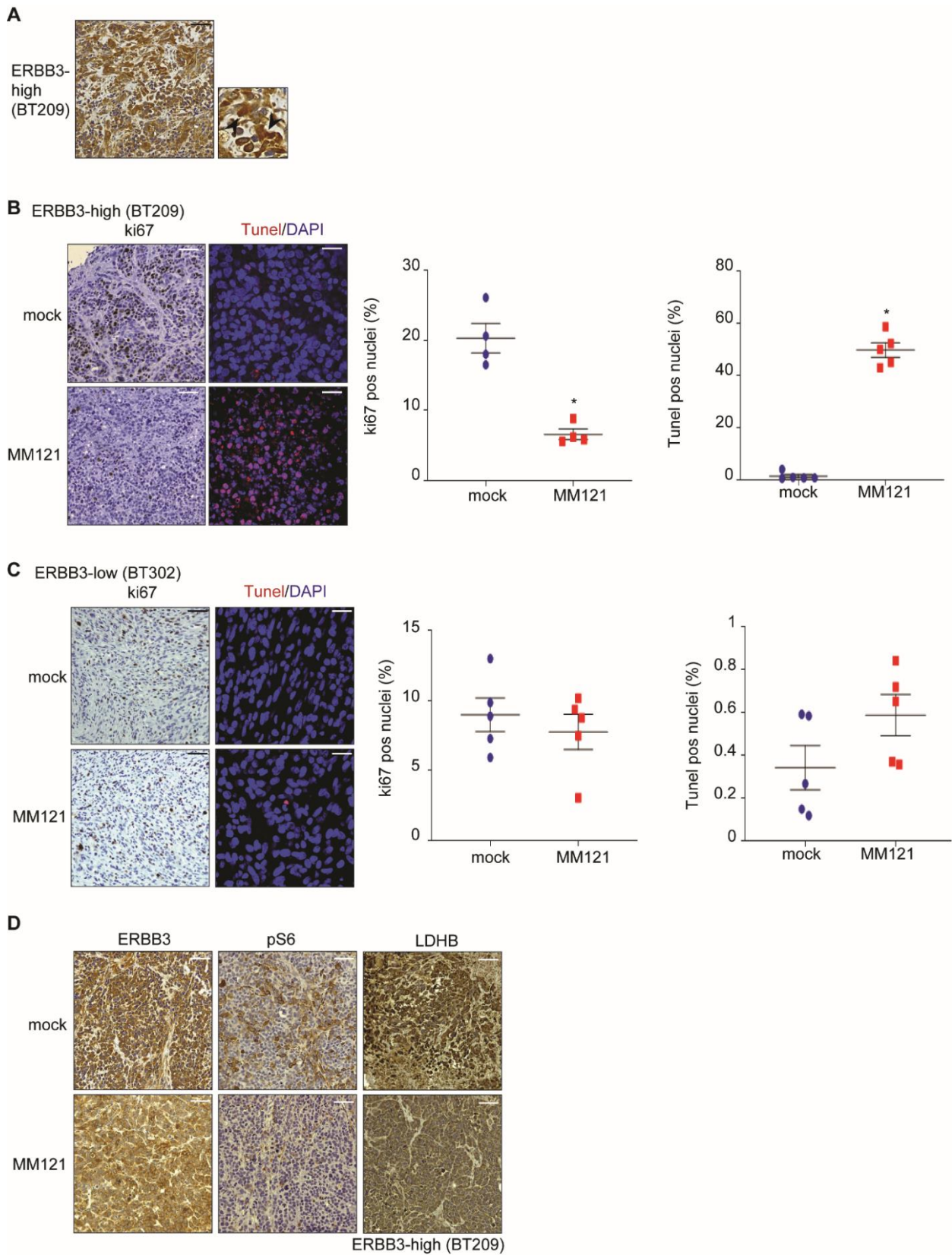


Figure S10. ERBB3 antibodies inhibit ERBB3-high experimental GBMs, related to Figure 7.

(A) Representative ERBB3 IHC staining in tumors generated by subcutaneous transplant of ERBB3-high NS (BT209). ERBB3-high tumors displayed ERBB3 nuclear staining (arrows). Scale bar, 100 μ m.

(B) Representative ki67 and TUNEL stainings of tumors generated as in (A), treated with or without MM121, and analyzed at the experimental end point (left). Quantification of the percentage of ki67 and TUNEL positive cells (n = 10 HPF/condition) (ki67: * p = 0.029; TUNEL: * p = 0.008; Kolmogorov-Smirnov test) (right). Scale bar, 100 μ m (ki67) and 25 μ m (TUNEL).

(C) Representative ki67 and TUNEL stainings of tumors generated by subcutaneous transplant of ERBB3-low NS (BT302) treated with or without MM121, and analyzed at the experimental end point (left). Quantification of the percentage of ki67 and TUNEL positive cells (n = 10 HPF/condition) (right). Scale bar, 100 μ m (ki67) and 25 μ m (TUNEL).

(D) Representative IHC staining of ERBB3, phospho-S6 (pS6) and LDHB on the same tumors as in (B). Scale bar, 100 μ m.

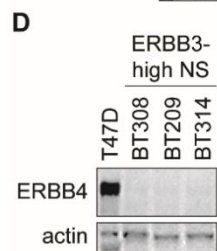
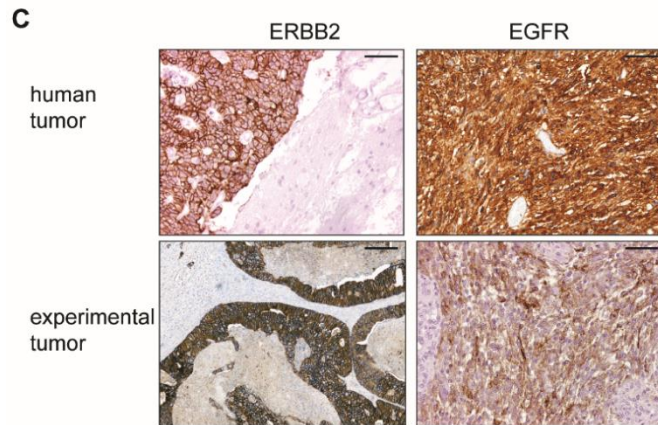
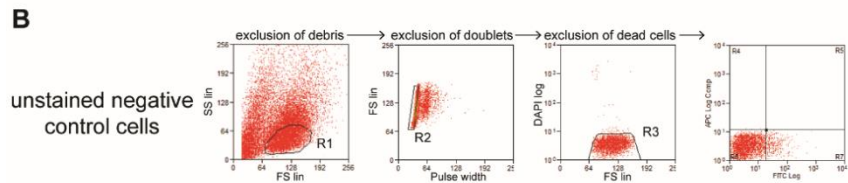
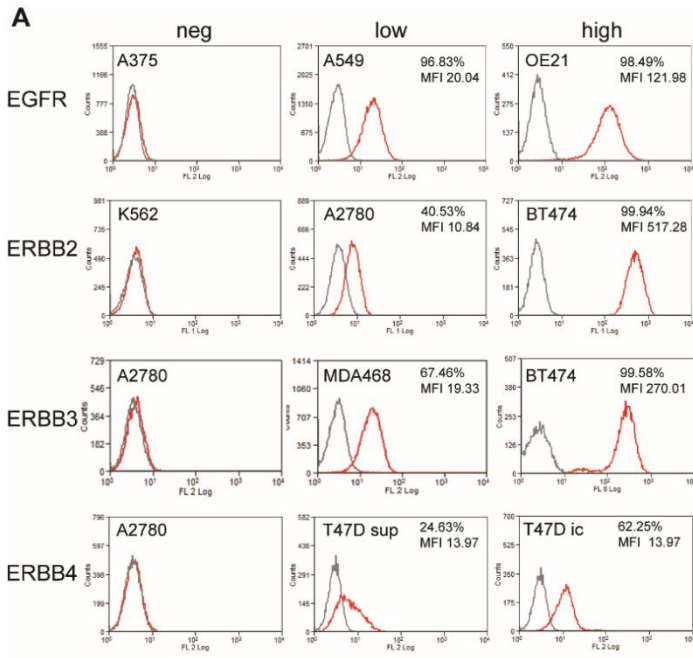


Figure S11. Antibody validation, related to STAR Methods.

(A) Validation of antibodies used for measuring expression of EGFR family receptors in NS by flow-cytometry. For each antibody, the indicated negative, low- and high-expressing conventional cell lines were used. The percentage of positive cells and the mean fluorescence intensity (MFI) were calculated by comparing stained (red line) versus unstained (grey line) cells in each sample.

(B) The flow-cytometric gating strategy is established for each sample in unstained negative control cells to exclude debris (R1), doublet cells (R2) and dead cells (R3), by analysis of physical parameters (SS, side scatter; FS, forward scatter; DAPI staining).

(C) Validation of ERBB2 and EGFR antibodies used in IHC staining. Human and experimental tumor tissues overexpressing ERBB2 (HER2⁺ human breast cancer metastasis, parental tumor and mouse xenograft) or EGFR (EGFR^{amp} GBM, parental and generated by NS (BT379) transplantation). Scale bar, 100 μ m.

(D) Validation of ERBB4 antibodies used in western blot analysis. Breast cancer cell line T47D was used as positive control and compared to representative ERBB3-high NS (BT308, BT209 and BT314). actin, loading control.

Table S1, related to Figures 1 and S1-S2. ERBB3 expression and NS classification

	NS code	ERBB3 (L2R)	Wang Q. subtype¹	Wang Z. subtype²
ERBB3-high NS	BT209	4.89	PN	II
	BT454	4.09	PN	II
	BT337	3.69	PN	II
	BT358	3.62	MES	II
	BT308	3.61	PN	II
	BT205	3.10	PN	II
	BT314	2.96	PN	II
ERBB3-low NS	BT373	2.49	PN	II
	BT430	2.28	PN	non I-II
	BT407	2.13	PN	non I-II
	BT326	1.85	PN	non I-II
	BT138	1.59	CL	non I-II
	BT443	1.49	PN	non I-II
	BT284	1.41	PN	I
	BT201	1.35	PN	non I-II
	BT419	1.24	CL	I
	BT414	1.16	CL	non I-II
	BT302	1.12	MES	non I-II
	BT434	1.03	CL	I
	BT446	0.85	CL	I
	BT334	0.82	CL	non I-II
	BT422	0.48	CL	non I-II
	BT283	0.47	PN	I
	BT428	0.46	CL	I
	BT437	0.44	MES	I
	BT418	0.43	PN	non I-II
	BT266	0.38	PN	non I-II
	BT500	0.37	CL	I
	BT235	0.36	PN	I
	BT299	0.27	MES	non I-II
	BT462	0.19	PN	I
	BT150	0.15	PN	I
	BT333	0.14	PN	non I-II
	BT294	0.14	CL	I
	BT245	0.09	PN	non I-II
BT442	0.04	CL	I	
BT415	0.03	CL	I	

continued

	NS code	ERBB3 (L2R)	Wang Q. subtype ¹	Wang Z. subtype ²
ERBB3-neg NS	BT483	-0.05	CL	I
	BT398	-0.06	MES	I
	BT470	-0.07	CL	non I-II
	BT517	-0.14	CL	non I-II
	BT404	-0.15	MES	non I-II
	BT159	-0.23	PN	I
	BT423	-0.25	CL	I
	BT275	-0.26	PN	non I-II
	BT273	-0.37	PN	non I-II
	BT513	-0.38	MES	II
	BT453	-0.42	CL	I
	BT479	-0.62	MES	non I-II
	BT408	-0.63	CL	I
	BT451	-0.69	CL	I
	BT261	-0.75	CL	I
	BT371	-0.87	MES	II
	BT297	-0.88	CL	I
	BT449	-1.04	MES	non I-II
	BT249	-1.05	PN	I
	BT328	-1.13	MES	non I-II
	BT379	-1.20	CL	non I-II
	BT413	-1.24	CL	I
	BT468	-1.28	CL	I
	BT332	-1.37	CL	I
	BT487	-1.38	MES	non I-II
	BT246	-1.41	CL	I
	BT279	-1.43	PN	non I-II
	BT202	-1.48	CL	non I-II
	BT421	-1.52	PN	II
	BT490	-1.54	CL	non I-II
	BT330	-1.57	MES	II
	BT232	-1.60	MES	non I-II
	BT274	-1.63	PN	non I-II
	BT445	-1.67	CL	I
	BT493	-1.70	CL	I
	BT155	-1.71	CL	non I-II
	BT287	-1.73	MES	II
	BT452	-1.74	MES	non I-II
	BT322	-1.75	MES	non I-II
	BT219	-1.78	MES	II
BT206	-1.81	PN	non I-II	
BT480	-1.82	MES	non I-II	
BT417	-1.83	CL	I	
BT157	-1.84	MES	II	
BT467	-1.86	MES	II	
BT456	-1.92	MES	II	
BT463	-1.93	PN	non I-II	

¹Based on Wang Q. *et al.*, 2017; CL, classical; MES, mesenchymal; PN, proneural;

²Based on Wang Z. *et al.*, 2020; I, Type I; II, Type II; non I-II, non-Type I&II. L2R, log2ratio.

Table S2, related to Figure 1. Clinical data of patients that originated the 84-NS panel (all untreated primary glioblastomas, WHO grade IV gliomas)

patient code	gender	age	location	PFS (months)	OS (months)
BT138	F	37	F-T left	2	6
BT150	M	59	P left	4	10
BT155	F	45	F-T right	9	13
BT157	M	53	T left	n.a.	9
BT159	M	52	F right	n.a.	1
BT201	M	61	P right	14	20
BT202	M	69	T-P right	n.a.	4
BT205	M	73	L right	n.a.	2
BT206	M	67	F left	n.a.	4.5
BT209	M	55	T-P left	3.5	4.5
BT219	M	54	T left	n.a.	5
BT232	M	49	T-P-O left	n.a.	7.5
BT235	M	68	F-T right	n.a.	24.5
BT245	F	53	T left	43	46
BT246	M	61	F left	3	4.5
BT249	M	63	T left	n.a.	n.a.
BT261	M	63	T-P right	n.a.	3
BT266	M	7	DIPG	n.a.	10
BT273	M	57	F-T-P right	n.a.	1
BT274	M	48	T right	9	18
BT275	F	66	P right	n.a.	14
BT279	F	58	P left	n.a.	15
BT283	F	44	P right	9	9.5
BT284	M	74	O left	7	23.5
BT287	M	70	F-T left	14	16
BT294	M	54	O-P right	18	28.5
BT297	M	53	T left	n.a.	14
BT299	M	48	T-P-O left	n.a.	6.5
BT302	F	17	F right	n.a.	n.a.
BT308	M	76	T left	n.a.	3
BT314	M	67	T right	n.a.	18
BT322	M	66	F left	3.5	11.5
BT326	M	27	F left	6	6.5
BT328	M	54	F-P left	n.a.	6
BT330	M	58	F right	n.a.	35.5
BT332	M	74	O-P left	n.a.	9
BT333	F	37	T left	n.a.	7
BT334	M	63	F-T right	n.a.	9
BT337	M	63	T-P-F left	9.5	17.5
BT358	F	62	F right	n.a.	20
BT371	F	46	F left	5	14.5
BT373	M	62	F right	9	22
BT379	M	72	F-P right	n.a.	3
BT398	M	48	Thm left	4	8
BT404	M	57	F left	3.5	9.5
BT407	M	55	T-F left	n.a.	11
BT408	F	61	P left	13	24
BT413	F	71	T left	n.a.	8.5
BT414	F	65	O-P left	n.a.	3
BT415	M	47	P right	14	18.5
BT417	M	50	F left	n.a.	24

continued

patient code	gender	age	location	PFS (months)	OS (months)
BT418	F	67	P left	29	33
BT419	M	64	P-T DX	n.a.	2
BT421	M	65	T right	n.a.	15
BT422	M	68	F left	7.5	11
BT423	F	39	F right	21	n.a.
BT428	M	64	O-P right	34	n.a.
BT430	F	70	T left	4	6
BT434	M	74	F left	n.a.	5
BT437	M	48	T left	10	12
BT442	F	58	T right	9	16
BT443	M	65	T left	5.5	18
BT445	M	60	I right	9	25
BT446	M	45	O-P left	n.a.	n.a.
BT449	M	68	T-O right	4.5	9
BT451	F	37	F left	n.a.	5
BT452	F	65	T right	n.a.	0
BT453	M	58	T right	33	22.5
BT454	M	75	P left	n.a.	5
BT456	M	60	T left	7.5	20
BT462	M	70	F right	4	6.5
BT463	M	69	T-P left	4.5	11
BT467	M	57	F left	n.a.	10.5
BT468	M	63	P-T SIN	11	14.5
BT470	M	41	F-P left	n.a.	13
BT479	M	52	O-P right	n.a.	10
BT480	F	68	F right	4	10
BT483	M	36	F-T right	8	13
BT487	M	70	T right	9	15
BT490	F	73	T left	11	24
BT493	M	43	F left	26	n.a.
BT500	F	64	P left	n.a.	20
BT513	M	57	T left	4	9.5
BT517	M	47	F left	7	13

RED: ERBB3-high patients matched with ERBB3-high NS. All other patients are matched with ERBB3-low or -neg NS. PFS, progression Free Survival; OS, overall survival; F, frontal; P, parietal; T, temporal; O, occipital; L, lenticular; I, insular; Thm, thalamic. n.a., not available.